UNIVERSITY OF CALIFORNIA

Los Angeles

# Impact of class I antigen presentation alterations in melanoma

A dissertation submitted in partial satisfaction of the requirements for

the degree Doctor of Philosophy in

Molecular and Medical Pharmacology

by

Mildred Galvez

2023

ABSTRACT OF THE DISSERTATION

Impact of class I antigen presentation alterations in melanoma

by

Mildred Galvez

Doctor of Philosophy in Molecular and Medical Pharmacology

University of California, Los Angeles, 2023

Professor Antoni Ribas, Chair

Immune checkpoint blockade (ICB) targeting programmed cell death-1 (PD-1) has led to prolonged clinical responses among several patients with melanoma and other cancer types. ICB response relies on effective immune recognition and elimination of tumor cells. This depends on the successful presentation of tumor-specific antigens on surface major histocompatibility complex (MHC) class I molecules by tumor cells to the T-cell receptor of cytotoxic CD8+ T cells. Currently, both primary and acquired mechanisms of resistance remain significant barriers to expanding the therapeutic benefits of anti-PD-1 treatment. Several studies have stressed the critical role of antigen processing machinery (APM) defects in mediating resistance to ICB therapies. More specifically, aberrations of the β-2-microglobulin (B2M) gene, which encodes a critical component of the MHC class I molecule, were found to be enriched in patients with melanoma who progressed during therapy. Nevertheless, there are cases of patients with B2M-deficient tumors that respond to ICB, but the exact mechanism mediating this response is currently unknown. Presently, the exact effect of MHC class I APM alterations on anti-PD-1 therapy response requires further characterization and the cells mediating the anti-tumorigenic

effects of PD-1 blockade in B2M-defective tumors have not been fully elucidated. In this work, we aim to holistically characterize alterations in components involved in class I antigen processing, presentation, and regulation in melanoma tumors, as well as to elucidate the main cell mediators of class I-deficient tumor removal in patient-derived biopsies and mouse models. Using a clinical dataset of patients with melanoma treated with ICB, whole-exome sequencing and bulk RNA-sequencing data from baseline tumor samples were analyzed to identify somatic class I APM alterations and evaluate correlative clinical outcomes, infiltrating immune cells, and gene expression patterns. Additionally, human melanoma cell lines and B2M-null mouse tumor models were utilized to validate these findings and further explore the impact of B2M and MHC class I defects on tumor intrinsic and extrinsic factors. Collectively, our findings may help offer alternative therapeutic targets and avenues for the treatment of tumors with class I-mediated ICB resistance.

The dissertation of Mildred Galvez is approved.

Valerie A. Arboleda

David A. Nathanson

Maureen A. Su

Antoni Ribas, Committee Chair

University of California, Los Angeles

2023

This work is dedicated to my family in the US and Mexico and to my friends who have supported me throughout.

TABLE OF CONTENTS

List of Figures

**Chapter 1: Class I antigen presentation and immune checkpoint blockade**



**Chapter 2: Anti-tumor immune responses in B2M deficient cancers**

**Chapter 3: Role of altered MHC class I antigen presentation machinery in response and resistance to immune checkpoint blockade in melanoma**

List of Tables

**Chapter 2: Anti-tumor immune responses in B2M deficient cancers**



**Chapter 3: Role of altered MHC class I antigen presentation machinery in response and resistance to immune checkpoint blockade in melanoma**



All supplementary tables are attached separately as Excel spreadsheets. The pages listed above are where the supplementary tables are first referenced in the text. Main tables are included within the chapter.

Acknowledgments

I would like to first express my greatest gratitude to my advisor, Dr. Antoni Ribas. Thank you for supporting me as I developed the project, learned from others, and continued my professional development under your guidance. Joining in the middle of a pandemic was not easy, but your patience and the guidance from others helped me greatly as I first started. Thank you for continuously encouraging me and supporting me as I applied for several things– the opportunities and networking that I gained through these experiences were invaluable and will follow me for the rest of my career. It has been such a privilege working in your lab and learning directly from you. You are an incredible role model and I aspire to follow in your footsteps. Out of all the things that I admire about you, what I admire most is the warmth and kindness with which you approach your patients– thank you and Dr. Amy Sun for giving me the opportunity to see this.

I would also like to express my utmost gratitude to the current and past members of the Ribas lab as well as our collaborators at the Parker Institute for Cancer Immunotherapy. I would like to especially thank Dr. Katie M. Campbell, Egmidio Medina, and Dr. Davis Y. Torrejon who performed the work that set the foundation for my project. I would also like to thank all the lab members that I worked with for giving me the opportunity to learn from them. I am particularly grateful for my fellow graduate students Daniel Karin and Justin Saco– thank you for all your support and I wish you the best during your graduate training!

And of course, I would love to thank all of my mentors and advisors from across all my associated programs. Beginning with my committee, I would like to thank Dr. David Nathanson, Dr. Maureen Su, and Dr. Valerie Arboleda for their extensive professional and personal support. From MSTP, I would like to thank Dr. Carlos Portera-Cailliau, Dr. David Dawson, Dr. Olujimi Ajijola, Dr. Maureen Su, Susie Esquivel, Maleka Decker, and Staci Chikami for their guidance, encouragement, and

support. From Molecular and Medical Pharmacology, I would like to express my appreciation for Dr. Ting-Ting Wu and Emily Fitch who have both helped me with countless things, as well as my amazing Ph.D. cohort who made this journey a million times better. From the Graduate Programs in Bioscience, I would like to thank Dr. Greg Payne and Dr. Diana Azurdia who have helped me in ways I cannot even begin to describe– thank you for always being there for me during the most difficult times. From the David Geffen School of Medicine at UCLA, thank you immensely to Dr. Lee Miller and Dr. Deborah Lehman for their never-ending encouragement and support. Lastly, from the Charles R. Drew University of Medicine of Science, thank you to Dr. Daphne Calmes, Kay Lynn Ceja, and many others for believing in me, supporting me, and guiding me from the very beginning.

Lastly, the biggest thank you to my family and friends. My Ph.D. training has been a long and arduous but incredibly rewarding road, something I could not have done without the encouragement, support, and motivation from all my family members and friends. Thank you to my wonderful peers, colleagues, and friends from my hometown, undergraduate training, past labs, medical school, graduate school, and MSTP– this really was a team effort! Thank you to my family– my mom, dad, brother, sister, grandma, grandpa, aunts and cousins, and all others– for teaching me the most valuable lessons in life. Thank you for the hard work and the obstacles that you all have overcome as you moved to a new country to give us better opportunities than you ever had. Thank you for instilling in me an unwavering perseverance in the face of personal and professional adversity. And, thank you for always believing in me.

**Article Submissions**

Chapter 2 was adapted from an article submission of work that was co-led by Davis Y. Torrejon and Mildred Galvez and supervised by Antoni Ribas. The manuscript is titled “Anti-tumor immune responses in B2M deficient cancers” co-authored by Davis Y. Torrejon,* Mildred Galvez,* Gabriel Abril-Rodriguez, Katie M. Campbell, Egmidio Medina, Agustin Vega-Crespo, Anusha Kalbasi, Begoña Comin-Anduix, and Antoni Ribas. It was submitted to *Cancer Immunology Research* on February 2023. *Equal contributions as first authors.

Chapter 3 is a manuscript in preparation of work that was led by Mildred Galvez and supervised by Antoni Ribas. The manuscript is titled “Role of altered MHC class I antigen presentation machinery in response and resistance to immune checkpoint blockade in melanoma” co-authored by Mildred Galvez, Egmidio Medina, Katie M. Campbell, and Antoni Ribas. The finalized version will be submitted for consideration for publication in 2024.

**Funding Sources**

Mildred Galvez was funded by the UCLA-Caltech MSTP Training Grant NIH NIGMS T32 GM008042 and the UCLA Tumor Cell Biology Training Program NIH T32 CA009056.

## VITA

### EDUCATION

| | |
|---|---|
| 2016 - Present | UCLA-Caltech Medical Scientist Training Program (MSTP)<br>UCLA Department of Molecular and Medical Pharmacology<br>David Geffen School of Medicine at UCLA<br>Charles R. Drew University of Medicine and Science<br>M.D./Ph.D. |
| 2009 - 2013 | UC Berkeley<br>B.A. Molecular and Cell Biology: Immunology and Pathogenesis<br>Minor in Anthropology |

### HONORS and AWARDS

| | |
|---|---|
| 2023 | St. Jude Future Fellow Research Conference |
| 2022 - 2023 | UCLA Edward A. Bouchet Graduate Honor Society |
| 2022 | American Association for Cancer Research Minority Scholar in Cancer Research Award |
| 2021 - 2023 | UCLA T32 Training Program in Tumor Cell Biology |
| 2016 - 2025 | David Geffen School of Medicine at UCLA Leaders of Tomorrow Scholarship |
| 2016 - 2017 | David Geffen School of Medicine at UCLA Merit Scholarship |
| 2013 | UC Berkeley Dean's Honors |
| 2013 | UC Berkeley Distinction in General Scholarship |
| 2013 | UC Berkeley Molecular and Cell Biology Departmental Honors |
| 2011 - 2013 | UC Berkeley Rose Hills Foundation Science and Engineer Scholarship |
| 2009 - 2013 | UC Berkeley Biology Scholars Program |
| 2009 - 2013 | UC Berkeley Coalition for Excellence and Diversity in Mathematics, Science, and Engineering |

### PRESENTATIONS

***Select Oral Presentations***

| | |
|---|---|
| 2023 | UCLA Jonsson Comprehensive Cancer Center Trainee Seminar |
| 2023 | UCLA Molecular and Medical Pharmacology Seminar |
| 2023 | UCLA Edward A. Bouchet Graduate Honor Society Luncheon |
| 2022 | UCLA Molecular and Medical Pharmacology Annual Retreat |
| 2022 | UCLA-Caltech MSTP Annual Research Conference |
| 2022 | UCLA Tumor Cell Biology T32 Seminar |
| 2022 | Parker Institute for Cancer Immunotherapy Annual Retreat |
| 2022 | UCLA Molecular and Medical Pharmacology Seminar |
| 2021 | UCLA-Caltech MSTP Tutorial Series |
| 2021 | UCLA Tumor Cell Biology T32 Seminar |

***Select Poster Presentations***

| | |
|---|---|
| 2023 | UCLA Jonsson Comprehensive Cancer Center Tumor Immunology Retreat |
| 2023 | St. Jude Future Fellow Research Conference, Memphis, TN |
| 2023 | UCLA Jonsson Comprehensive Cancer Center Annual Retreat |
| 2023 | American Association for Cancer Research Annual Conference, Orlando, FL |
| 2023 | Annual Yale Bouchet Conference on Diversity and Graduate Education, New Haven, CT |
| 2022 | UCLA Jonsson Comprehensive Cancer Center Annual Retreat |
| 2022 | American Association for Cancer Research Annual Conference, New Orleans, LA |

**PUBLICATIONS**

Abril-Rodriguez G, Torrejon DY, Karin D, Campbell KM, Medina E, Saco JD, **Galvez M,** Champhekar AS…Ribas A. Remodeling of the tumor microenvironment through PAK4 inhibition sensitizes tumors to immune checkpoint blockade. *Cancer Research Communications*. 2022;2(10):1214-1228. doi: 10.1158/2767-9764.CRC-21-0133.

Chuntova P,* Chow F,* Watchmaker PB,* **Galvez M**,* Heimberger AB, Newell EW, Diaz A, DePinho RA, Li MO, Wherry EJ, Mitchell D, Terabe M, Wainwright DA, Berzofsky JA, Herold-Mende C, Heath JR...Prins RM, Platten M, Okada H. Unique challenges for glioblastoma immunotherapy—discussions across neuro-oncology and non-neuro-oncology experts in cancer immunology. Meeting Report from the 2019 SNO Immuno-Oncology Think Tank. *Neuro-Oncology*. 2021;23(3):356-375. doi: 10.1093/neuonc/noaa277. *Co-first authors.

Davidson TB, Lee A, Hsu M, Sedighim S, Orpilla J, Treger J, Mastall M, Roesch S, Rapp C, **Galvez M**...Prins RM. Expression of PD-1 by T Cells in Malignant Glioma Patients Reflects Exhaustion and Activation. *Clinical Cancer Research*. 2019;25(6):1913-1922. doi: 10.1158/1078-0432.CCR-18-1176.

# Chapter 1:

# Class I antigen presentation and immune checkpoint blockade

**Response to PD-1 blockade and other immune checkpoint blockade therapies relies on tumor cell antigen presentation via MHC class I molecules**

Anti-programmed cell death-1 (PD-1) therapy has led to long-lasting, favorable clinical outcomes among several patients with melanoma (1,2). Despite this, about 60% of patients display primary resistance and 25% display acquired resistance (1,2). Thus, investigating mechanisms of response and resistance to anti-PD-1 therapy is critical in order to expand its therapeutic benefits. Response to anti-PD-1 treatment relies on the successful recognition and elimination of tumor cells by reinvigorated, tumor-specific cytotoxic CD8+ T cells. PD-1 is a negative regulator of immune cell function and it is often expressed on the surface of CD8+ T cells that have been continuously exposed to their target antigens (1,3). Tumor cells can upregulate the ligand of PD-1, programmed death-ligand 1 (PD-L1), to suppress CD8+ T cell activity and thus, escape immune elimination (1,3). Anti-PD-1 antibodies intercept the PD-1:PD-L1 interaction, thereby allowing CD8+ T cells to become activated (3). Tumor cells that present endogenous antigen on surface major histocompatibility complex (MHC) class I molecules are recognized by CD8+ T cells through T-cell receptor (TCR) binding to MHC class I complexes (1,3). Activated tumor-specific CD8+ T cells secrete interferon (IFN)-γ, which causes tumor cells to undergo cell cycle arrest, increase MHC class I expression, and secrete chemokines that attract more T cells, all of which promote tumor eradication (1,3). Therefore, tumors are more likely to respond to PD-1 blockade and be targeted by the immune system if they have intact IFN-γ and MHC class I antigen presentation pathways.

**Class I antigen presentation defects are found in melanoma, and many other cancers, and are associated with resistance to immune checkpoint blockade therapies**

Dysregulated class I antigen presentation is a common mechanism of tumor primary and acquired resistance to immune checkpoint blockade (ICB) therapies targeting cytotoxic T lymphocyte antigen-4 (CTLA-4) and PD-1 (4,5). MHC class I complexes are composed of intracellular

antigenic peptides, a light chain encoded by the β-2-microglobulin (B2M) gene, and a heavy chain encoded by the human leukocyte antigen (HLA) genes HLA-A, HLA-B, and HLA-C (5) (**Figure 1**). Effective class I antigen presentation relies on the successful processing, loading, and presentation of antigens on MHC class I molecules. This involves the concerted action of several gene products and their regulators, including those involved in immunoproteasome formation for peptide processing (LMP2, LMP7, LMP10), peptide transporters (TAP1, TAP2), and peptide chaperones (tapasin, calreticulin, calnexin, ERp57, TAPBPR) (6,7). In addition, this process also relies on components that activate and control the transcription of genes involved in regulating the class I antigen presentation pathway, such as IFN-γ signaling (JAK1, JAK2, IFNGR1, IFNGR2, IRF1) and NOD-like receptor family CARD domain containing 5 (NLRC5), the master transcriptional regular of class I genes (3,5,7). Any alteration in the class I antigen processing machinery (APM) and components regulating it that leads to lost or decreased MHC class I expression has the potential to promote tumor immune escape (5,6,8). In a study describing class I APM abnormalities across several different cancers, it was reported that the frequency of defective class I antigen expression ranges from about 35% to up to 90%, with another study similarly reporting that loss of MHC class I expression can be as high as 93% (8,9). Furthermore, another study evaluating genetic alterations (mutations, deletions, amplifications) in class I APM components across multiple cancers found that genetic alterations ranged from approximately <1% (thyroid cancer) to 15% (skin cutaneous melanoma) for the class I structural components, ranged from about <1% (thyroid cancer) to >30% (ovarian cancer) for class I APM, and ranged from <5% (thyroid cancer) to <30% (skin cutaneous melanoma) for MHC class I signaling, which includes IFN-γ signaling and NLRC5 (9). Currently, despite the several genes and gene products involved in the class I antigen presentation pathway, the most commonly implicated and studied alterations associated with ICB resistance involve mutations or deletions in the HLA, B2M, TAP, and JAK1/2 genes (4,5,9). Hence, it is critical to wholistically characterize class I antigen presentation defects in the context of ICB therapy response and resistance.

**B2M is a critical component of the MHC class I molecule and alterations are found at higher proportions in patients with melanoma who progress during PD-1 blockade therapy**

The B2M gene encodes the light chain of the MHC class I molecule, a critical component of the MHC class I complex that if lost, leads to improper complex folding and thus, degradation, which leads to loss of MHC class I cell surface expression (5,10). Consequently, the absence of B2M expression leads to the inability of tumor cells to present antigen via MHC class I, resulting in cancer cell evasion of CD8+ T cell anti-tumor activity (5,6,8). Thus, the co-occurrence of mutations and loss of heterozygosity (LOH) in B2M often act as mechanisms of primary and acquired resistance to anti-CTLA-4 and anti-PD-1 therapy among patients with melanoma (5). In Sade-Feldman *et al.*, the analysis of 17 longitudinal tumor biopsies from patients with metastatic melanoma receiving ICB demonstrated that B2M abnormalities were found more often in patients with progressive disease (11). Furthermore, they found that B2M mutations were present exclusively in tumors from patients who initially did not respond or in post-progression samples after initial response (11). Additional analyses of pre-treatment tumor samples from the Van Allen clinical cohort (105 patients with melanoma treated with the anti-CTLA-4 antibody) and the Hugo clinical cohort (38 patients with melanoma treated with the anti-PD-1 antibody) corroborated these findings (11). In these cohorts, B2M LOH was enriched approximately threefold in clinical non-responders (~30%) compared to responders (~10%) and was associated with worse overall survival (11). Similarly, in Liu *et al.,* they analyzed 144 baseline tumor biopsies of patients with melanoma treated with PD-1 blockade and found B2M LOH events in 25% of patients with progressive disease compared to 16% in responders (12). To date, the effect of B2M/MHC class I inactivation on anti-PD-1 treatment response requires further investigation, particularly in trying to identify the primary cell mediators of response that are independent of the CD8+ T cell: MHC class I axis.

In summary, understanding the biological and clinical impact of class I and B2M aberrations in patients with melanoma is of paramount importance to help identify novel treatment strategies for cancers with a compromised class I APM.

**Figure 1**

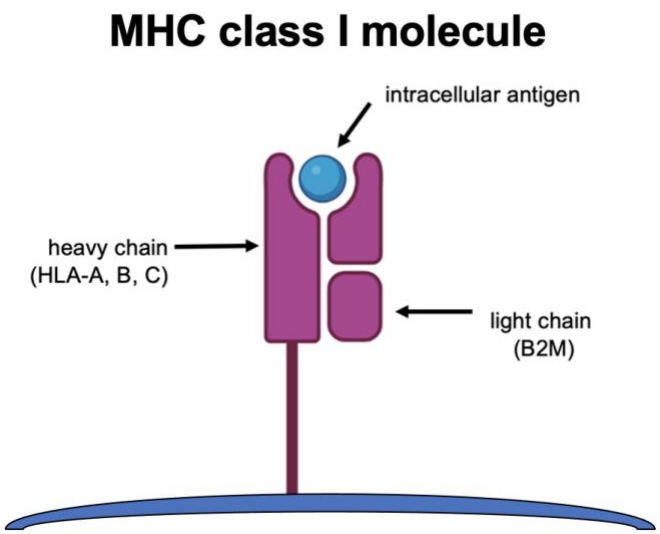


**Figure 1: MHC class I molecule**. The MHC class I molecule is composed of intracellular antigen, a heavy chain, and a light chain encoded by the B2M gene. It is found on the surface of all nucleated cells and interacts with the TCR of CD8+ T cells. Created with BioRender.com (13).

**References**


1. Eddy K, Chen S. Overcoming immune evasion in melanoma. IJMS 2020;21(23):8984 doi 10.3390/ijms21238984.
2. O'Donnell JS, Smyth MJ, Teng MWL. Acquired resistance to anti-PD1 therapy: checkmate to checkpoint blockade? Genome Med 2016;8(1):111 doi 10.1186/s13073-016-0365-1.
3. Marabelle A, Aspeslagh S, Postel-Vinay S, Soria J-C. *JAK* mutations as escape mechanisms to anti–PD-1 therapy. Cancer Discov 2017;7(2):128-130 doi: 10.1158/2159-8290.CD-16-1439.
4. Sharma P, Hu-Lieskovan S, Wargo JA, Ribas A. Primary, adaptive, and acquired resistance to cancer immunotherapy. Cell 2017;168(4):707-723 doi 10.1016/j.cell.2017.01.017.
5. Keenan TE, Burke KP, Van Allen EM. Genomic correlates of response to immune checkpoint blockade. Nature Medicine 2019;25(3):389-402 doi 10.1038/s41591-019-0382-x.
6. Mpakali A, Stratikos E. The role of antigen processing and presentation in cancer and the efficacy of immune checkpoint inhibitor immunotherapy. Cancers 2021;13(1):134 doi 10.3390/cancers13010134.
7. Kelly A, Trowsdale J. Genetics of antigen processing and presentation. Immunogenetics 2019;71(3):161-170 doi: 10.1007/s00251-018-1082-2.
8. Cai L, Michelakos T, Yamada T, *et al*. Defective HLA class I antigen processing machinery in cancer. Cancer Immunol Immunother 2018;67(6):999-1009 doi 10.1007/s00262-018-2131-2.
9. Dhatchinamoorthy K, Colbert JD, Rock KL. Cancer immune evasion through loss of mhc class i antigen presentation. Front Immunol 2021;12:636568 doi 10.3389/fimmu.2021.636568.

10. Germano G, Lu S, Rospo G, *et al*. CD4 T cell–dependent rejection of beta-2 microglobulin null mismatch repair–deficient tumors. Cancer Discovery 2021;11(7):1844-1859. doi 10.1158/2159-8290.CD-20-0987
11. Sade-Feldman M, Jiao YJ, Chen JH, *et al*. Resistance to checkpoint blockade therapy through inactivation of antigen presentation. Nat Commun 2017;8(1):1136 doi doi.org/10.1038/s41467-017-01062-w.
12. Liu D, Schilling B, Liu D, et al. Integrative molecular and clinical modeling of clinical outcomes to PD1 blockade in patients with metastatic melanoma. Nature Medicine 2019;25(12):1916-1927 doi 10.1038/s41591-019-0654-5
13. BioRender.com.

# Chapter 2:

# Anti-tumor immune responses in B2M deficient cancers

**Abstract**

β-2-microglobulin (B2M) is a critical component of the major histocompatibility complex (MHC) class I molecule and is required to present tumor antigens to T cells. Its loss results in acquired resistance to immune checkpoint blockade (ICB) therapies. However, there have been well-documented cases of *B2M*-inactivated tumors that responded to ICB, justifying the study of how an antitumor immune response can be generated to tumors without surface MHC class I. We knocked-out *B2M* in three murine models with varying baseline MHC class I expression and sensitivity to anti-programmed death receptor (PD-1) therapy to analyze the immune responses. MC38 and YUMMER2.1 without *B2M* responded to anti-PD-1 alone or with an interleukin-2 agonist, mediated by both CD4+ T cells and natural killer (NK) cells. The more aggressive B16 without *B2M* expression only partially responded to the interleukin-2 agonist, which was dependent on NK cells. When analyzing nearly 300 pre-treatment biopsies from patients with melanoma on PD-1 blockade-based therapies, we found infrequent *B2M* mutations or homozygous loss but more frequent loss of heterozygosity (LOH) or copy number gains. *B2M* LOH was enriched in biopsies from patients without response to therapy, and these biopsies were more frequently infiltrated by activated NK cells. We conclude that in the absence of *B2M,* activation of CD4+ T cells and NK cells can mediate responses to murine models of PD-1 blockade therapy. Additionally, in human melanoma the intratumoral presence of activated NK cells upon partial *B2M* loss likely selects against tumor escape through low surface MHC class I expression.

## Introduction

The success of immune checkpoint blockade (ICB) therapies relies on the antitumor activity of CD8+ T cells (1,2). However, CD8+ T cell-based therapies rely on functional antigen presentation by tumor cells, which opens avenues for the development of resistance mechanisms. Canonically, tumor antigens are presented to CD8+ T cells by surface major histocompatibility complex (MHC) class I molecules, which are composed of a heavy chain and β-2-microglobulin (B2M). B2M is necessary for the proper stabilization and folding of MHC class I molecules. In its absence, the MHC class I complex does not reach the cell surface and is degraded (3). The loss of MHC class I through *B2M* mutations or copy number losses results in the inability of CD8+ T cells to recognize cancer cells and has long been recognized to lead to tumor immunotherapy resistance (4-8). However, the use of ICB in highly immunogenic cancers that may have already gone through immune editing have demonstrated that some patients whose cancers do not express *B2M* can still respond to anti-PD-1-based therapies (9-15). Therefore, there is a need to study how the immune system can induce responses in *B2M*-null tumors by developing murine models and studying patient-derived biopsies. Previously, we reported that anti-PD-1 resistance due to *B2M* loss could be overcome with the activation of NK cells and CD4+ T cells in murine models (16). The role of CD4+ T cells in immune responses to *B2M*-knockout (KO) tumors has been corroborated in murine models and biopsy samples of patients with DNA mismatch repair deficient (MMR-d) cancers (13). Furthermore, γδ T cells have also been shown to increase in MMR-d cancers with *B2M* defects, and have a cytotoxic effect upon treatment with ICB (15). Nevertheless, the exact effect of MHC class I antigen presentation machinery defects on anti-PD-1 therapy response, and the cells capable of mediating the anti-tumorigenic effects of PD-1 blockade in *B2M*-defective human tumors, have not been fully characterized.

Here we used CRISPR/Cas9 to develop sublines through *B2M*-KO mutations in three murine models: MC38 and YUMMER2.1, which have high immunogenicity due to carcinogen-induced high mutational load and have CD4+ and CD8+ T cell co-dependency in response to anti-PD-1 therapy, and the lowly immunogenic B16 model with undetectable baseline MHC class I expression and primary CD8+ T cell dependency to respond to immunotherapy (17). These murine models allowed us to study the mechanisms by which immune cells orchestrate responses to PD-1 blockade in the context of *B2M* inactivation. To further corroborate these findings, we analyzed sequencing data from a large cohort of pre-treatment human melanoma biopsies for the presence of *B2M* somatic alterations and correlative infiltrating immune cell subsets. Our findings may support the development of combination strategies to potentiate the CD8+ T cell antitumor effects and avoid resistance to ICB therapies.

## Materials and Methods

### CRISPR/Cas9-mediated gene knockout

MC38, B16 and YUMMER2.1 murine cell lines were subjected to CRISPR/Cas9-mediated knockout of *B2M* and *JAK1* as previously described (16). The following single guide RNAs targeting *B2M* were used: forward: 5′-TCACGCCACCCACCGGAGAA-3′; reverse: 5′-TTCTCCGGTGGGTGGCGTGAC-3′. These were cloned into the pSpCas9(BB)-2A-GFP vector (Addgene, Watertown, MA) (18) and then transformed into One Shot Stbl3 Chemically Competent *E. coli* (Invitrogen) and cultured overnight in Lysogeny Broth (LB) plates containing ampicillin. Selected colonies were grown overnight in LB medium and DNA was isolated with the QIAprep midiprep kit (Qiagen, Valencia, CA). To verify the sequence of the plasmids, a U6 promoter primer forward 5′-GCCTATTTCCCATGATTCCTTC-3′ was utilized. Next, cells were transfected using Lipofectamine 3000 following the manufacturer's protocol (Thermo Fisher Scientific, Waltham, MA), and GFP-positive cells were collected and single-cell sorted 48 to 72 hours post-transfection at the UCLA Jonsson Comprehensive Cancer Center (JCCC) Flow Cytometry Core. For each clone, genomic DNA was isolated using the NucleoSpin Tissue XS kit (Macherey-Nagel), and a 700-base pair (bp) region including the sgRNA was amplified via PCR using the HotStarTaq Master Mix (Qiagen). Finally, disruption was verified by Sanger sequencing utilizing the Tracking of Indels by Decomposition (TIDE) (19) web tool and further confirmed via Western blot.

### Surface flow cytometry analysis of PD-L1 and MHC class I

On day 1, murine cells were plated at $2x10^5$ per 6-well plate and, when cell confluence reached 70-80%, cells were collected for surface staining. The day after, culture media was replaced with fresh media with or without IFNγ 100 ng/ml for 18 hours. On day 3 after incubation, cells were trypsinized and then incubated at 37°C for 2 hours with the same concentrations of IFNγ. Next, cells were centrifuged to remove the media and resuspended in 100% FBS. Cells were first

stained with Zombie Green viability dye (BioLegend, San Diego, CA) for 15 minutes, then washed and stained with anti-mouse PE, anti-PD-L1, APC anti-MHC I and AF700 anti-MHC II, and left on ice for 20 minutes. Cells were then washed once with 3 ml PBS and resuspended in 300 µL of PBS. Following staining, samples were analyzed using the Attune Flow Cytometer (Thermo Fisher Scientific) platform at the UCLA JCCC Flow Cytometry Core. Data were analyzed using FlowJo software (version 10.0.8r1, Tree Star Inc., San Carlos, CA). Experiments were performed at least in duplicate per cell line.

**Characterization of the tumor immune infiltrate by flow cytometry**

To characterize and quantify the dendritic, T and myeloid cell populations, mouse tumor samples from MC38 WT or *B2M*-KO cells were collected and treated with anti-PD-1 or isotype at day 9 and day 16. Tumor samples were processed using the mouse tumor dissociation kit (Miltenyi Biotec) per the manufacturer's protocol. Samples were stained using the three antibody panels listed in **Supplementary Table S1**. Following staining, samples were analyzed using the LSRII (Becton, Dickinson and Company, Franklin Lakes, NJ) at the UCLA JCCC Flow Cytometry Core and analyzed using FlowJo software (version 10.0.8r1, Tree Star Inc., San Carlos, CA).

**Mice, cell lines and reagents**

All mouse studies were approved by the UCLA Animal Research Committee under protocol #2004-159-43I. C57BL/6 mice were bred and kept under defined flora and pathogen-free conditions at the Association for the Assessment and Accreditation of Laboratory Animal Care (AAALAC) approved animal facility of the Division of Experimental Radiation Oncology, UCLA. The MC38 mouse colon adenocarcinoma cell line was initially generated at the NCI Surgery Branch (originally Colo38), and was obtained from Dr. Robert Prins, UCLA Department of Neurosurgery. The B16-F10 mouse melanoma cell line was purchased from ATCC. The YUMM2.1 UV mouse melanoma cell line was obtained from Dr. Marcus Bosenberg, Yale University. The

MC38, B16-F10 and YUMM2.1 UV mouse cell lines and established knockout cell lines were cultured at 37° C with 5% $CO_2$ in Dulbecco's Modified Eagle Medium (DMEM) (Invitrogen, Carlsbad, CA) supplemented with 10 % FBS, 100 units/ml penicillin, 100 µg/ml streptomycin, and 0.25 µg/ml amphotericin B. Cell lines were tested for mycoplasma contamination using the MycoAlert Mycoplasma Detection Kit (Lonza), and were regularly tested for authentication. For *in vivo* experiments, early passage cell lines (no more than ten passages) were utilized.

Antibodies for *in vivo* experiments: anti-mouse-PD-1 (clone RMP1-14), anti-mouse CD8 (clone YTS 169.4, BE0117), anti-mouse CD4 (clone GK1.5, BE0003), anti-mouse NK1.1 (clone PK136, BE0036), anti-mouse CD40L (clone MR-1, BP0017), anti-mouse IFNγ (clone XMG1.2, BE0055) and isotype control antibody (clone 2A3, BE0089), all from BioXCell (West Lebanon, NH). Bempegaldesleukin (NKTR-214) (20) was provided by Nektar Therapeutics through a Materials Transfer Agreement (MTA) and was diluted in the recommended product formulation buffer for *in vivo* studies.

**Antitumor studies in mouse models**

To seed subcutaneous (s.c.) tumors in mice, $0.3x10^6$ MC38, $0.3x10^6$ B16, $1x10^6$ YUMMER2.1 wild-type or established *B2M*-KO cells were injected into the flanks of C57BL/6 mice. Once tumors became palpable, four to six doses of 300 µg of anti-PD-1 or isotype control antibody were injected intraperitoneally (i.p.) every 3 days. Bempegaldesleukin was injected at 0.8 mg/kg every 9 days for one to two doses intravenously (tail vein). For depletion studies, 300 µg of anti-CD8, 300 µg of anti-CD4, 300 µg of anti-NK1.1, 200 µg of anti-CD40L, 200 µg of anti-IFNγ or the combination were administered every 3 days starting the day before anti-PD-1 or bempegaldesleukin treatment and up until the end of the experiment. To validate depletion efficacy, splenocytes from control and depleted corresponding mice were harvested for comparisons. Tumor growth was followed using caliper measurements two or three times per week and tumor volume was

calculated using the following formula: tumor volume= ((width)2 x length)/2. Mean and standard error of the tumor volumes per group was calculated.

**Mass cytometry (CyTOF) analysis**

A total of $0.3x10^6$ MC38 wild-type or established *JAK1* and *B2M* KO tumor cells were implanted into the flanks of C57BL/6 mice. On day 13 post-implantation, tumors were harvested from mice at predefined treatments. Tumors were digested using the mouse tumor dissociation kit (Miltenyi, Biotec). Spleens were dissociated and filtered using a 70-μm filter, followed by digestion with the ACK lysis buffer (Lonza). Sample staining and data acquisition were performed as previously described with the additional modifications that 3% paraformaldehyde was utilized and samples were not barcoded (16). The immune marker panel has been previously described (16). Samples were analyzed using the Fluidigm Helios (San Francisco, CA) mass cytometry system at the UCLA JCCC Flow Cytometry Core. Samples were manually gated for cells, singlets and double expression of the viable CD45 single-cell-positive population using FlowJo software (version 10.4.2), and data files were analyzed using the standard settings in OMIQ data analysis software (www.omiq.ai).

**Clinical dataset**

For human tumor biopsy analyses, a clinical dataset of patients with advanced melanoma (n=514) that has been previously harmonized for somatic variant detection and gene expression profiling was utilized (21). This dataset contains clinical response, whole-exome sequencing (WES), and bulk RNA-sequencing (RNAseq) data across seven clinical trials of patients with advanced melanoma who received immune checkpoint blockade therapy (ICB; anti-PD-1, anti-CTLA-4, or combination therapy). Copy number alterations (CNAs), loss of heterozygosity (LOH), and tumor purity estimates were determined using Sequenza (22). For gene expression analysis, the normalized log-CPM file that was batch-effect corrected with ComBat-seq was utilized (23).

The Liu cohort (24), CheckMate 038 (9), CheckMate 064 (25), and CheckMate 067 (26) cohorts were analyzed since these are the only trials that have both WES and RNAseq data (**Supplementary Figure S1**). For these analyses, pre-treatment melanoma tumors of cutaneous, mucosal, acral, unknown, and uveal origins were utilized. Samples with best overall response (BOR) categories of complete response (CR), partial response (PR), and progressive disease (PD) to ICB therapy were used for clinical response group comparisons, with CR/PR representing clinical responders and PD representing clinical non-responders (RECIST v1.1 criteria) (27). Stable disease (SD) tumors were excluded from clinical response group comparisons but included in somatic variant analysis.

### *B2M* genetic alteration analysis

Using the WES data of samples with greater than 10% tumor purity, baseline tumors were analyzed for *B2M* genetic alterations (n=295) (**Supplementary Table S2**). Tumors were considered *B2M* altered if they had non-silent mutations, CNAs, or LOH at the *B2M* locus. Non-silent mutations correspond to single nucleotide variants (SNVs) and insertions and deletions (indels) with a high or moderate Ensembl VEP impact designation (https://uswest.ensembl.org/index.html). CNAs refer to somatic alterations that result in gained or lost copies of a genetic region. LOH describes events where one copy of an allele is lost, irrespective of copy number status. For *B2M* group comparisons, tumors with *B2M* gains were excluded since they do not correspond to downregulating *B2M* genetic alterations. Additionally, SD tumors were excluded from the dataset for clearer responder versus non-responder comparisons (**Supplementary Figure S1**).

**Tumor microenvironment analysis**

Immune cell deconvolution was performed with CIBERSORTx (https://cibersortx.stanford.edu) using the LM22 signature matrix of 22 functionally defined mature human immune cell subsets (28-30), which distinguishes different cell types and cell states (naïve, memory, resting, and activated) based on 547 significantly differentially expressed genes (**Supplementary Table S3**). Each cohort was run separately using the uncorrected RNAseq FPKM values to infer cell fractions and total cell numbers (absolute mode) per tumor sample (**Supplementary Table S4**). Each job was run following the recommended parameters using 1000 permutations. The p-values calculated by CIBERSORTx ranged from 0-0.857 in regular mode (median 0.065) and 0-0.836 (median 0.075) in absolute mode (**Supplementary Figure S2**), and these values were loosely correlated with estimated tumor purity by Sequenza (WES) (**Supplementary Figure S3**). We performed comparisons of immune cell types across clinical groups two ways: all samples or excluding samples with p>0.5. The significance in comparison across immune cell types was not different across these analyses, so the findings from the first comparison, including all samples, was reported. Differences in immune cell populations between groups were visualized and evaluated in R/RStudio (http://www.R-project.org/) by comparing the medians using a Wilcoxon test and were considered significantly different if the p-value was less than 0.05.

**Bioinformatics statistical analysis**

Statistical analyses were performed using R/RStudio v2022.07.1+554 (http://www.R-project.org/). All plots analyzing *B2M* groups were generated using the R package ggplot2 (https://ggplot2.tidyverse.org/). For median group comparisons, p-values less than 0.05 were considered statistically significant.

## Data availability

The genomics data used in this study are from a previous publication (21), with the raw sequencing data available through the Sequence Read Archive accession identifier PRJNA923698. Processed data from the harmonized biopsy sequencing dataset, including annotated variants and gene expression values, are available at https://github.com/ParkerICI/MORRISON-1-public.

## Results

### Different constitutive and induced MHC class I expression on MC38, B16 and YUMMER 2.1

Cancer cell lines have different levels of constitutive surface MHC class I expression and frequently do not express MHC class II, but both can be increased by exposure to interferon-gamma (IFNγ); thus, using flow cytometry we first characterized the baseline and inducible surface expression of MHC class I and II on three murine cell lines, MC38, B16, and YUMMER 2.1. We also analyzed expression of programmed death-ligand 1 (PD-L1) as it is readily induced by IFNγ (31). To determine the role of B2M on the expression of these surface markers, we generated corresponding *B2M*-KO sublines using CRISPR/Cas9 gene editing (16). Constitutive MHC class I surface expression was highest in MC38, intermediate in YUMMER2.1 and lowest in B16. The same trend was observed when staining for the constitutive surface expression of MHC class II. Exposure to IFNγ resulted in increased MHC class I and II expression in the three models. In all three models, *B2M* KO led to the loss of surface expression of both MHC class I and II, but maintained the upregulation of surface expression of PD-L1 in response to IFNγ (**Figure 1**). We reasoned that these different levels of MHC class I expression may result in different sensitivities to effector immune cells *in vivo*, as MHC class I is required for CD8+ T cell tumor recognition, and loss of MHC class I sensitizes target cells to natural killer (NK) cell cytotoxicity.

### CD4+ T cells are instrumental in controlling MC38 *B2M*-deficient tumor growth

To analyze the role of effector immune cell subsets in antitumor responses to MC38 murine colon adenocarcinoma tumors, we inoculated C57BL/6 mice with MC38 wild-type (WT) or MC38 *B2M*-KO tumors, followed by antibody-mediated CD4+ T-cell and CD8+ T-cell depletion in both groups, and antibody-mediated NK1.1+ cell depletion in *B2M*-KO tumors. In the MC38 WT control group, depletion of CD4+ T cells, CD8+ T cells, or both, abrogated the anti-PD-1 therapy antitumor

response, while for WT untreated tumors, there were no significant effects with either immune cell depletion **(Figure 2A)**. On the other hand, MC38 *B2M*-KO tumors did not respond to anti-PD-1 therapy. Untreated MC38 *B2M*-KO tumors grew with similar kinetics as the WT control group, but CD4+ T-cell depletion led to significant tumor overgrowth of MC38 *B2M*-KO tumors for both untreated and treated with anti-PD-1 therapy groups **(Figure 2B)**. NK depletion in MC38 *B2M*-KO tumors had a lower impact, both in tumor growth and in response to anti-PD-1 therapy. Therefore, CD4+ T cells are critical for controlling the growth of MC38 *B2M*-KO tumors regardless of antitumor treatment.

**cDC1 but not cDC2 were reduced in MC38 *B2M*-deficient tumors**

To analyze the immune cells infiltrating MC38 WT and MC38 *B2M*-KO tumors, mice were inoculated with MC38 WT or MC38 *B2M*-KO lines and treated with isotype control or anti-PD-1 antibody (n=3 mice per group). We harvested spleens and tumors nine and 16 days after tumor inoculation and studied the cell populations by multiplex flow cytometry (**Supplementary Figure S4).** Regardless of the anti-PD-1 treatment, no differences were observed in the infiltration by CD4+ T cells, T regulatory cells (Tregs), CD8+ T cells or NK cells**.** The percentage of CD62L+CD44+ central memory CD4+ T cells was significantly higher in MC38 *B2M*-KO tumors compared to MC38 WT tumors at day 9 post tumor-cell inoculation. The percentages of CD8+PD1+, CD8+Ki67+ and CD62L-CD44+ effector CD8+ T cells were significantly decreased in MC38 *B2M*-KO tumors compared to MC38 WT tumors at day 16 post tumor-cell inoculation (**Supplementary Figure S5A)**, indicating that T cell proliferation is occurring in favor of CD4+ T cells (without Tregs) over CD8+ T cells in MC38 *B2M*-KO tumors.

No significant differences in the percentages of macrophages, M1, M2, CD4 or CD8+ T cells per gram were observed at day 9. However, M1 macrophage infiltration and the M1/M2 ratio were significantly decreased at day 16 in the MC38 *B2M*-KO tumors (anti-PD-1 resistant tumors)

compared to MC38 WT tumors **(Supplementary Figure S5B)**. Additionally, the number of NK cells per gram at day 9 in MC38 *B2M*-KO tumors was significantly lower relative to WT tumors **(Supplementary Figure S5C)**. In the MC38 *B2M*-KO tumors, we observed a sharp decrease in the percentage of cDC1 (migratory CD11c$^{int}$MHC-II$^{hi}$CD103$^{+}$DCs and resident CD11c$^{hi}$MHC-II$^{int}$CD8a$^{+}$DCs), a subset of dendritic cells that have been specialized for priming CD8+ T cell responses through cross-presentation (32). In contrast, MC38 *B2M*-KO tumors had an increased percentage of cDC2, resident CD11c$^{hi}$MHC-II$^{int}$CD11b$^{+}$ DCs **(Figure 3 and Supplementary Figure S5B)**. These data suggest that loss of *B2M* in MC38 tumors abrogates the activation and migration of cDC1 regardless of anti-PD-1 treatment and promotes cDC2 attraction, which are more potent activators of CD4+ T cells, into the tumor microenvironment (32).

**CD4+ T cells and NK cells increased while cDC1 CD103+ cells decreased in MC38 *B2M*-KO tumors treated with an IL-2 pathway agonist**

As we demonstrated previously (16), treatment with the CD122-preferential interleukin-2 (IL-2) agonist bempegaldesleukin alone or in combination with anti-PD-1 overcame therapeutic resistance to anti-PD-1 therapy in MC38 *B2M*-KO tumors. Depletion studies suggested that NK and CD4+ T cells, which are not restricted by MHC class I, played a key role in this antitumor immunity. We also demonstrated that despite tumor-intrinsic IFNγ defects, MC38 *JAK1*-KO tumors with sufficient basal expression of MHC class I could overcome anti-PD-1 therapy resistance with Toll-like receptor 9 (TLR9) agonist co-administration, an effect mediated mainly by CD8+ T cells. Both loss and downregulation of MHC class I antigen presentation are considered major immune escape mechanisms (6-8), but they have varying effects on effector immune cells. Thus, we next used mass cytometry by time-of-flight (CyTOF) analysis of the tumor microenvironment to characterize the effects of bempegaldesleukin and anti-PD-1 plus bempegaldesleukin on the immunological response changes in MC38 WT, MC38 *B2M*-KO, and MC38 *JAK1*-KO tumors, as these readily respond to bempegaldesleukin combined with anti-PD-

1 **(Supplementary Figure S6)**. At 13 days post-tumor inoculation, the combination of bempegaldesleukin with anti-PD-1 led to increased CD4+ T and NK cells and reduced CD8+ T cells in MC38 *B2M*-KO tumors. In contrast, CD8+ T, CD4+ T and NK cells all increased in bempegaldesleukin and anti-PD-1-treated MC38 *JAK1*-KO tumors **(Figure 4A-E)**. This is consistent with our previous findings in which CD8+ T cells were the main immune effectors in MC38 *JAK1*-KO tumors with sufficient basal MHC class I expression (16). CD103+ murine dendritic cells decreased in MC38 *B2M*-KO tumors regardless of treatment **(Figure 3A, Figure 4C, and Supplementary Figure S7A)**. On the other hand, bempegaldesleukin significantly expanded CD103+ murine dendritic cells, which are required for cross-presentation, in both MC38 WT and *JAK1*-KO tumors. Altogether, our results support that the infiltration of cDC1 CD103+ murine dendritic cells decreases in MC38 *B2M*-KO tumors regardless of treatment, and that anti-PD-1 therapy resistance can be overcome with an IL-2 pathway agonist by activating CD4+ T cell and NK cell responses.

**Depletion of CD4+ T cells promotes pro-tumorigenic macrophage differentiation**

Because our data suggests that CD4+ T cells play a key role in MC38 *B2M*-KO tumors, we further explored the role that tumor-infiltrating CD4+ T cells may play in determining macrophage differentiation. While bempegaldesleukin treatment led to a minimal expansion of tumor-associated macrophages (TAM), isotype control and bempegaldesleukin with CD4+ T cell depletion (where tumors grew faster) led to a dramatic increase in macrophages (**Supplementary Figure S7B**). Additionally, immunosuppressive M2 TAMs were significantly increased in bempegaldesleukin with CD4+ T cell depletion, with a decrease in the M1/M2 index at day 13 after tumor inoculation. These data suggest that CD4+ T cells limit macrophage differentiation and/or proliferation toward an immunosuppressive M2 state.

**NK cells and IFNγ control tumor growth in B16 *B2M*-KO tumors**

B16 murine melanoma has low basal expression of MHC class I, which can be increased with IFNγ exposure (33), and is mainly dependent on CD8+ T cells for the antitumor response in the setting of anti-PD-L1 therapy (34). To investigate how to overcome primary resistance to PD-1 blockade in this aggressive model when MHC class I loss is due to *B2M* inactivation, we treated B16 *B2M*-KO tumors with bempegaldesleukin alone or in combination with anti-PD-1 therapy. Our prior work showed that in B16 *B2M*-KO tumors, bempegaldesleukin or bempegaldesleukin in combination with anti-PD-1 overcame therapeutic resistance to anti-PD-1 (16). We then investigated the cell types responsible for the antitumor activity in B16 *B2M*-KO tumors. Depletion of NK cells abolished the therapeutic effect **(Figure 5A-B)**. In contrast, depletion of CD4+ or CD8+ T cells had no effect. We further studied the molecules involved in the immune cell interactions by administering blocking antibodies against IFNγ or CD40L. We observed that the antitumor activity was lost when blocking IFNγ, but not when blocking CD40L **(Figure 5A-B)**, which is canonically expressed on CD4+ T cells and plays an important role in the T cell-mediated activation of dendritic cells (35,36). These data suggest that NK cells and IFNγ were essential for overcoming anti-PD-1 therapy resistance in B16 *B2M*-KO tumors. In addition, these results show that CD4+ T cells and T cell help through CD40L were not crucial for developing an effective antitumor immune response in this model.

**YUMMER2.1 *B2M*-KO tumors respond to anti-PD-1 therapy**

The YUMM2.1 murine melanoma is a *BRAF*$^{V600E}$*/PTEN*-null-driven model that has been previously shown to be responsive to anti-PD-1 therapy (37), with CD4+ T cell depletion completely abrogating the antitumor effect and CD8+ T cell depletion only having a partial effect (17). To generate a model that not only included melanoma driver oncogenes but also had increased ultraviolet (UV) light-induced mutational burden, as it is frequently found in human cutaneous melanomas (38), we obtained a polyclonal YUMM2.1 by UV exposure and expanded

single cell clones to generate 24 UV-homogeneous sublines. This resulted in sublines with truncal UV-induced mutations able to respond to anti-PD-1 therapies (39). We evaluated the *in vitro* and *in vivo* growth curves in order to identify the subline that behaved most similarly to the parental UV-heterogeneous cell line to select for subsequent *in vivo* studies (**Supplementary Figure S8A**). The resulting YUMM2.1 UV-clone 2, named YUMMER2.1, is a model that more closely resembles human melanomas with $BRAF^{V600E}$ and $PTEN^{-/-}$ oncogenic driver alterations, a high mutational load induced by UV carcinogenesis, and anti-PD-1 therapy responsiveness (**Figure 6A-B**). Next, we generated a *B2M*-KO subline of YUMMER2.1 using CRISPR/Cas9 gene editing and validated the phenotype by protein analysis (**Supplementary Figure S8**). To model the *in vivo* response to PD-1 blockade in YUMMER2.1 *B2M*-deficient tumors, we injected YUMMER2.1 *B2M*-KO tumors subcutaneously into the lower flank of C57BL/6 mice. When tumors became palpable, mice received the first out of six injections of anti-PD-1 therapy or isotype control. Even with *B2M* loss, YUMMER2.1 *B2M*-KO tumors responded to anti-PD1 therapy, showing that this model is largely sensitive to PD-1 blockade treatment (**Figure 6C**), even in the absence of MHC class I surface expression.

**Depletion of CD4+ T cells, NK cells, and CD40L abrogates anti-PD-1 therapy response in YUMMER2.1 *B2M*-KO tumors**

To investigate the cell types responsible for the anti-PD-1 response in YUMMER2.1 *B2M*-KO tumors, we depleted CD4+ T cells, CD8+ T cells, NK cells, CD40L, and IFNγ. In agreement with previous data with YUMM2.1 (17), CD8+ T cell depletion only partially abrogated the response, whereas CD4+ T cell depletion and CD40L blockade completely abrogated the anti-PD-1 therapy response in YUMMER2.1 tumors (**Figure 6D-E**). Depletion of CD4+ T cells, NK cells and CD40L, but not CD8+ T cells or IFNγ, significantly curbed tumor growth inhibition by anti-PD-1 therapy (**Figure 6F-G**). These results suggest that in YUMMER2.1 *B2M*-KO tumors, CD4+ T cells and NK cells are the main cells responsible and necessary for anti-PD-1 antitumor activity. Additionally,

we further identified the involvement of CD40L in the antitumor response in this *B2M*-deficient murine model.

**In human melanoma biopsies, *B2M* loss of heterozygosity is the most prevalent downregulating genetic alteration**

We next wanted to study the immune cells infiltrating human melanoma biopsies with and without *B2M* downregulation or complete loss. To determine the *B2M* genetic status in biopsies of patients with advanced melanoma who received ICB therapy, we analyzed data from a harmonized clinical cohort (21). Baseline whole-exome sequencing (WES) samples (n=295) (**Supplementary Table S2 and Supplementary Figure S1**) were analyzed for the presence of *B2M* somatic alterations, specifically non-silent mutations, copy number alterations, or loss of heterozygosity (LOH). We found that none of the patients in this cohort had tumors with non-silent mutations in *B2M*. However, 49.5% of the cohort (n=146) had tumors with copy number alterations in *B2M*. Of the 295 patients analyzed, 0.7% of patients had biopsies with *B2M* homozygous loss (n=2), 19% had *B2M* LOH with total copy numbers ranging from 1-5 (n=56), and 30% had *B2M* copy number gains with total copy numbers ranging from three to seven (n=88) (**Supplementary Figure S9**).

***B2M* LOH in melanoma correlates with progressive disease status and decreased *B2M* expression**

In order to elucidate the effects of downregulating *B2M* genetic alterations in the context of clinical response, we compared the clinical outcomes of patients whose tumors had *B2M* homozygous loss or LOH and unaltered status using the response RECIST criteria v1.1 (27), separating patients with complete and partial response (CR/PR) from patients with disease progression (PD) following ICB therapy. This criterion, however, eliminated the two cases with stable disease and *B2M* homozygous loss (**Supplementary Figure S9**), leaving only *B2M* LOH (n=45) and unaltered tumors (n=119) for analysis (**Supplementary Figure S1**). We found that the presence of *B2M*

LOH events in progressive disease tumors (n=32/95) was significantly higher compared to responsive tumors (n=13/69), occurring approximately twice as often in biopsies of patients with no response to therapy (34% versus 19%; $X^2_{Pearson}$ test, p=0.04) (**Figure 7A**). Next, to determine whether *B2M* LOH was associated with reduced *B2M* expression, bulk tumor RNA-sequencing (RNAseq) data (n=100) was analyzed for *B2M* expression differences (**Supplementary Figure S1**). We found that *B2M* expression was lower in *B2M* LOH tumors compared to unaltered tumors (Wilcoxon test, p=0.05) (**Figure 7B**). These results agree with prior studies that describe *B2M* LOH events as potential precursors to *B2M* loss and thus, reduced *B2M* expression (7).

**Melanomas with *B2M* loss of heterozygosity have more activated NK cells**

To determine the immune cell subtypes present in *B2M* LOH (n=25) versus unaltered tumors (n=75), we performed immune cell deconvolution analysis on samples with paired WES and RNAseq data using CIBERSORTx (https://cibersortx.stanford.edu). We found that *B2M* LOH tumors had significantly higher fractions (Wilcoxon test, p=0.032) and quantified amounts (Wilcoxon test, p=0.021) of activated NK cells (**Figure 7C and Supplementary Figure S10A**). It is also worth noting that compared to unaltered tumors, *B2M* LOH tumors had trends supporting greater fractions and numbers of M1 macrophages, γδ T cells, memory resting CD4+ T cells, plasma cells, memory B cells, CD8+ T cells, activated mast cells, and follicular helper T cells **(Figure 7C and Supplementary Figure S10A**).

Furthermore, when examining the immune cell composition of *B2M* LOH tumors across ICB response groups, the fractions of monocytes were significantly higher in *B2M* LOH responsive tumors (n=6, Wilcoxon test, p=0.026), while the fractions of memory activated CD4+ T cells were significantly higher in *B2M* LOH progressive tumors (n=19, Wilcoxon test, p=0.014) (**Figure 7D**). These patterns were also observed with the absolute scores, where only monocytes and memory activated CD4+ T cells were significantly different between both groups (**Supplementary Figure**

**S10B).** Notably, *B2M* LOH progressive tumors also had greater fraction and absolute score values for activated NK cells, γδ T cells, and CD8+ T cells; and a greater absolute score value for M1 macrophages (**Figure 7D and Supplementary Figure S10B).**

Next, to assess which subsets may be playing a more prominent role in mediating response to ICB therapy, we focused exclusively on responsive (CR/PR) melanoma tumors, comparing the estimated immune cell populations between *B2M* LOH tumors (n=6) and *B2M* unaltered tumors (n=35). It was observed that compared to unaltered samples, only monocytes were significantly higher in *B2M* LOH responsive tumors for both fractions (Wilcoxon test, p=0.018) and absolute values (Wilcoxon test, p=0.03) (**Supplementary Figure S11**). However, it is also important to note that *B2M* LOH responsive tumors had higher fractions and total numbers of activated NK cells and memory resting CD4+ T cells relative to *B2M* unaltered tumors (**Supplementary Figure S11).** Our results support that in human melanoma biopsies with *B2M* dysregulation, activated NK cells are the most significantly elevated immune cell type infiltrating the tumors, with potential roles for other immune cells, such as CD4+ T cells, monocytes/M1 macrophages, and γδ T cells.

## Discussion

It has been well-documented that cancers with *B2M* homozygous loss could still respond to PD-1 blockade-based therapies (9-15), which challenges the conventional thinking on the mode of action of anti-PD-1 by reinvigorating cytotoxic CD8+ T cells that recognize tumor antigens presented by MHC class I (2). The effector arm of a cellular antitumor immune response has two main cytotoxic cells, CD8+ T cells recognizing MHC class I antigen complexes and NK cells recognizing the absence of or a mismatched MHC class I. The need to avoid NK cell killing seems to be a major driver for cancers to not lose MHC class I expression completely (40), even if this would allow the cancer to acquire resistance to ICB therapies (6-8). In addition, CD4+ T cells can have effector functions that induce cytotoxic cancer cell death, either directly or indirectly through the secretion of cytokines that promote bystander cytotoxicity. Furthermore, the helper function of CD4+ T cells, which involves cytokines such as IFNγ and CD40L engagement through dendritic cells, results in increased cytotoxic activity of CD8+ T cells and NK cells (41).

We reasoned that identifying the immune cell mediators capable of exerting the anti-tumorigenic effects of anti-PD-1 therapy response in the absence of *B2M* is of critical importance in order to not only address antigen presentation-mediated therapeutic resistance, but also to better understand the mechanism of action of PD-1 blockade therapies. In this study, we used a combination of three different murine models with varying immune cell dependencies and human melanoma biopsy samples to interrogate the dominant immune cell subtypes and molecular markers associated with the immune response of *B2M*-deficient tumors. The YUMMER2.1 model is highly immunogenic and is able to respond to anti-PD-1 therapy, even in the absence of MHC class I presentation due to *B2M* loss, through CD4+ T cell and T cell helper functions. The MC38 model has intermediate immunogenicity and does not respond to anti-PD-1 single agent therapy when there is no MHC class I presentation. However, it can respond to therapy adding an IL-2

pathway agonist, and in this case, the antitumor response is mediated by CD4+ T cells and NK cells, with a critical requirement for T cell help and intratumoral dendritic cells. The low immunogenicity B16 model is resistant to anti-PD-1 with or without *B2M* loss, but can respond with an IL-2 pathway agonist and the response is completely dependent on NK cells with no added role for CD4+ T cells or T cell helper functions. Our work in murine models has shown that CD4+ T cells are critical for the antitumor immunity in *B2M*-KO models. This opposite of what has been reported in prior studies where it was observed that CD4+ T cell depletion led to increased tumor reactivity and increased intratumoral infiltration of CD8+ T cells (42,43). However, in our models Tregs are not expected to play a significant role in tumor reactivity and response, as demonstrated by the MC38 line where WT and *B2M*-KO tumors had similar quantities of Tregs; thus, depleting CD4+ T cells in this scenario would not decrease the amount of immunosuppressive CD4+ T cells in the tumor microenvironment. Furthermore, since these are *B2M*-KO lines with a compromised MHC class I-CD8+ T cell immunity axis, an increase in tumor-specific CD8+ T cells due to CD4+ T cell depletion would not lead to a therapeutic benefit. Our findings in these mouse models highlight the complexity of investigating immune responses in the context of *B2M* loss, stressing that tumor-intrinsic immune cell dependencies as well tumor microenvironmental factors can impact which effector cells control *B2M*-null tumor growth. Nonetheless, our work suggests that NK and CD4+ T cells are the dominant cell types curbing MHC class I-defective tumor expansion.

In our analysis of pre-treatment human melanoma biopsies, we identified *B2M* LOH due to copy number alterations as the most prevalent downregulating genetic alteration and found no non-silent mutations in *B2M*, which is in accordance with prior series (7,24). We also observed that *B2M* LOH occurred approximately twice as often in biopsies from patients who did not respond to ICB therapy compared to those who had a clinical response. This falls in line with what was found in two independent melanoma clinical cohorts, where the frequency of *B2M* LOH events at baseline was roughly three times higher in biopsies of patients with progressive disease (7). Our

immune cell deconvolution analysis of *B2M* LOH melanoma biopsies showed that, among the immune cell types analyzed, only activated NK cells were significantly higher in *B2M* LOH tumors when compared to *B2M* unaltered tumors. Additionally, we also observed higher amounts of activated NK cells in *B2M* LOH responsive tumors compared to *B2M* unaltered responsive tumors. This is consistent with the notion that MHC class I loss leaves tumor cells susceptible to NK cell-mediated killing (40,44). Furthermore, this is consistent with similar work analyzing the transcriptional profiles of two datasets of patients with non-small cell lung cancer (NSCLC) comparing tumors with low *B2M* expression against tumors with high *B2M* expression, where the fraction of activated NK cells was higher in *B2M*-low tumors (45). These results lend support toward NK cells potentially being the main mediators of MHC class I-negative tumor removal. We hypothesize that low or lost MHC class I expression in tumors leads to NK cell activation. However, despite the greater numbers and proportions of activated NK cells found in *B2M* LOH melanomas, these biopsies were still associated with progressive disease, and it was the *B2M* LOH progressive tumors that had the greatest amount of activated NK cells and other cytotoxic immune cell types. This suggests that there may be inhibitory molecules present in the tumor microenvironment that are impeding NK cell cytotoxic activity, stressing the need for more in-depth studies into the tumor microenvironment of *B2M*-dysregulated tumors. Additionally, in our samples, we found that M1 macrophages, memory resting CD4+ T cells, and γδ T cells were higher in *B2M* LOH tumors, with responsive tumors having greater amounts of monocytes and memory resting CD4+ T cells. Another striking observation since, as demonstrated by our murine models and previous studies, M1 macrophages that are no longer inhibited by the interaction of B2M with LILRB1 (46), and CD4+ T cells that are not dependent on surface MHC class I expression (13), can also play a role in eradicating *B2M*-null tumors. Similarly, it has recently been shown that γδ T cells, which are also not restricted by surface MHC class I expression, had high infiltration rates in *B2M*-inactivated MMR-d cancers and were associated with enhanced reactivity and cytotoxic activity against MHC class I-negative tumors (15).

In conclusion, cancers may induce different immune cell subset responses depending on their inherent immunogenicity and the level of surface MHC class I expression. The main immune cell subset mediating antitumor responses induced by PD-1 blockade in humans are CD8+ T cells (1), with the need for costimulation and help from CD4+ T cells when using PD-1 blockade therapies in implantable murine models where the immune system needs to be primed to induce tumor regression (17,47,48). As cancers attempt to evade the immune system by decreasing their immunogenicity through decreased tumor antigen presentation by MHC class I downregulation or loss, it triggers an alternate immune surveillance process mediated by NK cells, and potentially γδ T cells, with differing roles for CD4+ T cells depending on the model system.

**Acknowledgments**

This study was funded in part by the Parker Institute for Cancer Immunotherapy (PICI), NIH grants R35 CA197633 and P01 CA168585, the Ressler Family Fund, and the support from Ken and Donna Schultz, Todd and Donna Jones, Karen and James Witemyre, and Thomas Stutz through the Jonsson Cancer Center Foundation, and Jonathan Isaacson through the Melanoma Research Foundation (to A.R.). D.Y.T was supported by a Young Investigator Award from ASCO, a grant from the Spanish Society of Medical Oncology for Translational Research in Reference Centers and the V Foundation-Gil Nickel Family Endowed Fellowship in Melanoma Research. M.G. is a pre-doctoral fellow supported by the UCLA Tumor Cell Biology Training Program USHHS Ruth L. Kirschstein Institutional National Research Service Award T32 CA009056 and the UCLA Medical Scientist Training Program (MSTP) NIH NIGMS Training Grant T32 GM008042. G.A-R. was supported by the Isabel & Harvey Kibel Fellowship award and the Alan Ghitis Fellowship Award for Melanoma Research. K.M.C. is supported by the Cancer Research Institute Irvington Postdoctoral Fellowship Program, the V Foundation Gil Nickel Melanoma Research Fellowship, and the Parker Institute for Cancer Immunotherapy and V Foundation Bridge Fellows Program. Flow and mass cytometry were performed in the UCLA Jonsson Comprehensive Cancer Center (JCCC) and Center for AIDS Research Flow Cytometry Core Facility that is supported by NIH awards P30 CA016042 and 5P30 AI028697, and by the JCCC, the UCLA AIDS Institute, and the David Geffen School of Medicine at UCLA.

**Conflict of Interest Statement**

D.Y.T. is currently a full-time employee of Ascendis Pharma. K.M.C. has received consulting fees from PACT Pharma, Tango Therapeutics, and Geneoscopy LLC, and is a shareholder in Geneoscopy LLC. G.A-R. has received honoraria from consulting with Arcus Biosciences. A.R. has received honoraria from consulting with Amgen, Bristol-Myers Squibb, Chugai, Jazz, Merck, Novartis, RAPT, is or has been a member of the scientific advisory board and holds stock in Advaxis, Appia, Apricity, Arcus, Compugen, CytomX, Highlight, ImaginAb, ImmPact, ImmuneSensor, Inspirna, Isoplexis, Kite-Gilead, Larkspur, Lutris, MapKure, Merus, PACT, Pluto, RAPT, Synthekine and Tango, has received research funding from Agilent and from Bristol-Myers Squibb through Stand Up to Cancer (SU2C), and patent royalties from Arsenal Bio.

**Figure 1**

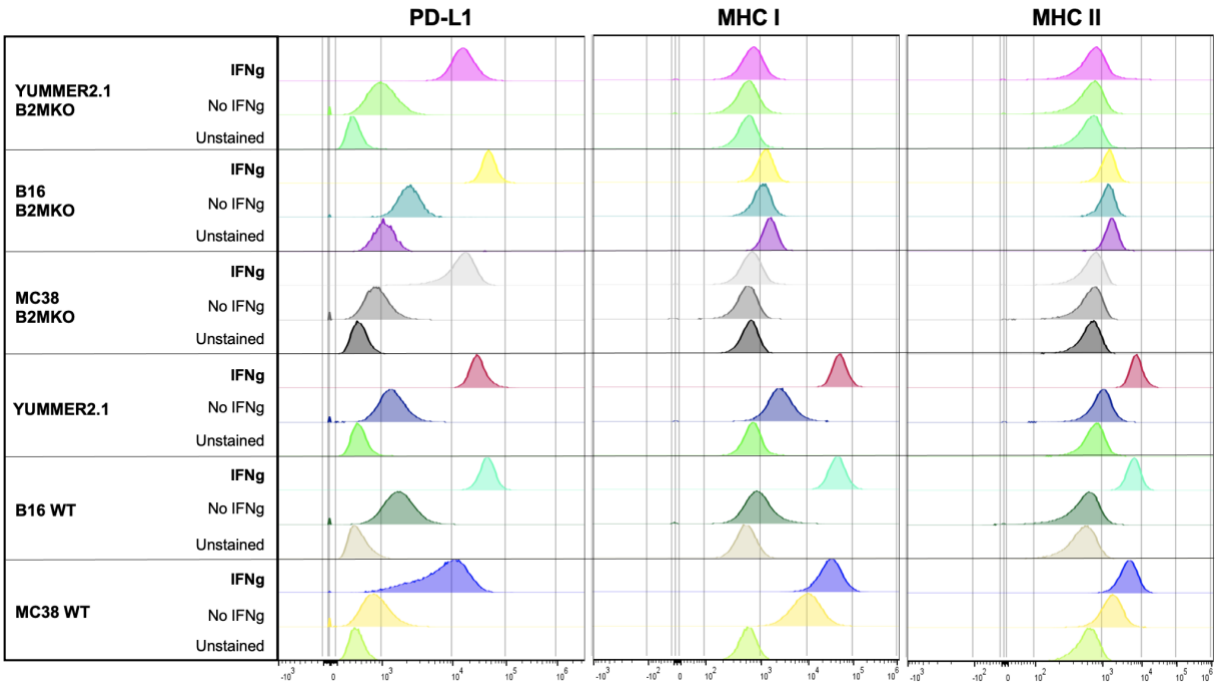


**Figure 1. Surface expression of PD-L1, MHC class I and II in murine cell lines.** Wild type (WT) and *B2M*-knockout (KO) sublines of MC38, B16 and YUMMER2.1 were stained for flow cytometry analysis with and without IFNγ stimulation. Histograms represent changes in mean fluorescence intensity (MFI) by flow cytometry.

**Figure 2**

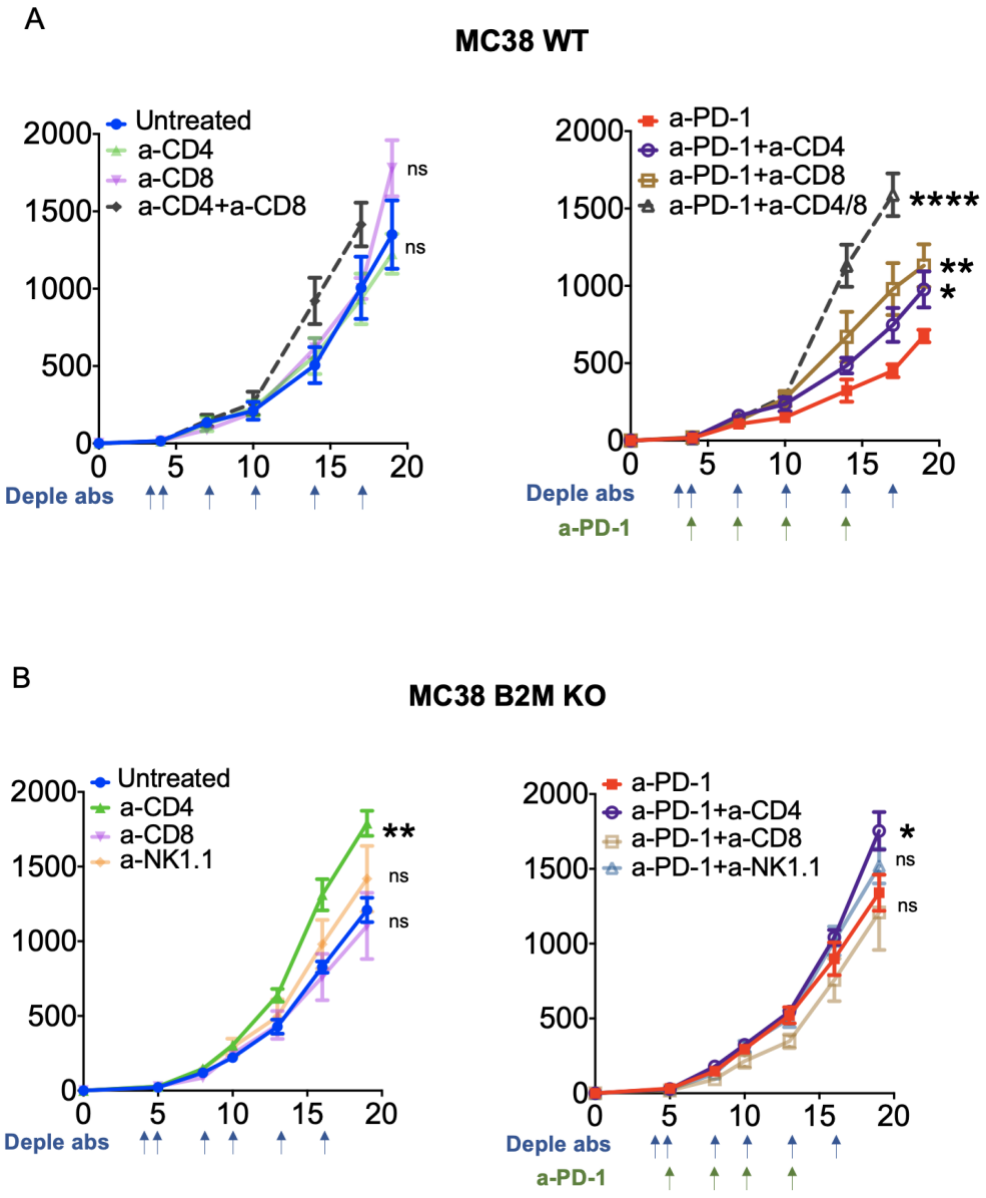


**Figure 2. Immune cell subsets inducing antitumor responses in MC38 with and without *B2M* expression.** *In vivo* tumor growth curves of (A) wild type (WT) and (B) *B2M*-knockout (KO) sublines of MC38 with 5 mice in each group. Data represented as mean ± SEM. The arrow indicates the days of treatment with depletion antibodies or when a–PD-1 was started. ns, not significant; *, P < 0.05; **, P < 0.01; ****, P < 0.0001.

**Figure 3**

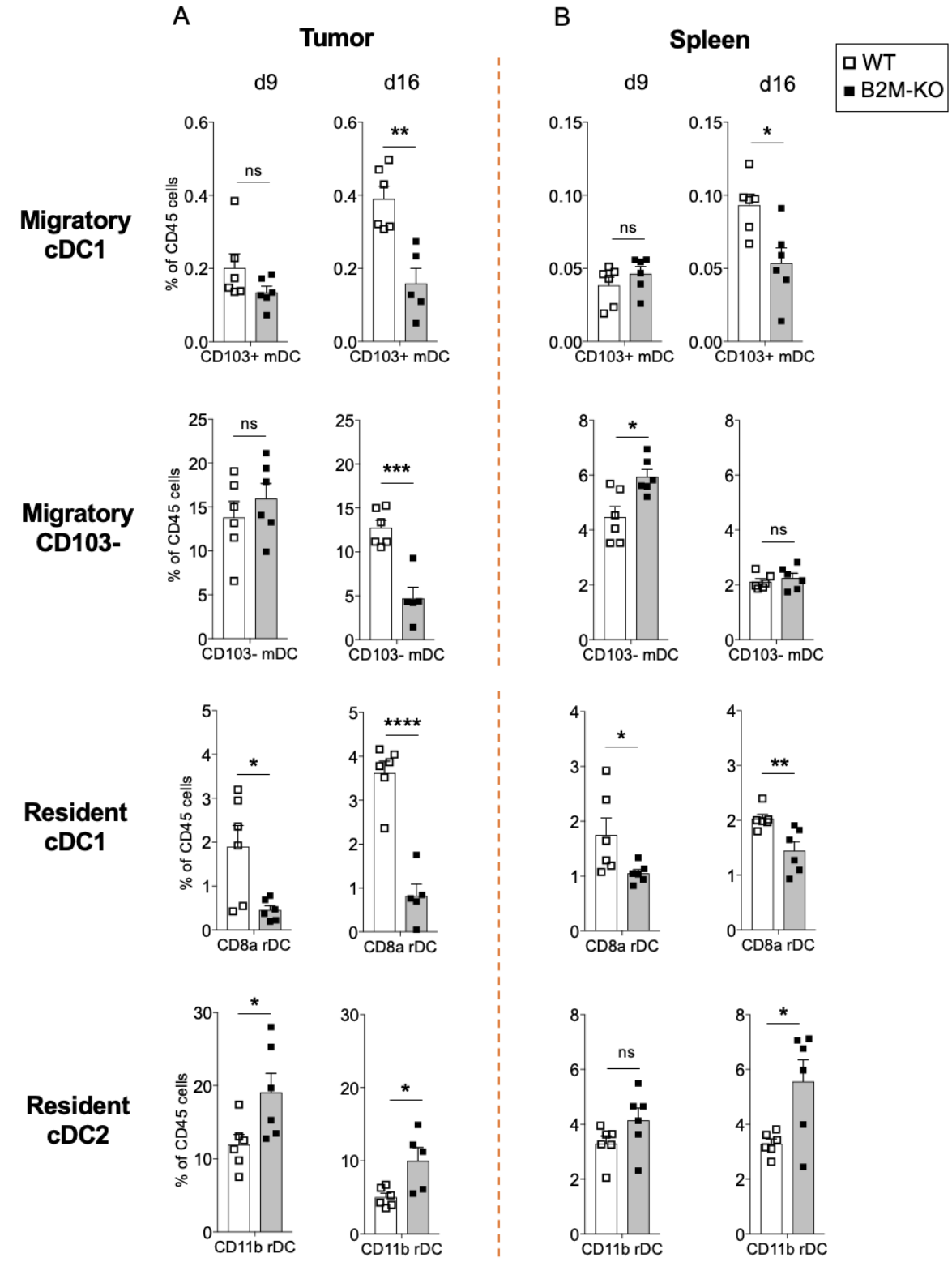
A
Tumor
B
Spleen
d9
d16
WT
B2M-KO
Migratory cDC1
Migratory CD103-
Resident cDC1
Resident cDC2
% of CD45 cells
CD103+ mDC
CD103- mDC
CD8a rDC
CD11b rDC
ns
*
**
***
****

**Figure 3. Dendritic cell subsets in MC38 with and without *B2M* expression.** Differences in the infiltration of CD103+ mDCs, CD103- mDCs, CD8+ rDCs and CD11b+ rDCs in MC38 WT and *B2M*-KO in (A) tumors and (B) spleens. Tumors were collected on day 9 (two doses of isotype or a-PD-1) and day 16 (four doses of isotype or a-PD-1). After processing and staining, samples were gated as indicated in Supplementary Figure 2. Mean ± SEM, Unpaired *t* test, *n* = 6. ns, not significant; *, P < 0.05; **, P < 0.01; ***, P < 0.001; ****, P < 0.0001.

**Figure 4**

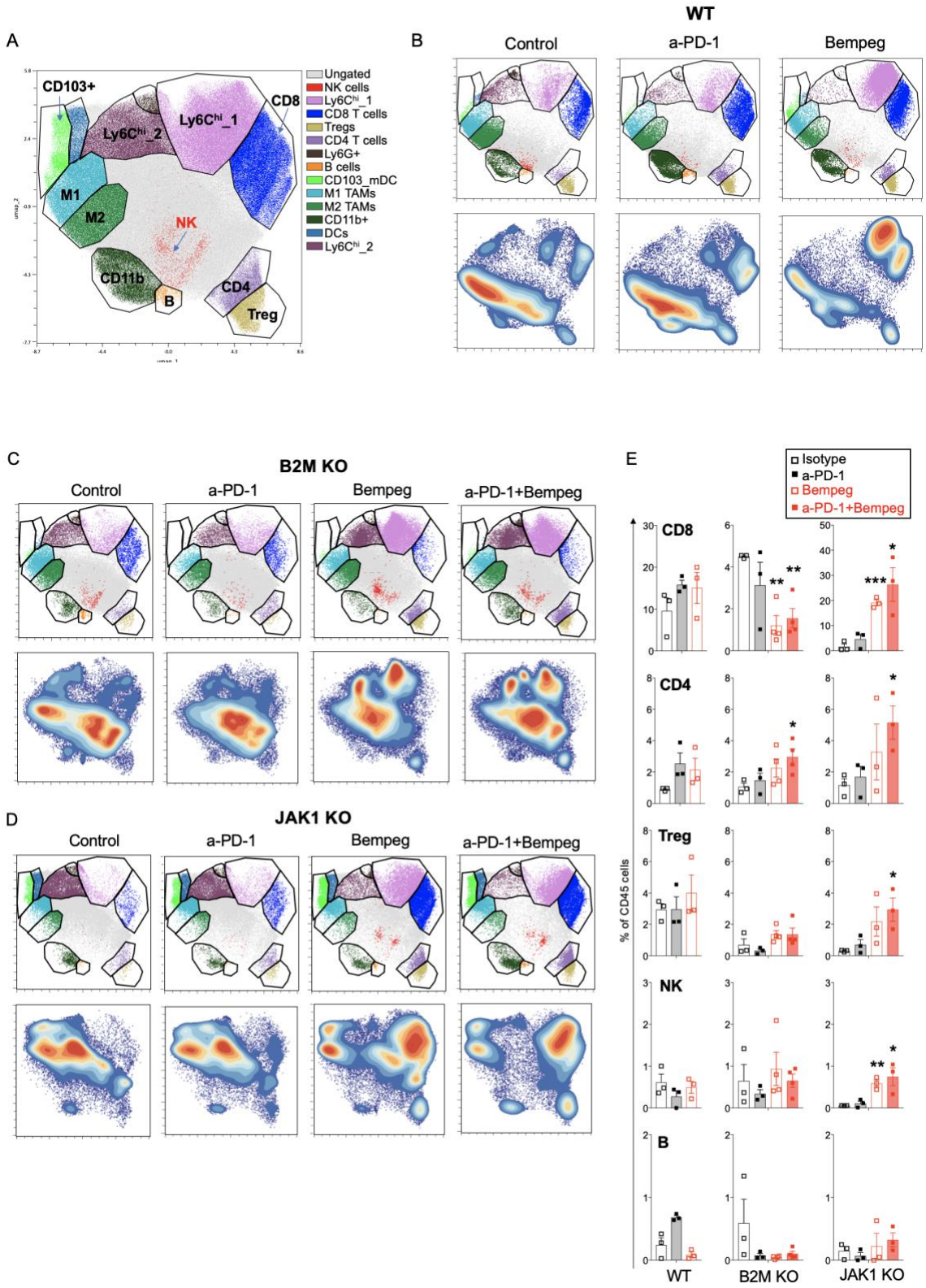
A
CD103+
Ly6C$^{hi}$_2
Ly6C$^{hi}$_1
CD8
M1
M2
NK
CD11b
B
CD4
Treg
Ungated
NK cells
Ly6C$^{hi}$_1
CD8 T cells
Tregs
CD4 T cells
Ly6G+
B cells
CD103_mDC
M1 TAMs
M2 TAMs
CD11b+
DCs
Ly6C$^{hi}$_2
B
WT
Control
a-PD-1
Bempeg
C
B2M KO
Control
a-PD-1
Bempeg
a-PD-1+Bempeg
D
JAK1 KO
Control
a-PD-1
Bempeg
a-PD-1+Bempeg
E
Isotype
a-PD-1
Bempeg
a-PD-1+Bempeg
CD8
CD4
Treg
NK
B
% of CD45 cells
WT
B2M KO
JAK1 KO

**Figure 4. Characterization of the tumor immune infiltration by CyTOF using OMIQ platform.** Plots showing UMAP views providing comprehensive manually gated immune cell populations in (A) all samples (B) MC38 WT (C) MC38 *B2M*-KO and (D) MC38 *JAK1*-KO treated with isotype-control, a-PD-1, bempegaldesleukin (bempeg) and a-PD-1 plus bempeg. (E) Percentage of CD8+ T, CD4+ T, T regs, NK and B cells from CD45+ cells. Mean ± SEM, Unpaired *t* test, *n* = 3-4. *, P < 0.05; **, P < 0.01; ***, P < 0.001.

**Figure 5**

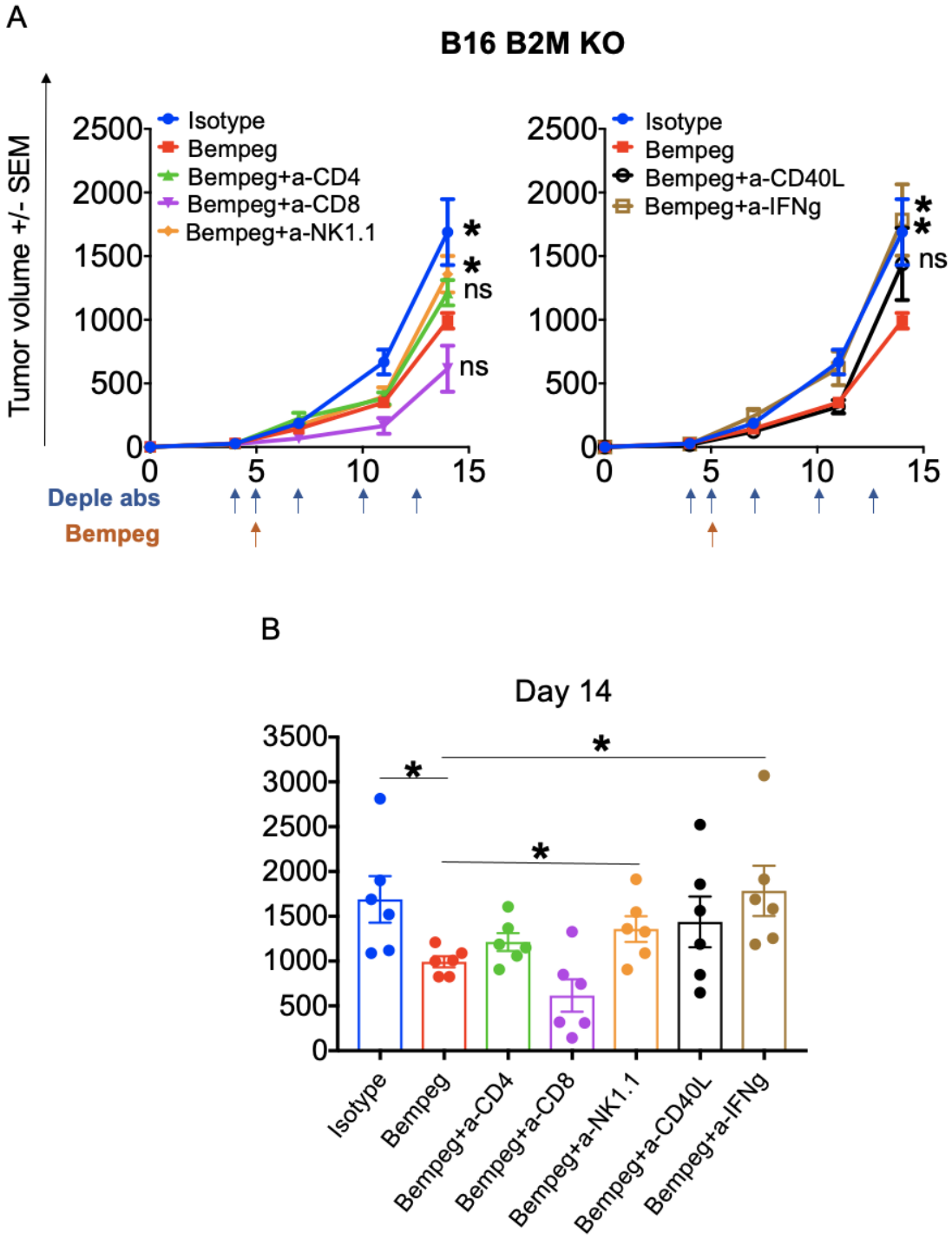
A
B16 B2M KO
Tumor volume +/- SEM
Isotype
Bempeg
Bempeg+a-CD4
Bempeg+a-CD8
Bempeg+a-NK1.1
Bempeg+a-CD40L
Bempeg+a-IFNg
Deple abs
Bempeg
ns
B
Day 14
Isotype
Bempeg
Bempeg+a-CD4
Bempeg+a-CD8
Bempeg+a-NK1.1
Bempeg+a-CD40L
Bempeg+a-IFNg

**Figure 5. Immune cell subsets inducing antitumor responses in B16 with and without *B2M* expression.** (A) *In vivo* tumor growth curves and (B) tumor volumes at day 14 for B16 *B2M*-KO tumors with anti-CD4, anti-CD8, and anti-NK1.1, anti-CD40L and anti-IFNγ depletion studies after 0.8 mg/kg intravenous bempegaldesleukin. Data represented as mean ± SEM from an *n* of 6 per group. The arrow indicates the days of treatment with depletion antibodies or when bempegaldesleukin was started. Dunnett multiple comparisons tests for bempegaldesleukin versus each condition: control, anti-CD4, anti-CD8, anti-NK1.1, anti-CD40L, anti-IFNγ. ns, not significant; *, $P < 0.05$.

**Figure 6**

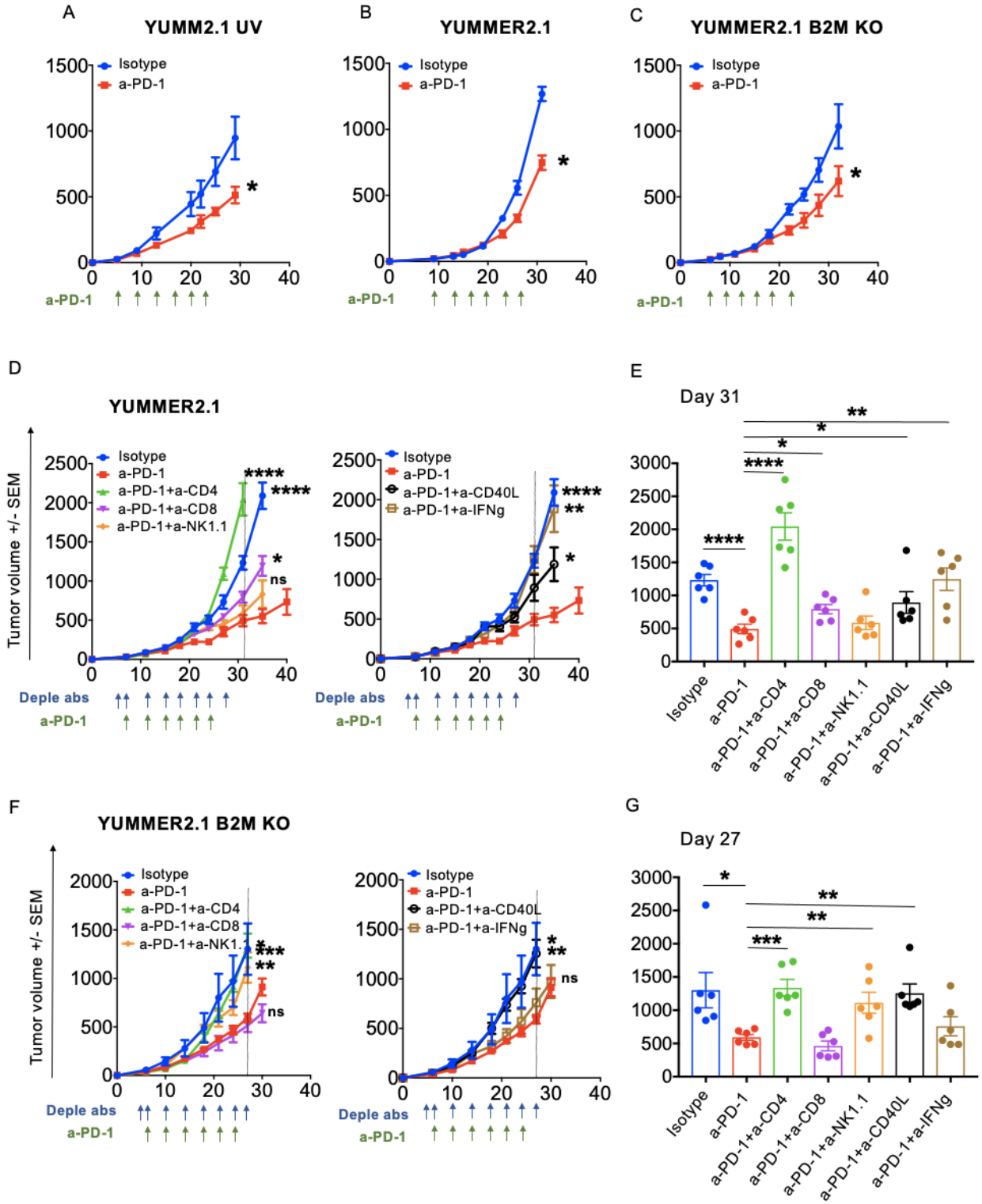
A
YUMM2.1 UV
B
YUMMER2.1
C
YUMMER2.1 B2M KO
Isotype
a-PD-1
a-PD-1
D
YUMMER2.1
Tumor volume +/- SEM
a-PD-1+a-CD4
a-PD-1+a-CD8
a-PD-1+a-NK1.1
a-PD-1+a-CD40L
a-PD-1+a-IFNg
Deple abs
E
Day 31
Isotype
a-PD-1
a-PD-1+a-CD4
a-PD-1+a-CD8
a-PD-1+a-NK1.1
a-PD-1+a-CD40L
a-PD-1+a-IFNg
F
YUMMER2.1 B2M KO
G
Day 27

**Figure 6. Immune cell subsets inducing antitumor responses in YUMMER2.1 with and without *B2M* expression.** *In vivo* tumor growth curves of (A) YUMM2.1 UV (B) YUMMER2.1 and (C) YUMMER2.1 *B2M*-KO tumors after isotype-control or anti-PD-1 therapy. In YUMM2.1 UV, *n* = 4 per group; YUMMER2.1, *n* = 10 per group and in YUMMER2.1 *B2M*-KO, *n* = 5 per group. (D) In *vivo* tumor growth curves and (E) tumor volumes at day 31 for YUMMER2.1 with anti-CD4, anti-CD8, and anti-NK1.1, anti-CD40L and anti-IFNγ depletion after anti-PD-1 therapy. Data represented as mean ± SEM from an *n* of 6 per group. (F) In *vivo* tumor growth curves and (G) tumor volumes at day 27 for YUMMER2.1 *B2M*-KO with anti-CD4, anti-CD8, and anti-NK1.1, anti-CD40L and anti-IFNγ depletion after anti-PD-1 therapy. Data represented as mean ± SEM from an *n* of 6 per group. In (A-D) and (F) the arrow indicates the days of treatment with depletion antibodies or when a-PD-1 was started. In (A-F) ns, not significant; *, $P < 0.05$; **, $P < 0.01$; ***, $P < 0.001$; ****, $P < 0.0001$.

**Figure 7**

A

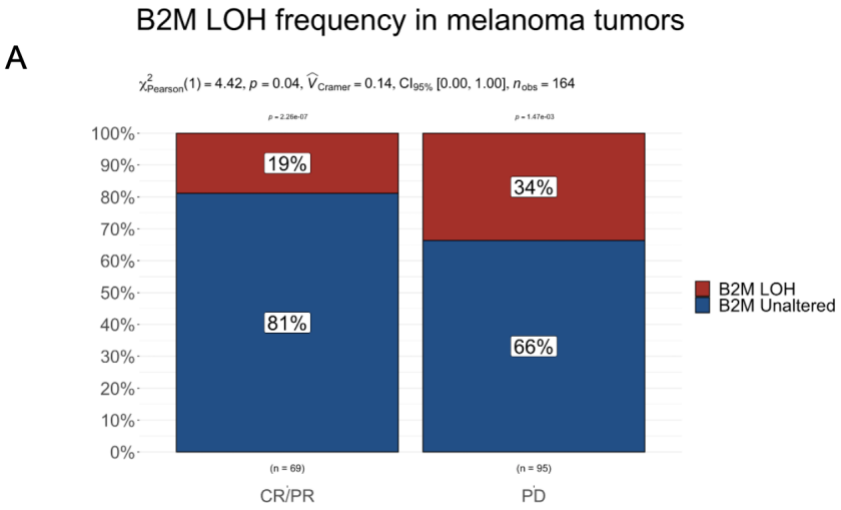
B2M LOH frequency in melanoma tumors
$\chi^2_{Pearson}(1) = 4.42$, $p = 0.04$, $\widehat{V}_{Cramer} = 0.14$, $CI_{95\%}$ [0.00, 1.00], $n_{obs} = 164$
100%
90%
80%
70%
60%
50%
40%
30%
20%
10%
0%
19%
81%
34%
66%
(n = 69)
(n = 95)
CR/PR
PD
B2M LOH
B2M Unaltered

B

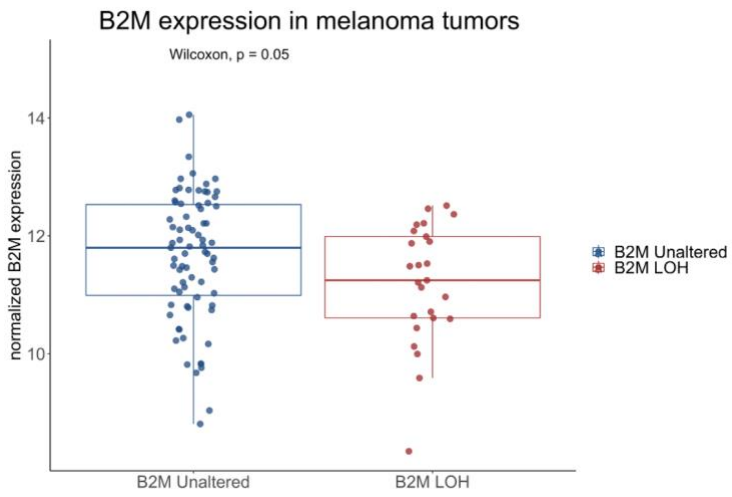
B2M expression in melanoma tumors
Wilcoxon, p = 0.05
normalized B2M expression
14
12
10
B2M Unaltered
B2M LOH
B2M Unaltered
B2M LOH

**Figure 7 *continued***

C

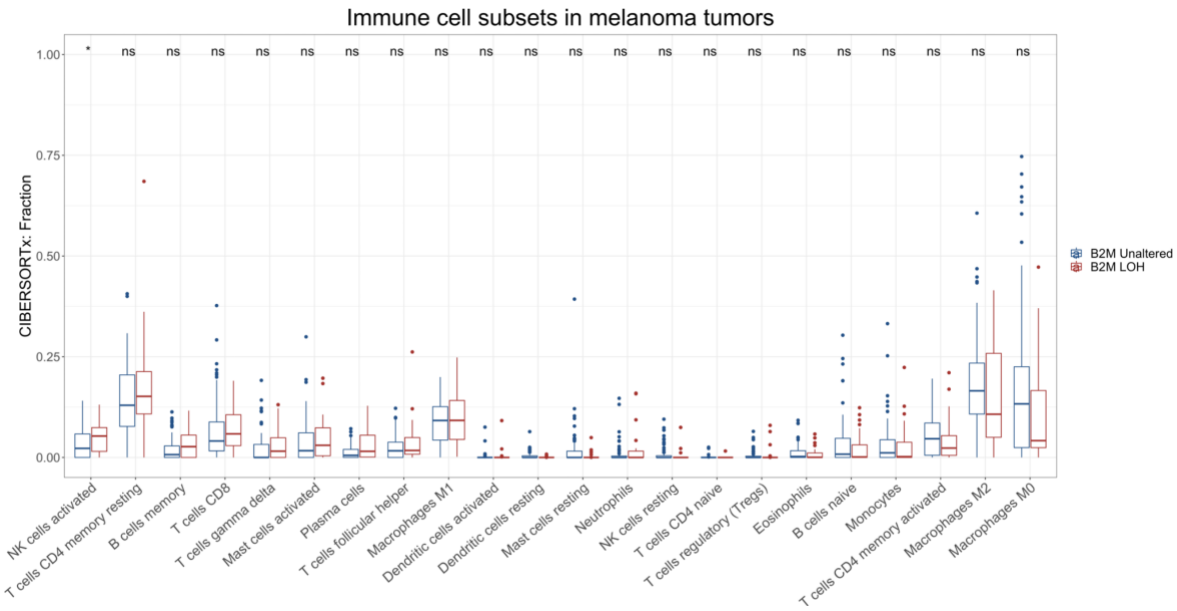


D

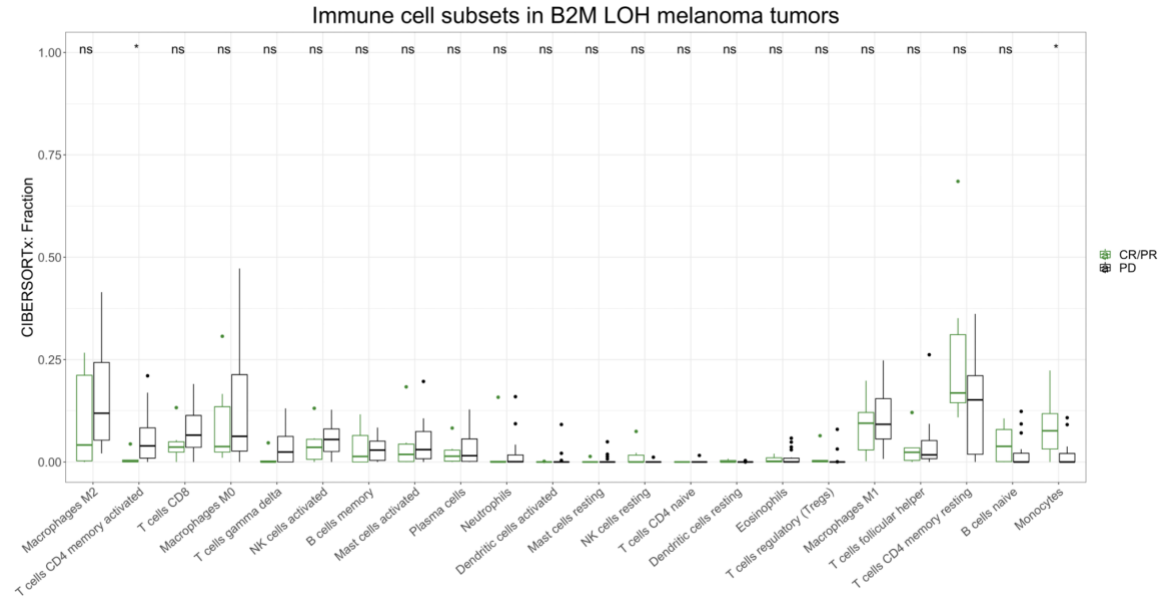

**Figure 7. Baseline melanoma biopsies with and without *B2M* loss of heterozygosity (LOH).** (A) The frequency of LOH events in baseline responsive (n=69) versus progressive melanoma tumors (n=95); $X^2_{Pearson}$ test, p=0.04, n=164. (B) *B2M* expression levels in *B2M* unaltered (n=75) versus tumors with *B2M* LOH (n=25) determined using the normalized bulk RNAseq data (logcpm). Wilcoxon test, p=0.05, n=100. CIBERSORTx immune cell deconvolution analysis using bulk RNAseq data showing (C) fractions of immune cell types in *B2M* unaltered (n=75) versus *B2M* LOH tumors (n=25), and (D) fractions of immune cell subtypes in *B2M* LOH progressive (n=19) versus responsive tumors (n=6). Cell types are sorted by greatest difference in median score between groups; Wilcoxon test, ns= not significant, * p<0.05.

**Supplementary Figure S1**

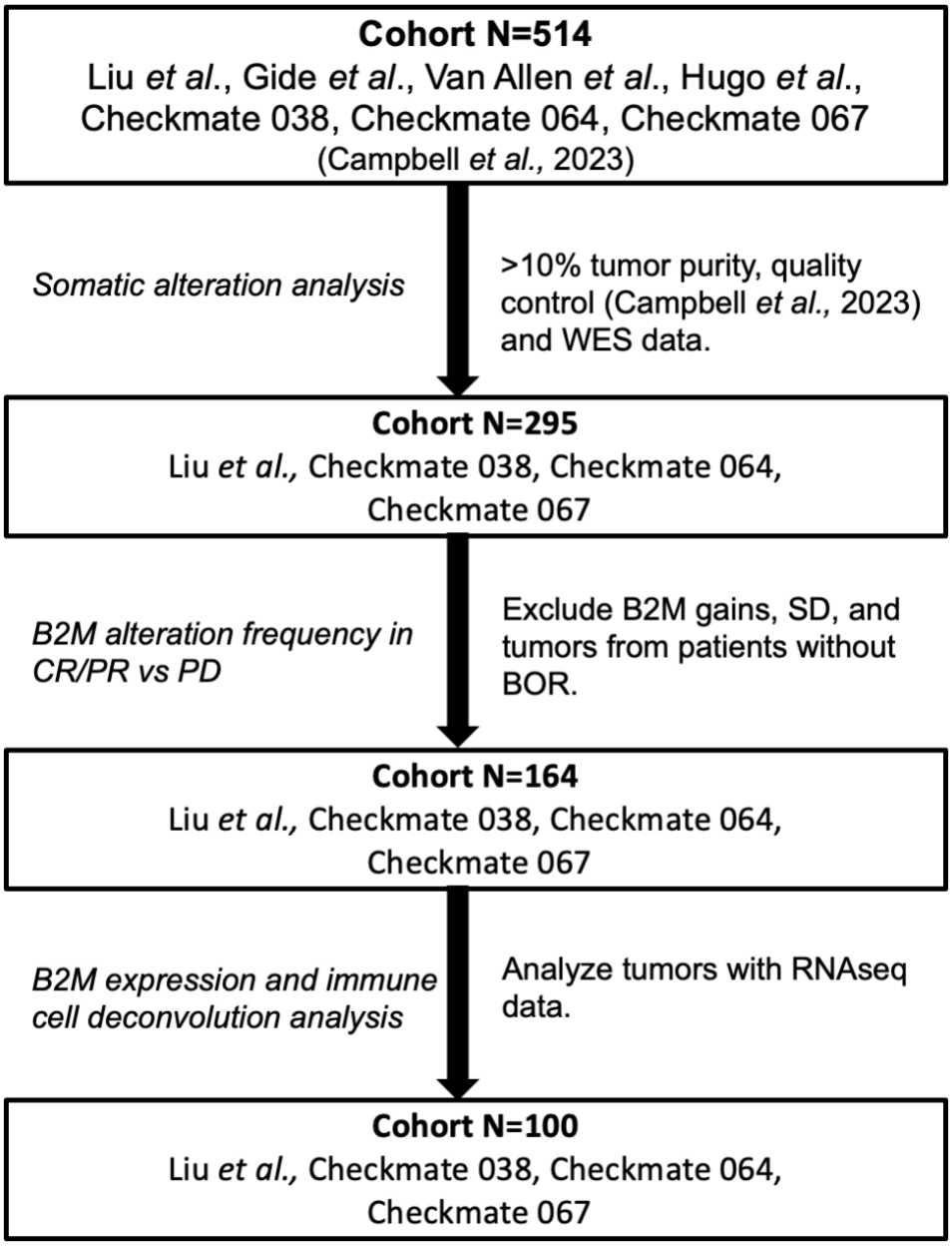


**Supplementary Figure S1: Clinical dataset and analysis workflow.**

**Supplementary Figure S2**

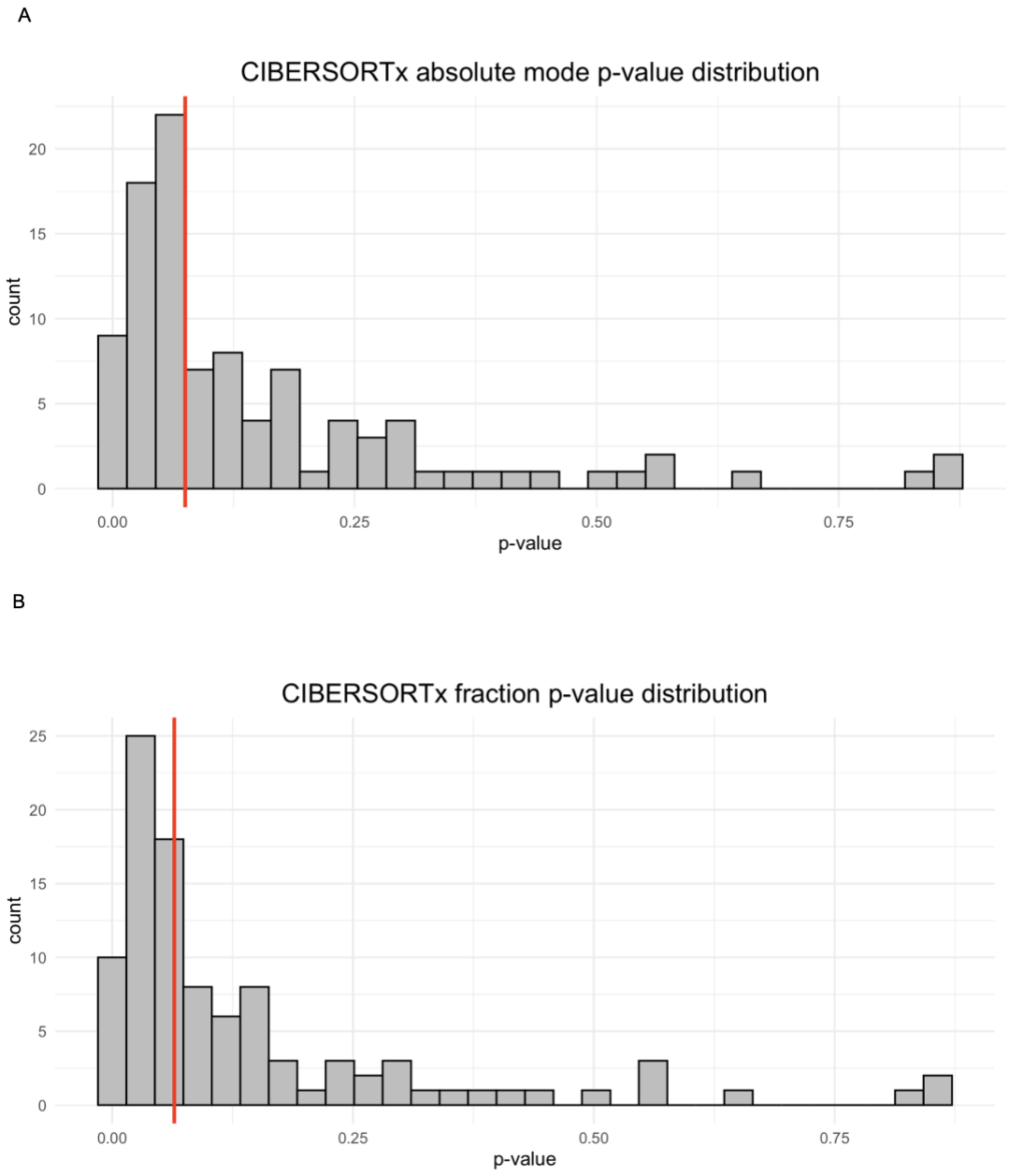


**Supplementary Figure S2: CIBERSORTx p-value distribution.** Histograms of the p-value distributions of the samples (n=100) analyzed through CIBERSORTx for (A) absolute mode (median=0.075) and (B) fractions (median=0.065). Red line represents the median.

**Supplementary Figure S3**

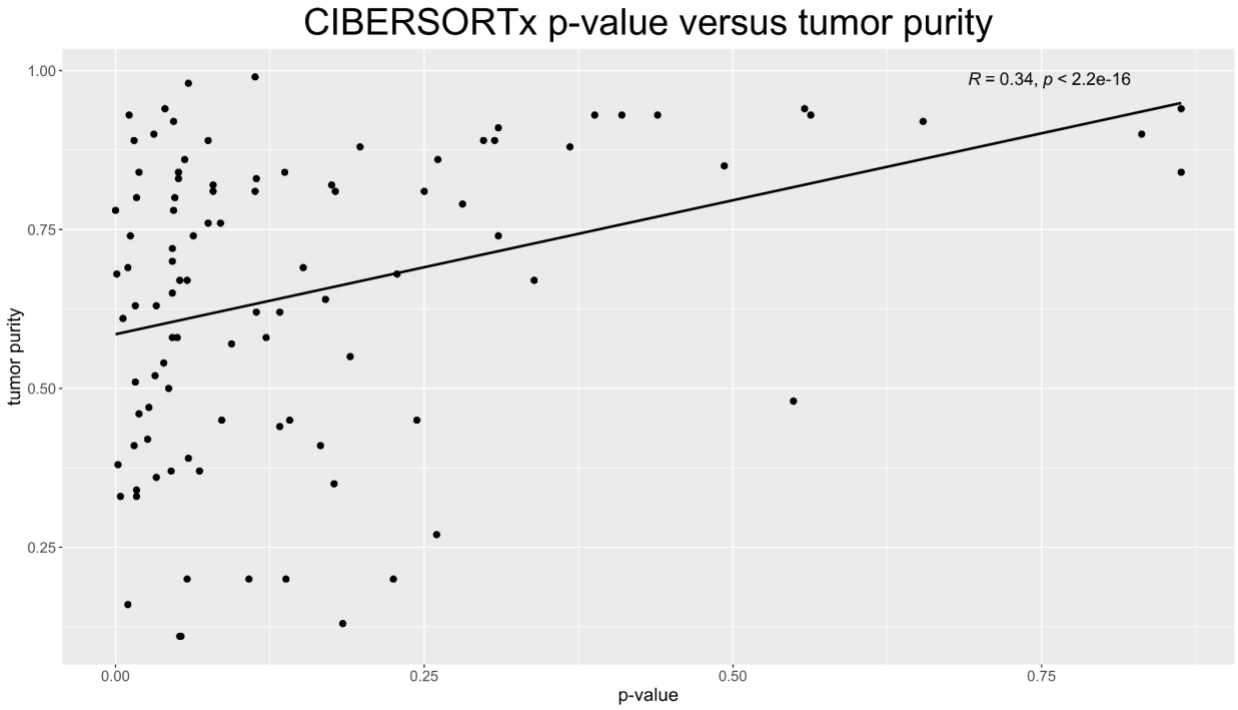


**Supplementary Figure S3: CIBERSORTx p-value versus tumor purity.** Scatterplot of the samples (n=100) analyzed through CIBERSORTx with p-value readout on the x-axis and tumor purity (WES) on the y-axis; Pearson correlation $R^2$= 0.11, p<2.2 x $10^{-16}$.

## Supplementary Figure S4

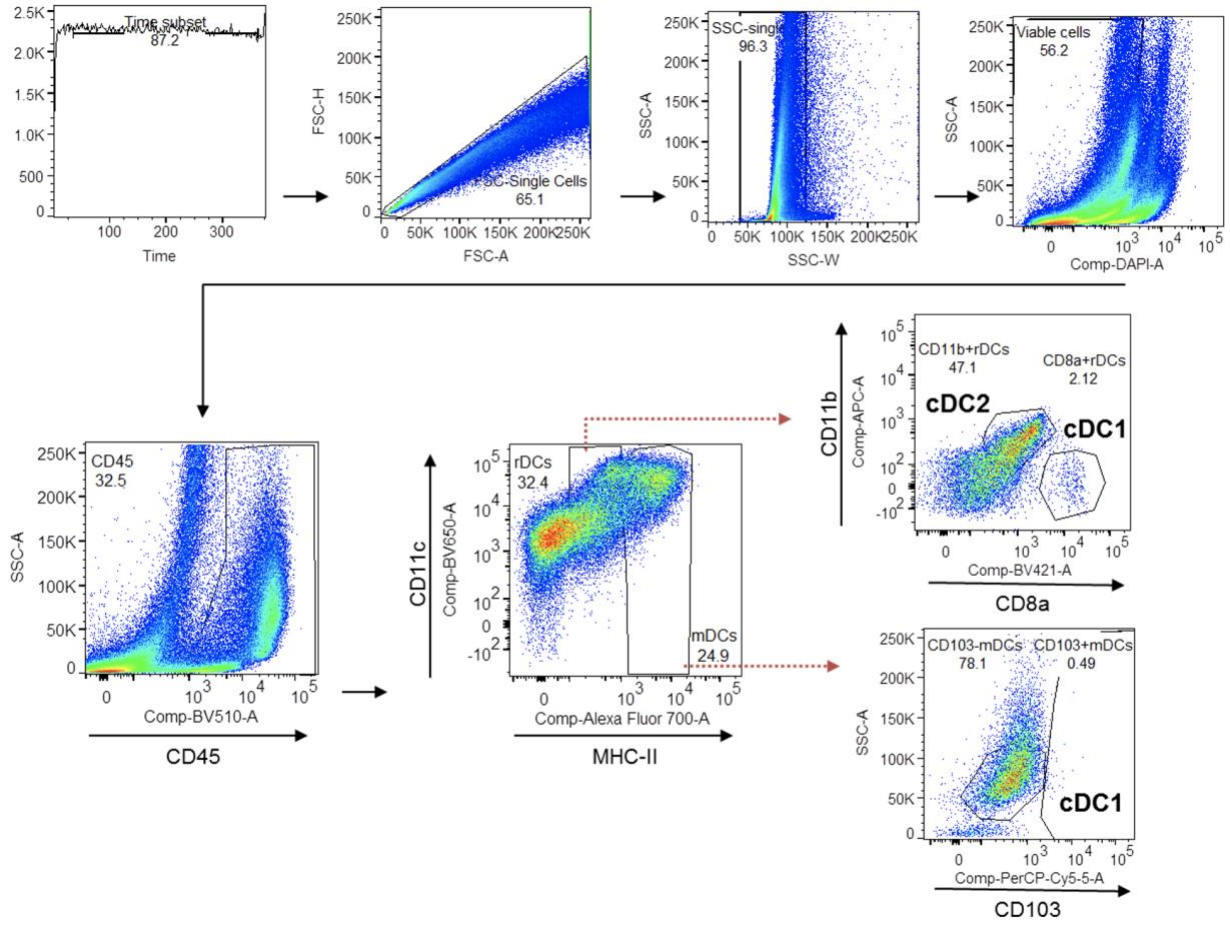


**Supplementary Figure S4: Gating strategy in dendritic cell panel.**

## Supplementary Figure S5

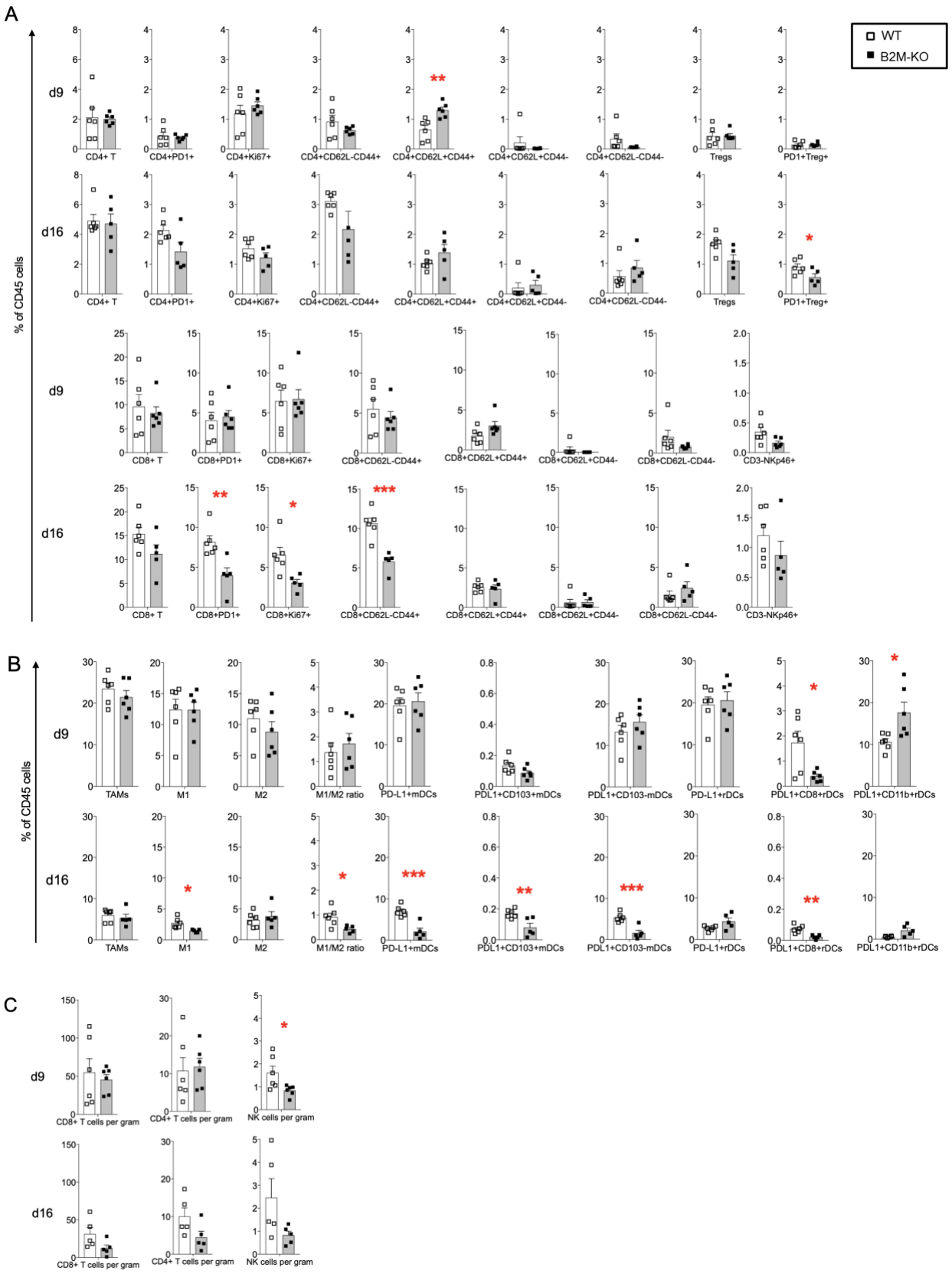

**Supplementary Figure S5: (A) T cell subsets and (B) myeloid and dendritic cell subsets in MC38 with and without *B2M* expression.** Differences in the infiltration of immune cells in MC38 WT and *B2M*-KO tumors. Tumors were collected on day 9 (two doses of isotype or a-PD-1) and day 16 (four doses of isotype or a-PD-1). (C) Numbers of CD8+ T, CD4+ T and NK cells per gram in MC38 WT and B2M-KO tumors. Mean ± SEM, Unpaired t test, n = 6. ns, not significant; *, $P < 0.05$; **, $P < 0.01$; ***, $P < 0.001$.

**Supplementary Figure S6**

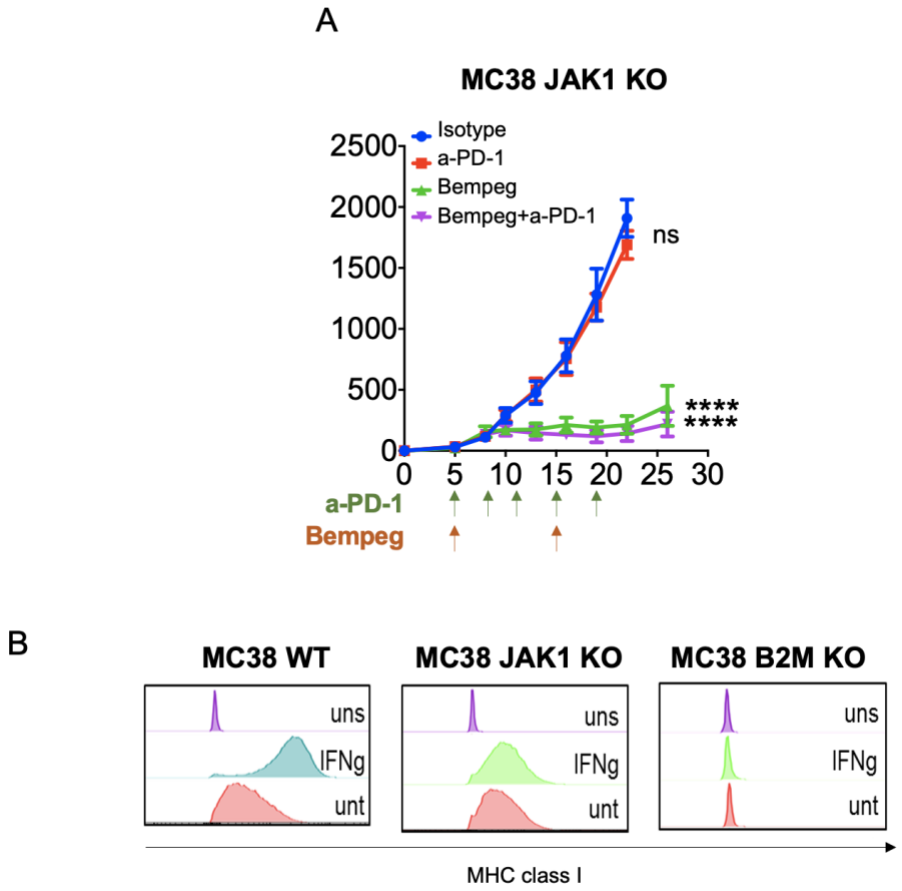


**Supplementary Figure S6: Bempegaldesleukin to reverse resistance in *JAK1*-deficient tumors.** (A) *In vivo* tumor growth curves for MC38 *JAK1*-KO tumors treated with 0.8 mg/kg intravenous bempegaldesleukin every 9 days x 2 doses, or anti-PD-1 therapy, or the combination. Data represented as mean ± SEM from an *n* of 4 per group. The arrow indicates the days of treatment with bempegaldesleukin or when anti -PD-1 therapy was started. Dunnett multiple comparisons tests for control versus anti-PD-1, or bempegaldesleukin, or bempegaldesleukin plus anti-PD-1. ns, not significant; ****, $P < 0.0001$. (B) The measure of MHC class I expression by flow cytometry after IFNγ stimulation in MC38 WT, *JAK1*-KO and *B2M*-KO. *JAK1*-KO maintains its MHC class I basal expression upon IFNγ. Histograms represent changes in MFI by flow cytometry.

**Supplementary Figure S7**

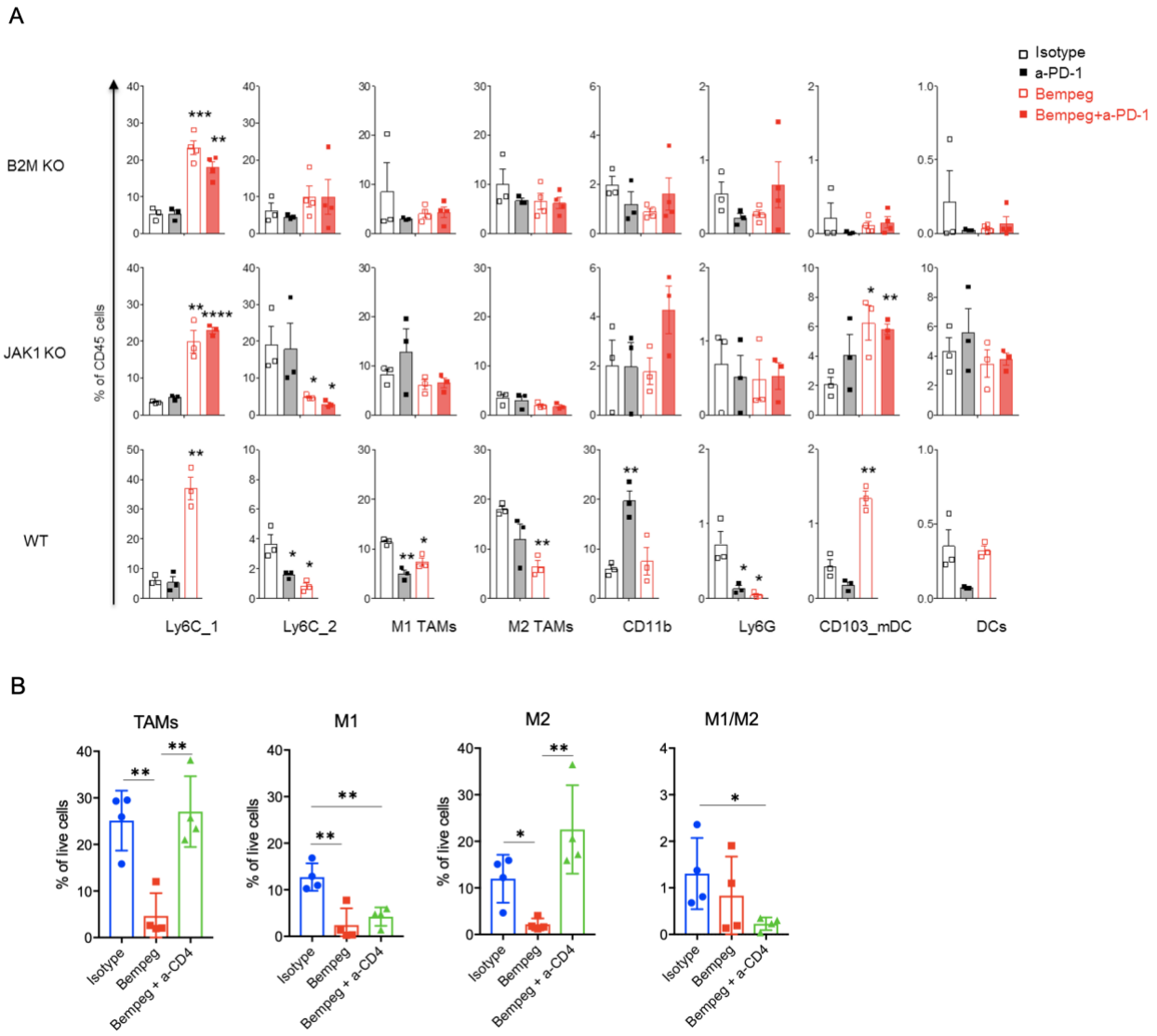


**Supplementary Figure S7: (A) Identification of tumor immune cell infiltration by CyTOF.** Percentage of Ly6C+, TAMs, CD11b+, Ly6G+, CD103 mDCs and DCs cells from CD45+ cells. Mean ± SEM, Unpaired t test, n = 3-4. *, P < 0.05; **, P < 0.01; ***, P < 0.001; ****, P < 0.0001. (B) Percentages of TAMs, M1, M2 and index M1/M2 from live cells in MC38 *B2M*-KO tumors treated with isotype monoclonal antibody, bempegaldesleukin, or bempegaldesleukin plus anti-CD4. Mean ± SEM, Unpaired t test, n = 4. *, P < 0.05; **, P < 0.01.

**Supplementary Figure S8**

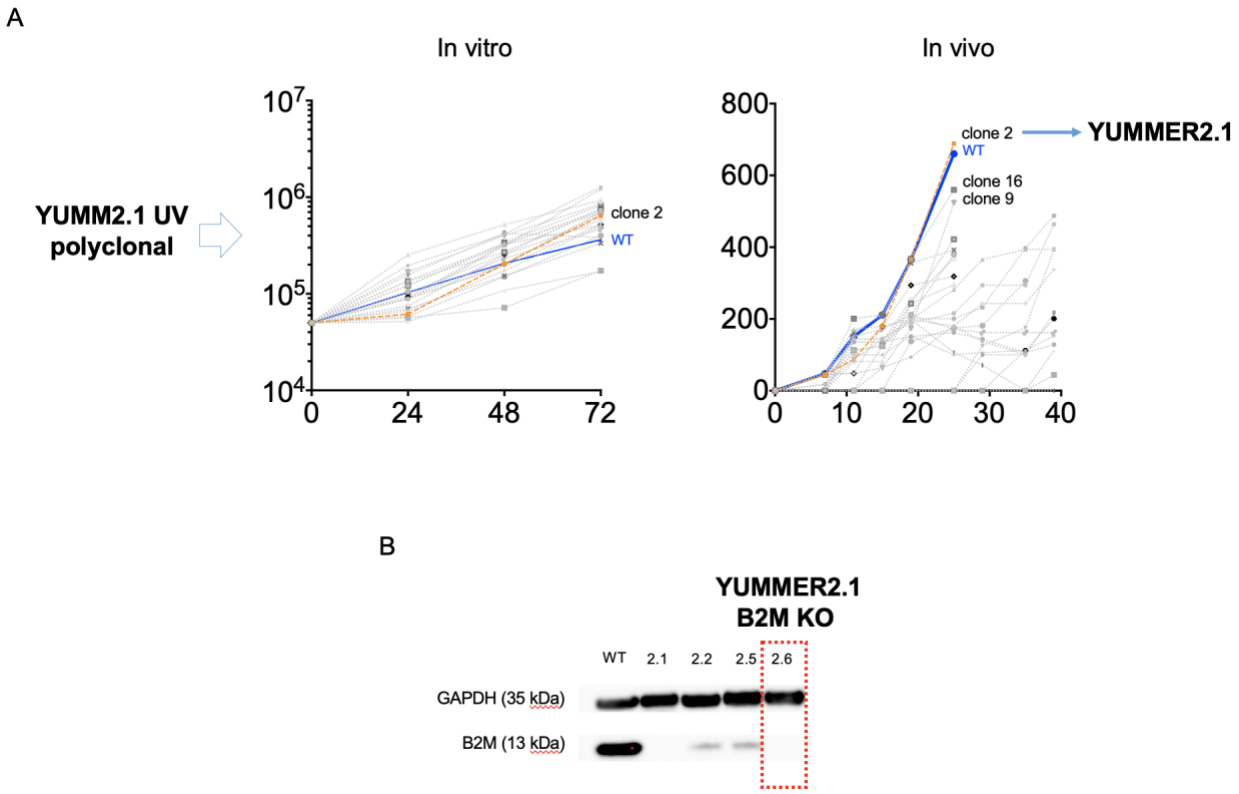


**Supplementary Figure S8: Validation of YUMMER2.1 and YUMMER2.1 *B2M*-KO.** (A) *In vitro* and *in vivo* growth curves in twenty-four clones from the YUMM2.1 UV cell line compared to WT. *In vitro* growth curves represent the percent confluence of cells (y-axis) over time (x-axis) as measured by IncuCyte continuous live-cell imaging. Error bars reflect the standard error of the mean across six replicates of each subline. YUMM2.1 UV clone 2 had similar proliferation rates and *in vitro* and *in vivo* growth curves compared to the parental cell line and was used for *in vivo* studies (YUMMER2.1). (B) Validation of *B2M*-KO by CRISPR/Cas9 gene editing from YUMMER2.1 using Western blot.

**Supplementary Figure S9**

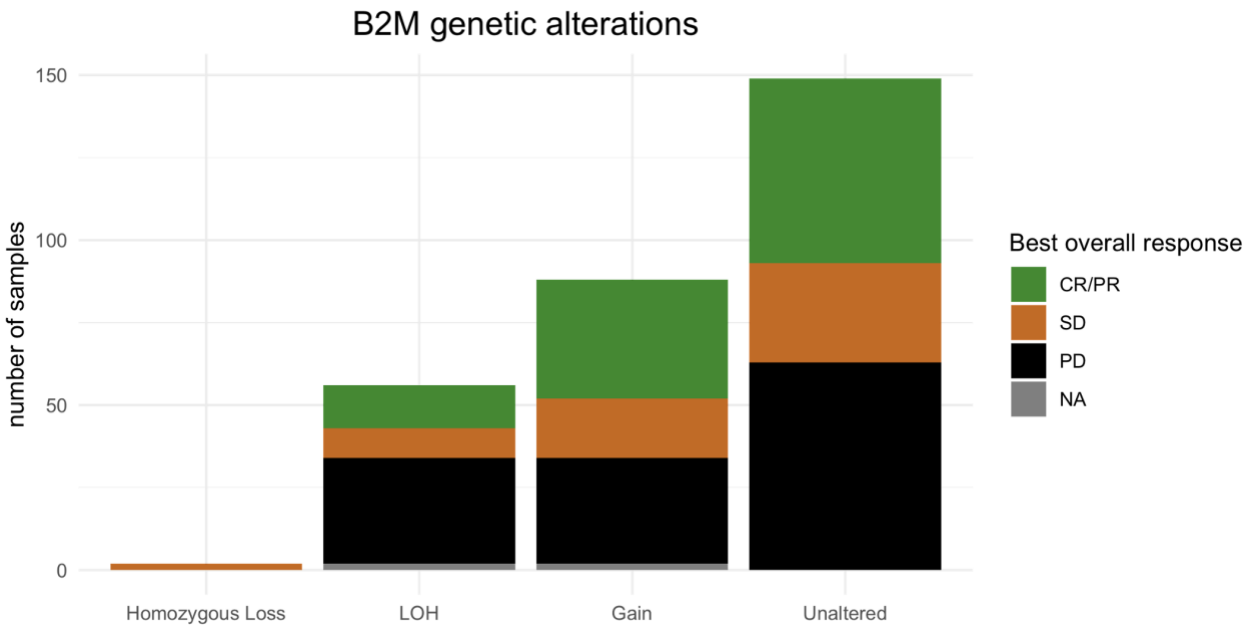


**Supplementary Figure S9: *B2M* genetic alterations in pre-treatment human melanoma biopsies.** Summary of *B2M* genetic alterations in pre-treatment human melanoma biopsies (n=295) determined by analyzing WES data processed by Sequenza. *B2M* homozygous loss n=2, LOH n=56, copy number gains n=88, unaltered n=149.

## Supplementary Figure S10

A

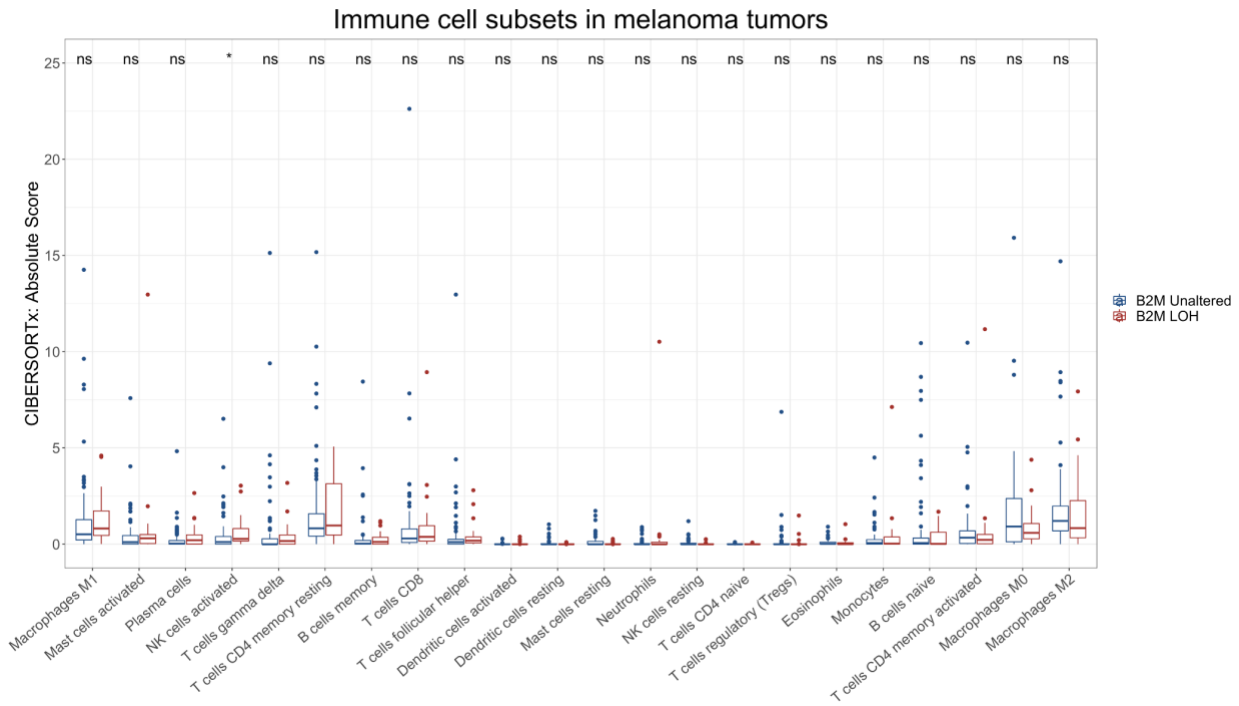


B

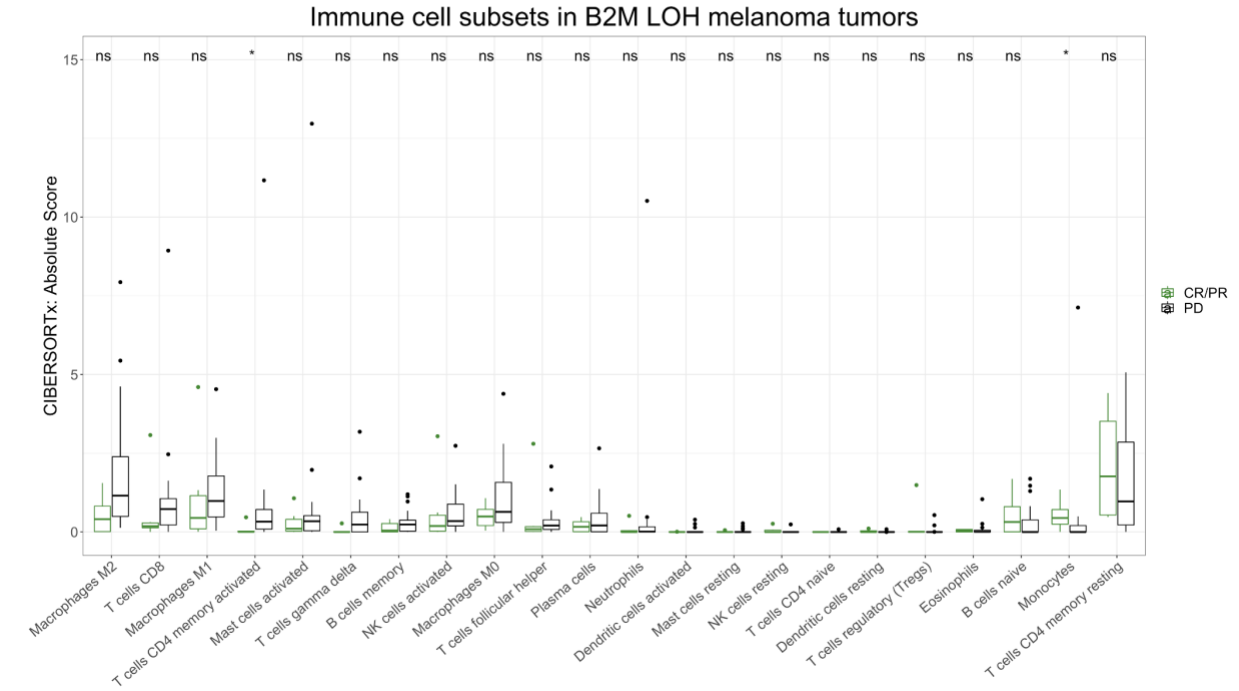

**Supplementary Figure S10: Immune cell subsets in baseline human melanoma tumors**. CIBERSORTx immune cell deconvolution analysis using bulk RNAseq data showing (A) absolute scores of immune cell types in *B2M* unaltered (n=75) versus *B2M* LOH (n=25) tumors, and (B) absolute scores of immune cell subtypes in *B2M* LOH progressive (n=19) versus responsive tumors (n=6). Cell types are sorted by greatest difference in median score between groups; Wilcoxon test, ns= not significant, * $p<0.05$.

## Supplementary Figure S11

A

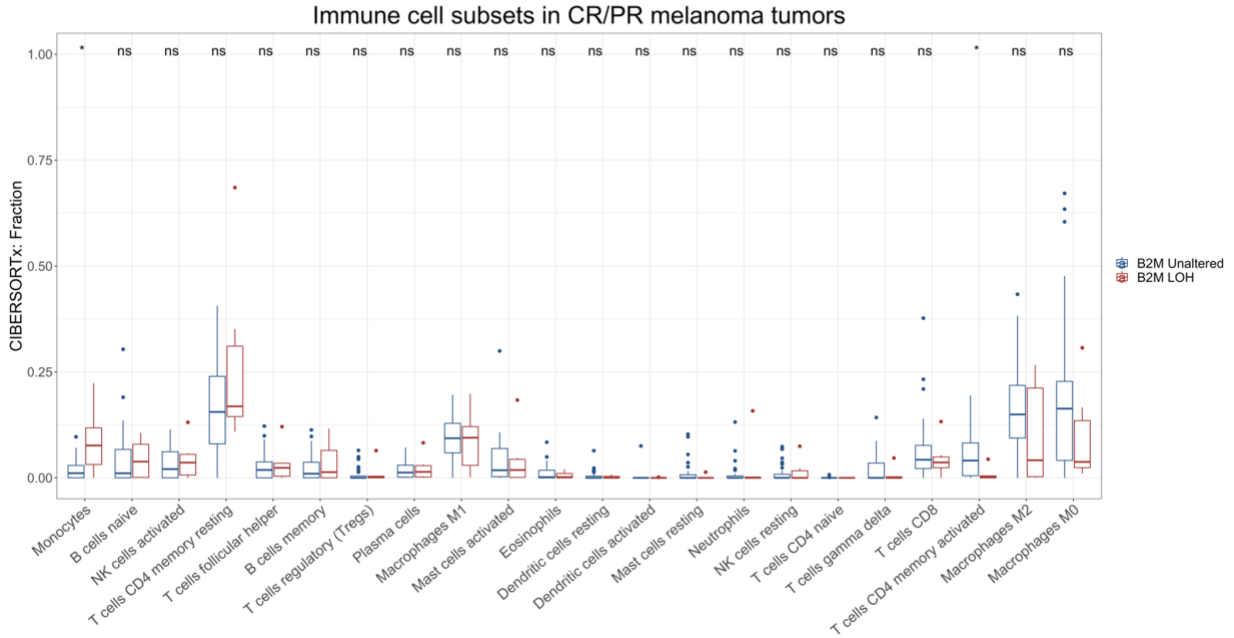


B

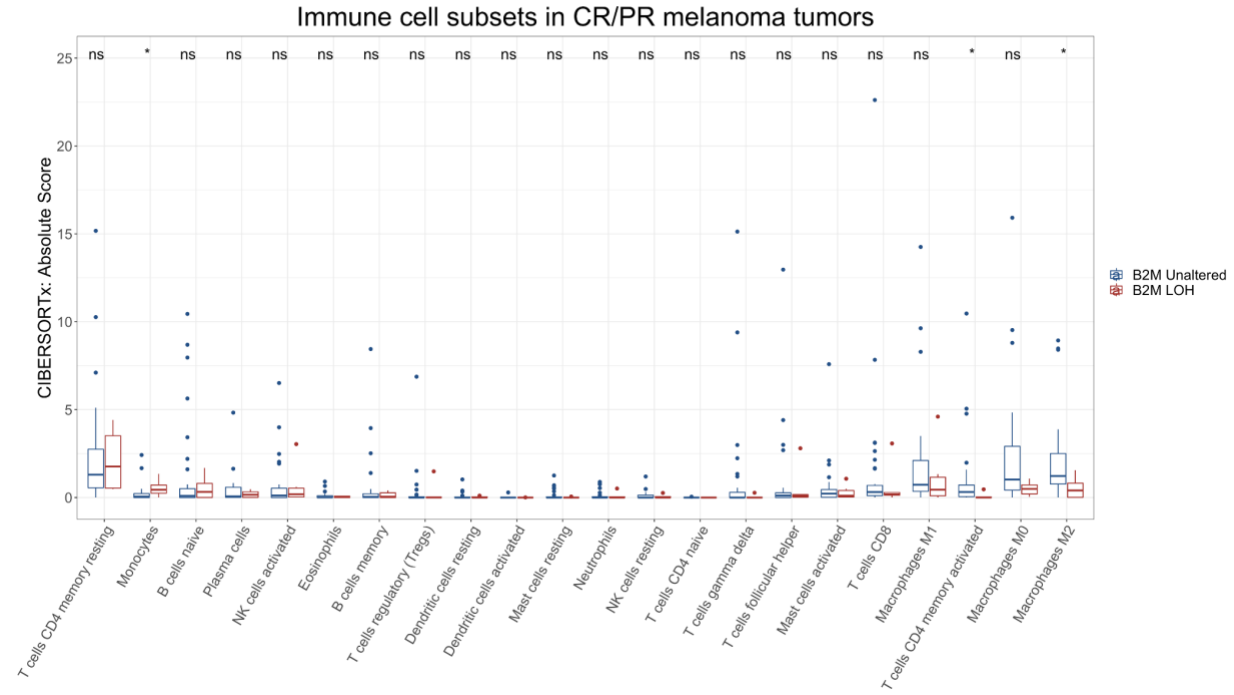

**Supplementary Figure S11: Immune cell subsets in responsive human melanoma tumors.** CIBERSORTx immune cell deconvolution analysis using bulk RNAseq data showing (A) fraction and (B) absolute scores of immune cell types in responsive (CR/PR) *B2M* unaltered (n=35) versus *B2M* LOH (n=6) tumors. Cell types are sorted by greatest difference in median score between groups; Wilcoxon test, ns= not significant, * $p<0.05$.

**Supplementary Table Index**

**References**


1. Tumeh PC, Harview CL, Yearley JH, Shintaku IP, Taylor EJ, Robert L*, et al.* PD-1 blockade induces responses by inhibiting adaptive immune resistance. Nature 2014;515(7528):568-71 doi 10.1038/nature13954.
2. Ribas A, Wolchok JD. Cancer immunotherapy using checkpoint blockade. Science 2018;359(6382):1350-5 doi 10.1126/science.aar4060.
3. Ploegh HL, Orr HT, Strominger JL. Major histocompatibility antigens: the human (HLA-A, -B, -C) and murine (H-2K, H-2D) class I molecules. Cell 1981;24(2):287-99 doi 10.1016/0092-8674(81)90318-4.
4. D'Urso CM, Wang ZG, Cao Y, Tatake R, Zeff RA, Ferrone S. Lack of HLA class I antigen expression by cultured melanoma cells FO-1 due to a defect in B2m gene expression. J Clin Invest 1991;87(1):284-92.
5. Restifo NP, Marincola FM, Kawakami Y, Taubenberger J, Yannelli JR, Rosenberg SA. Loss of functional beta 2-microglobulin in metastatic melanomas from five patients receiving immunotherapy. J Natl Cancer Inst 1996;88(2):100-8.
6. Zaretsky JM, Garcia-Diaz A, Shin DS, Escuin-Ordinas H, Hugo W, Hu-Lieskovan S*, et al.* Mutations Associated with Acquired Resistance to PD-1 Blockade in Melanoma. N Engl J Med 2016;375(9):819-29 doi 10.1056/NEJMoa1604958.
7. Sade-Feldman M, Jiao YJ, Chen JH, Rooney MS, Barzily-Rokni M, Eliane JP*, et al.* Resistance to checkpoint blockade therapy through inactivation of antigen presentation. Nat Commun 2017;8(1):1136 doi 10.1038/s41467-017-01062-w.
8. Gettinger S, Choi J, Hastings K, Truini A, Datar I, Sowell R*, et al.* Impaired HLA Class I Antigen Processing and Presentation as a Mechanism of Acquired Resistance to Immune Checkpoint Inhibitors in Lung Cancer. Cancer Discov 2017 doi 10.1158/2159-8290.CD-17-0593.

9. Riaz N, Havel JJ, Makarov V, Desrichard A, Urba WJ, Sims JS*, et al.* Tumor and Microenvironment Evolution during Immunotherapy with Nivolumab. Cell 2017;171(4):934-49 e16 doi 10.1016/j.cell.2017.09.028.

10. Benci JL, Johnson LR, Choa R, Xu Y, Qiu J, Zhou Z*, et al.* Opposing Functions of Interferon Coordinate Adaptive and Innate Immune Responses to Cancer Immune Checkpoint Blockade. Cell 2019;178(4):933-48 e14 doi 10.1016/j.cell.2019.07.019.

11. Grasso CS, Giannakis M, Wells DK, Hamada T, Mu XJ, Quist M*, et al.* Genetic Mechanisms of Immune Evasion in Colorectal Cancer. Cancer Discov 2018;8(6):730-49 doi 10.1158/2159-8290.CD-17-1327.

12. Keenan TE, Burke KP, Van Allen EM. Genomic correlates of response to immune checkpoint blockade. Nat Med 2019;25(3):389-402 doi 10.1038/s41591-019-0382-x.

13. Germano G, Lu S, Rospo G, Lamba S, Rousseau B, Fanelli S*, et al.* CD4 T Cell-Dependent Rejection of Beta-2 Microglobulin Null Mismatch Repair-Deficient Tumors. Cancer Discov 2021;11(7):1844-59 doi 10.1158/2159-8290.CD-20-0987.

14. Middha S, Yaeger R, Shia J, Stadler ZK, King S, Guercio S*, et al.* Majority of B2M-Mutant and -Deficient Colorectal Carcinomas Achieve Clinical Benefit From Immune Checkpoint Inhibitor Therapy and Are Microsatellite Instability-High. JCO Precis Oncol 2019;3 doi 10.1200/PO.18.00321.

15. de Vries NL, van de Haar J, Veninga V, Chalabi M, Ijsselsteijn ME, van der Ploeg M*, et al.* gammadelta T cells are effectors of immunotherapy in cancers with HLA class I defects. Nature 2023 doi 10.1038/s41586-022-05593-1.

16. Torrejon DY, Abril-Rodriguez G, Champhekar AS, Tsoi J, Campbell KM, Kalbasi A*, et al.* Overcoming genetically-based resistance mechanisms to PD-1 blockade. Cancer Discov 2020;(epub):May 28: CD-19-1409. doi: 10.158/2159-8290.

17. Homet Moreno B, Zaretsky JM, Garcia-Diaz A, Tsoi J, Parisi G, Robert L*, et al.* Response to Programmed Cell Death-1 Blockade in a Murine Melanoma Syngeneic Model Requires

Costimulation, CD4, and CD8 T Cells. Cancer immunology research 2016;4(10):845-57 doi 10.1158/2326-6066.CIR-16-0060.

18. Ran FA, Hsu PD, Wright J, Agarwala V, Scott DA, Zhang F. Genome engineering using the CRISPR-Cas9 system. Nat Protoc 2013;8(11):2281-308 doi 10.1038/nprot.2013.143.
19. Brinkman EK, Chen T, Amendola M, van Steensel B. Easy quantitative assessment of genome editing by sequence trace decomposition. Nucleic Acids Res 2014;42(22):e168 doi 10.1093/nar/gku936.
20. Charych DH, Hoch U, Langowski JL, Lee SR, Addepalli MK, Kirk PB*, et al.* NKTR-214, an Engineered Cytokine with Biased IL2 Receptor Binding, Increased Tumor Exposure, and Marked Efficacy in Mouse Tumor Models. Clin Cancer Res 2016;22(3):680-90 doi 10.1158/1078-0432.CCR-15-1631.
21. Campbell KM, Amouzgar M, Pfeiffer SM, Howes TR, Medina E, Travers M*, et al.* Prior anti-CTLA-4 therapy impacts molecular characteristics associated with anti-PD-1 response in advanced melanoma. Cancer Cell 2023;41(4):791-806 e4 doi 10.1016/j.ccell.2023.03.010.
22. Favero F, Joshi T, Marquard AM, Birkbak NJ, Krzystanek M, Li Q*, et al.* Sequenza: allele-specific copy number and mutation profiles from tumor sequencing data. Ann Oncol 2015;26(1):64-70 doi 10.1093/annonc/mdu479.
23. Zhang Y, Parmigiani G, Johnson WE. ComBat-seq: batch effect adjustment for RNA-seq count data. NAR Genom Bioinform 2020;2(3):lqaa078 doi 10.1093/nargab/lqaa078.
24. Liu D, Schilling B, Liu D, Sucker A, Livingstone E, Jerby-Amon L*, et al.* Integrative molecular and clinical modeling of clinical outcomes to PD1 blockade in patients with metastatic melanoma. Nat Med 2019;25(12):1916-27 doi 10.1038/s41591-019-0654-5.
25. Weber JS, Gibney G, Sullivan RJ, Sosman JA, Slingluff CL, Jr., Lawrence DP*, et al.* Sequential administration of nivolumab and ipilimumab with a planned switch in patients

with advanced melanoma (CheckMate 064): an open-label, randomised, phase 2 trial. Lancet Oncol 2016;17(7):943-55 doi 10.1016/S1470-2045(16)30126-7.

26. Wolchok JD, Chiarion-Sileni V, Gonzalez R, Rutkowski P, Grob JJ, Cowey CL*, et al.* Overall Survival with Combined Nivolumab and Ipilimumab in Advanced Melanoma. N Engl J Med 2017;377(14):1345-56 doi 10.1056/NEJMoa1709684.

27. Schwartz LH, Litiere S, de Vries E, Ford R, Gwyther S, Mandrekar S*, et al.* RECIST 1.1-Update and clarification: From the RECIST committee. Eur J Cancer 2016;62:132-7 doi 10.1016/j.ejca.2016.03.081.

28. Chen B, Khodadoust MS, Liu CL, Newman AM, Alizadeh AA. Profiling Tumor Infiltrating Immune Cells with CIBERSORT. Methods Mol Biol 2018;1711:243-59 doi 10.1007/978-1-4939-7493-1_12.

29. Newman AM, Liu CL, Green MR, Gentles AJ, Feng W, Xu Y*, et al.* Robust enumeration of cell subsets from tissue expression profiles. Nat Methods 2015;12(5):453-7 doi 10.1038/nmeth.3337.

30. Newman AM, Steen CB, Liu CL, Gentles AJ, Chaudhuri AA, Scherer F*, et al.* Determining cell type abundance and expression from bulk tissues with digital cytometry. Nat Biotechnol 2019;37(7):773-82 doi 10.1038/s41587-019-0114-2.

31. Garcia-Diaz A, Shin DS, Moreno BH, Saco J, Escuin-Ordinas H, Rodriguez GA*, et al.* Interferon Receptor Signaling Pathways Regulating PD-L1 and PD-L2 Expression. Cell reports 2017;19(6):1189-201 doi 10.1016/j.celrep.2017.04.031.

32. Sanchez-Paulete AR, Cueto FJ, Martinez-Lopez M, Labiano S, Morales-Kastresana A, Rodriguez-Ruiz ME*, et al.* Cancer Immunotherapy with Immunomodulatory Anti-CD137 and Anti-PD-1 Monoclonal Antibodies Requires BATF3-Dependent Dendritic Cells. Cancer Discov 2016;6(1):71-9 doi 10.1158/2159-8290.CD-15-0510.

33. Seliger B, Wollscheid U, Momburg F, Blankenstein T, Huber C. Characterization of the major histocompatibility complex class I deficiencies in B16 melanoma cells. Cancer Res 2001;61(3):1095-9.

34. Ji S, Lee J, Lee ES, Kim DH, Sin JI. B16 melanoma control by anti-PD-L1 requires CD8+ T cells and NK cells: application of anti-PD-L1 Abs and Trp2 peptide vaccines. Hum Vaccin Immunother 2021;17(7):1910-22 doi 10.1080/21645515.2020.1866951.

35. Grewal IS, Foellmer HG, Grewal KD, Xu J, Hardardottir F, Baron JL*, et al.* Requirement for CD40 ligand in costimulation induction, T cell activation, and experimental allergic encephalomyelitis. Science 1996;273(5283):1864-7.

36. Schoenberger SP, Toes RE, van der Voort EI, Offringa R, Melief CJ. T-cell help for cytotoxic T lymphocytes is mediated by CD40-CD40L interactions [see comments]. Nature 1998;393(6684):480-3.

37. Meeth K, Wang JX, Micevic G, Damsky W, Bosenberg MW. The YUMM lines: a series of congenic mouse melanoma cell lines with defined genetic alterations. Pigment Cell Melanoma Res 2016;29(5):590-7 doi 10.1111/pcmr.12498.

38. Wang J, Perry CJ, Meeth K, Thakral D, Damsky W, Micevic G*, et al.* UV-induced somatic mutations elicit a functional T cell response in the YUMMER1.7 mouse melanoma model. Pigment Cell Melanoma Res 2017;30(4):428-35 doi 10.1111/pcmr.12591.

39. Wolf Y, Bartok O, Patkar S, Eli GB, Cohen S, Litchfield K*, et al.* UVB-Induced Tumor Heterogeneity Diminishes Immune Response in Melanoma. Cell 2019;179(1):219-35 e21 doi 10.1016/j.cell.2019.08.032.

40. Karre K. NK cells, MHC class I molecules and the missing self. Scand J Immunol 2002;55(3):221-8.

41. Janeway CA, Jr., Bottomly K. Signals and signs for lymphocyte responses. Cell 1994;76(2):275-85.

42. Selby MJ, Engelhardt JJ, Johnston RJ, Lu LS, Han M, Thudium K*, et al.* Preclinical Development of Ipilimumab and Nivolumab Combination Immunotherapy: Mouse Tumor Models, In Vitro Functional Studies, and Cynomolgus Macaque Toxicology. PLoS One 2016;11(9):e0161779 doi 10.1371/journal.pone.0161779.

43. Ueha S, Yokochi S, Ishiwata Y, Ogiwara H, Chand K, Nakajima T*, et al.* Robust Antitumor Effects of Combined Anti-CD4-Depleting Antibody and Anti-PD-1/PD-L1 Immune Checkpoint Antibody Treatment in Mice. Cancer Immunol Res 2015;3(6):631-40 doi 10.1158/2326-6066.CIR-14-0190.

44. Freeman AJ, Vervoort SJ, Ramsbottom KM, Kelly MJ, Michie J, Pijpers L*, et al.* Natural Killer Cells Suppress T Cell-Associated Tumor Immune Evasion. Cell reports 2019;28(11):2784-94 e5 doi 10.1016/j.celrep.2019.08.017.

45. Zhao Y, Cao Y, Chen Y, Wu L, Hang H, Jiang C*, et al.* B2M gene expression shapes the immune landscape of lung adenocarcinoma and determines the response to immunotherapy. Immunology 2021;164(3):507-23 doi 10.1111/imm.13384.

46. Barkal AA, Weiskopf K, Kao KS, Gordon SR, Rosental B, Yiu YY*, et al.* Engagement of MHC class I by the inhibitory receptor LILRB1 suppresses macrophages and is a target of cancer immunotherapy. Nat Immunol 2018;19(1):76-84 doi 10.1038/s41590-017-0004-z.

47. Kamphorst AO, Wieland A, Nasti T, Yang S, Zhang R, Barber DL*, et al.* Rescue of exhausted CD8 T cells by PD-1-targeted therapies is CD28-dependent. Science 2017;355(6332):1423-7 doi 10.1126/science.aaf0683.

48. Hui E, Cheung J, Zhu J, Su X, Taylor MJ, Wallweber HA*, et al.* T cell costimulatory receptor CD28 is a primary target for PD-1-mediated inhibition. Science 2017;355(6332):1428-33 doi 10.1126/science.aaf1292.

# Chapter 3:

# Role of altered MHC class I antigen presentation machinery in response and resistance to immune checkpoint blockade in melanoma

**Abstract**

Response to cancer immunotherapies depends on effective recognition and eradication of tumor cells by the immune system. This is largely mediated by the successful presentation of tumor-specific antigens by major histocompatibility complex (MHC) class I molecules on the surface of tumor cells. The impact of defects in components regulating (*NLRC5)* and composing (*B2M*) the MHC class I antigen processing and presentation machinery require more extensive characterization. We analyzed whole-exome sequencing and bulk RNA-sequencing data from a harmonized clinical dataset of baseline tumor biopsies derived from patients with advanced melanoma treated with immune checkpoint blockade, and from a panel of patient-derived melanoma cell lines, to identify somatic alterations in genes involved in MHC class I antigen presentation and to evaluate correlative clinical outcomes and transcriptomic profiles. We report that the functionally similar transcriptional activators of antigen presentation, *NLRC5* and *CIITA,* had mutations that were mutually exclusive from one another. Furthermore, melanomas with *NLRC5* non-silent mutations within the NACHT domain had lower transcript levels of MHC class I pathway genes and were associated with progressive disease. Among the human melanoma cell lines, we demonstrate that interferon (IFN)-γ exposure led to increased expression of MHC class I pathway genes, even in lines with *NLRC5* non-silent mutations. Among this cohort, we also report that tumors with *B2M* loss of heterozygosity (LOH) had higher expression of *HLA-G*, an NK cell inhibitory ligand, which correlated with increased numbers of activated NK cells and progressive disease. We propose that among tumors with diminished MHC class I expression through *NLRC5* mutations, *CIITA* or IFN-γ could be utilized to restore surface MHC class I expression. Additionally, we postulate that *HLA-G* could be impeding NK cell function among *B2M*-dysregulated tumors. Thus, we also propose that targeting HLA-G could modulate NK cell-tumor interactions to restore a stunted anti-tumor immune response in tumors with MHC class I deficiency.

## Introduction

Dysregulated major histocompatibility complex (MHC) class I antigen presentation has been reported as a common mechanism of tumor primary and acquired resistance to immune checkpoint blockade (ICB) therapies (1,2). The MHC class I molecules present on the surface of tumor cells are responsible for presenting endogenous antigen to cytotoxic CD8+ T cells, thereby making cancer cells “visible” for an anti-tumor immune response (2,5). In their absence, tumor cells go unrecognized and escape immune-mediated elimination (2-5). The MHC class I complex is composed of intracellular antigenic peptides, a light chain encoded by the *β-2-microglobulin (B2M)* gene, and a heavy chain encoded by the human leukocyte antigen (HLA) genes *HLA-A, HLA-B,* and *HLA-C* (2). MHC class I antigen presentation relies on the successful processing, loading, and presentation of antigens on MHC class I molecules (6). This involves the concerted action of several molecules, including immunoproteasome components, peptide transporters, and peptide chaperones (3,6). In addition, this process also relies on components that activate and control the transcription of MHC class I genes, such as the interferon (IFN)-γ signaling pathway and NOD-like receptor family CARD domain containing 5 (NLRC5), the master transcriptional regular of MHC class I genes (2,6,7). Any alteration in the MHC class I antigen processing machinery (APM), and components regulating it, that leads to lost or diminished MHC class I expression can result in tumor immune escape (2-5). The most commonly implicated and studied alterations associated with ICB resistance have been mutations or deletions in the *HLA, B2M,* and *TAP1/2* genes (1,2,5). Nonetheless, there are reported cases of patients with defective MHC class I antigen presentation, including *B2M* loss, that can still respond to ICB therapy independently of the MHC class I: CD8+ T cells axis, but the exact mechanism remains unknown (2,8-10). Hence, it is critical to wholistically characterize MHC class I antigen presentation defects in the context of ICB therapy resistance and to further explore the role of other immune cells in mediating response in MHC class I-defective tumors.

In melanoma, although *B2M* loss-of-function alterations have been associated with worst outcomes during anti-programmed cell death-1 (PD-1) therapy, there are patients who respond to treatment (9,11-13). This has been similarly observed in patients with non-small cell lung cancer (NSCLC), Hodgkin lymphoma, and mismatch repair-deficient (MMR-d) colorectal cancer (2,9,10). Work analyzing biopsy samples of patients with MMR-d *B2M* low tumors that still responded to ICB found increased CD4+ T cell and γδ T cell infiltration (10,14). Similarly, our work in *B2M*-null mouse tumor models found that activated CD4+ T cells and natural killer (NK cells) could overcome anti-PD-1 resistance (8). We previously reported that in pre-treatment melanoma biopsies with *B2M* loss of heterozygosity (LOH), there were higher amounts of activated NK cells (Chapter 2: Anti-tumor immune responses in *B2M* deficient cancers). Additionally, when comparing *B2M*-LOH biopsies from patients that responded to ICB therapy, we found higher numbers of activated NK cells in responsive *B2M*-LOH samples compared to responsive *B2M*-unaltered samples (Chapter 2: Anti-tumor immune responses in *B2M* deficient cancers). In this work, we further explored this clinical dataset (15) by analyzing the sequencing data to characterize somatic alterations in MHC class I structural and regulatory genes and to more extensively compare *B2M*-altered versus unaltered tumors. To corroborate our findings in this melanoma cohort, we also analyzed sequencing data from human melanoma cell lines. Our goal is to offer alternative therapeutic targets and strategies for the treatment of tumors with MHC class I-mediated ICB resistance.

## Results

### Top mutated MHC class I pathway genes in melanoma biopsies

Mutations in MHC class I and class I-related genes are often implicated in immune escape and resistance to ICB therapies (1-5). Therefore, to identify the most commonly mutated genes involved in MHC class I antigen processing, presentation, and regulation (*NLRC5*, IFN-γ signaling), we analyzed the somatic variants of baseline biopsies of patients with advanced melanoma who received ICB therapies (n=242) (**Supplementary Table S1**). Our group has previously harmonized this clinical dataset for somatic variant detection and gene expression profiling (15). Somatic variants were determined by comparing pre-treatment tumor whole-exome sequencing (WES) to patient-matched normal WES. Among the cohort, 64% of patients (n=155/242) had tumors with non-silent mutations in the MHC class I genes corresponding to elements involved in antigen processing and presentation and IFN-γ signaling (n=164 genes) (**Figure 1**). The top mutated genes were: *NCAM1* (9.9%, n=24/242), *NLRC5* (8.7% n=21/242), *CIITA* (8.3% n=20/242), *VCAM1* (5.4%, n=13/242), and *TRIM48* (5.4%, n=13/242) (**Figure 1**). *NCAM1, VCAM1,* and *TRIM48* were derived from the IFN-γ list (Reactome), *NLRC5* was added onto the list, and *CIITA* came from the antigen processing and presentation list (KEGG). Interestingly, we did not find any non-silent mutations in the structural genes, *HLA-A, HLA-B, HLA-C,* and *B2M*. However, the second and third most recurrently mutated genes were *NLRC5* and *CIITA*, the master transcriptional activators of MHC class I and class II gene expression, respectively (6). *NLRC5* only had missense variants, while *CIITA* had two stop gain variants and 18 missense variants (**Figure 1**).

***NLRC5* and *CIITA* mutations are mutually exclusive and non-silent mutations cluster within the NACHT domain coding region**

Both NLRC5 and CIITA can regulate class I gene expression, particularly in the context of IFN-γ exposure (5,16-18). Although studies have been limited, it has been shown that CIITA activation can control MHC class I gene transcription and induce MHC class I surface expression (17,18). NLRC5 and CIITA are NOD-like receptors (NLRs) that share a similar function and structure (19-21). Both contain C-terminus leucine-rich repeats (LRRs) and a central NACHT domain, also called the nucleotide-binding domain, which is required for oligomerization, activation, and nucleotide binding (19-21). Thus, we next wanted to determine whether *NLRC5* and *CIITA* mutations co-occur within the same sample and to evaluate where the mutations localize within the chromosomal domains. We found that for non-silent mutations, there is a trend toward mutual exclusivity within the tumor samples (p=0.08) (**Table 1**). Of the samples analyzed, four contained mutations in both *NLRC5* and *CIITA*, 17 only had mutations in *NLRC5*, 16 only had mutations in *CIITA*, and 205 samples were wildtype for both genes (**Table 1**). When looking at all mutations, both silent and non-silent, we found a significant trend toward mutual exclusivity (p=0.00004), with 26 samples having both genes mutated, 34 only having *NLRC5* mutations, 30 only having *CIITA* mutations, and 152 samples not having any mutations in these genes (**Table 2**).

Next, we mapped the mutations to the chromosomal region. For *NLRC5*, there were 60 tumor samples containing mutations, 21 with non-silent variants and 39 with silent variants (**Figure 2A**). For *CIITA*, there were 56 tumors with mutations, 20 with non-silent variants and 36 with silent variants (**Figure 2B).** Non-silent mutations for both *NLRC5* and *CIITA* clustered within the NACHT domain coding region, whereas the silent mutations were more spread out through the chromosomal position (**Figure 2C** and **Figure 2D**). Notably, for *CIITA* both silent and non-silent mutations occurred closer to the NACHT domain coding region, unlike the *NLRC5* mutations which occurred largely throughout most of the region (**Figure 2C** and **Figure 2D**).

### *NLRC5* non-silent mutant tumors have lower median expression of *NLRC5* and MHC class I transcripts

Due to its central role in modulating MHC class I gene transcription, for subsequent analyses we explored the role of *NLRC5* mutational status in the context of gene expression levels. First, we compared the relative expression levels of *NLRC5* in *NLRC5* non-silent versus silent mutants and wildtype tumors using the normalized gene expression data (RNAseq n=178). Among *NLRC5* mutant tumors, non-silent mutant tumors (n=11) had the lowest median expression of *NLRC5,* with silent mutant tumors (n=37) and wildtype tumors (n=130) having comparable median *NLRC5* expression (p=0.6) (**Supplementary Figure S1A**). For the ensuing studies, we split the tumors as *NLRC5* mutant, corresponding to non-silent mutants, and *NLRC5* wildtype, referring to tumors with silent mutations or no mutations. *NLRC5* mutant samples (n=11) demonstrated lower median expression compared to wildtype samples (n=167) (p=0.44) (**Supplementary Figure S1B**).

Next, we wanted to determine whether the *NLRC5* non-silent mutations were associated with lower target gene expression. We assessed the relative expression levels of MHC class I genes that are regulated by NLRC5 (*HLA-A, HLA-B, HLA-C, B2M, LMP2/PSMB9, LMP7/PSMB8, TAP1*) and of a non-NLRC5-regulated MHC class I gene (*ERAP1*) (22). For all genes analyzed, *NLRC5* mutant tumors had a trend toward lower median expression compared to wildtype: *HLA-A* (p=0.27), *HLA-B* (p=0.11), *HLA-C* (p=0.26), *B2M* (p=0.23), *LMP2/PSMB9* (p=0.07), *LMP7/PSMB8* (p=0.095), and *TAP1* (p=0.62) (**Figure 3**). In contrast, for *ERAP1* (p=0.35), the gene that is not regulated by *NLRC5,* the median expression level was comparable between both groups (**Figure 3**).

### *NLRC5* non-silent, progressive mutant tumors have the lowest transcript expression for *NLRC5* and *B2M*

In order to determine if there were any differences based on clinical group, we similarly compared the relative expression levels of MHC class I genes among mutant and wildtype tumors split based on best overall clinical response to therapy as determined by the RECIST v1.1 criteria (23). First, we compared expression for *NLRC5* and found that among mutant samples, tumors that were derived from patients with progressive disease had lower median expression of *NLRC5* (p=0.36) (**Figure 4A**). This trend was also apparent with *HLA-B* (p=0.72) and *B2M* (p=0.02), with it being more notable in *B2M* transcript expression (**Supplementary Figure S2B** and **Figure 4B**). *HLA-A* (p=0.58)*, HLA-C* (p=0.72), *PSMB9* (p=1), and *ERAP1* (p=0.86) had similar expression levels between responsive and non-responsive mutant tumors (**Supplementary Figure S2**). On the other hand, *TAP1* (p=0.72) and *PSMB8* (p=0.47) progressive, mutant tumors had higher expression of their targets compared to responsive, mutant tumors (**Supplementary Figure S2).** Among the *NLRC5* wildtype tumors, responsive samples had higher median expression compared to progressive samples for all the genes, except *PSMB8, PSMB9,* and *ERAP1*, which had comparable values (**Figure 4** and **Supplementary Figure S2**).

### *NLRC5* non-silent mutations in progressive tumors largely localize to the NACHT domain

Due to the observable clinical difference in *NLRC5* and *B2M* median expression among mutant *NLRC5* tumors (n=21), we next sought to identify where the non-silent mutations localize among the protein position and whether there is a difference based on clinical response state. Notably, among progressive tumors with *NLRC5* non-silent mutations, most of the mutations clustered within the NACHT domain (**Figure 4C**). The frequency of NACHT domain non-silent mutations in progressive tumors was much higher when compared to responsive tumors (p=0.056) (**Table 3**), occurring at a frequency of 71% in progressive samples versus 23% in responsive samples (**Figure 4D** and **Table 3**).

**Melanoma cell lines with *NLRC5* non-silent mutations have lower expression of *NLRC5***

To corroborate the findings from the patient biopsies and to assess the effects of mutational status on intrinsic gene expression, we studied the impact of *NLRC5* non-silent mutations in characterized patient-derived human melanoma cell lines (24) (**Supplementary Table S2**). First, we analyzed the WES data (n=54) for MHC class I pathway mutations as described above and found that all cell lines in the panel had non-silent mutations in MHC class I pathway genes (**Supplementary Figure S3**). The top mutated genes were: *GBP4* (76%, n=41/54), *CTSB* (72%, n=39/54), *TRIM5* (68.5%, n=37/54), *PML* (68.5%, n=37/54), and *NLRC5* (68.5%, n=37/54), with *TRIM5, PML,* and *NLRC5* all sharing the same mutation frequency (**Supplementary Figure S3**). Thus, *NLRC5* was the third most recurrently mutated gene and it only had missense non-silent variants. When taking into account silent and non-silent mutations, 96% of the cell lines had mutations in *NLRC5* (n=52/54) (**Supplementary Figure S4A**).

Next, we compared the relative expression levels of *NLRC5* in *NLRC5* non-silent mutant (n=22), silent mutant (n=8), and wildtype (n=2) cell lines using the raw count gene expression data (RNAseq n=32). Non-silent mutant cells had the lowest median expression of *NLRC5,* followed by cells with silent mutations, and wildtype cells had the highest median expression of *NLRC5* (p=0.54) (**Supplementary Figure S4B**). Notably, the median expression for silent mutants and wildtype samples was fairly similar. Hence, for the next set of analyses, samples with silent mutations were aggregated with the wildtype samples. When comparing mutant to wildtype samples, *NLRC5* mutant cell lines (n=22) had lower median expression of *NLRC5* than wildtype cell lines (n=10) (p=0.28) (**Supplementary Figure S4C**).

**IFN-γ exposure in melanoma cell lines led to increased expression of MHC class I pathway genes, including *NLRC5, CIITA,* and *B2M,* with greater increases observed in *NLRC5* mutant cell lines**

Exposure to IFN-γ leads to the induction of MHC class I genes (7); thus, we compared the expression levels of NLRC5-regulated MHC class I pathway genes and *CIITA* in cell lines that were either cultured in IFN-γ or vehicle control for six hours (8). We found that exposure to IFN-γ led to a significantly higher transcript expression for *NLRC5* ($p=1.7x10^{-10}$), *CIITA* ($p=2.7x10^{-9}$), *B2M* (p=0.0022), *HLA-B* (p=0.029), *HLA-C* (p=0.0049), *TAP1* ($p=9.2x10^{-10}$), *PSMB8* ($p=1.8x10^{-8}$), *PSMB9* ($p<2.2x10^{-16}$), and the non-NLRC5-regulated gene *ERAP1* (p=0.0017) (**Supplementary Figure S5**). The only gene without a significant difference between both groups was *HLA-A* (p=0.13); however, the median expression value was still higher for IFN-γ-cultured cells compared to cells cultured in vehicle control.

Next, we wanted to compare the effect of culturing with IFN-γ in mutant versus wildtype cell samples. In the *NLRC5* wildtype cell lines, IFN-γ exposure led to a significant increase in the transcript expression for *NLRC5* ($p=1.1x10^{-5}$), *CIITA* (p=0.00049), *TAP1* (p=0.00032), *PSMB8* (p=0.00073), *PSMB9* ($p=1.1x10^{-5}$), and *ERAP1* (p=0.029) (**Figure 5**). For the other genes, *B2M* (p=0.063), *HLA-A* (p=0.17), *HLA-B* (p=0.19), and *HLA-C* (p=0.14), although not statistically significant, the median transcript expression was higher in the IFN-γ-cultured group (**Figure 5**). In the mutant cell lines, IFN-γ exposure led to a significant increase in the transcript expression for *NLRC5* ($p=2.9x10^{-7}$), *CIITA* ($p=1x10^{-6}$), *B2M* (p=0.0085), *HLA-C* (p=0.016), *TAP1* ($p=6.7x10^{-8}$), *PSMB8* ($p=2x10^{6}$), *PSMB9* ($p=2.9x10^{-11}$), and *ERAP1* (p=0.025), with higher median expression for *HLA-A* (p=0.32) and *HLA-B* (p=0.069) (**Figure 5**). Of note, the increase of MHC class I pathway gene expression with IFN-γ was consistently higher and more significant among the cell lines that had *NLRC5* mutations. Interestingly, the effects of IFN-γ exposure were greater among the non-structural MHC class I components and the non-NLRC5-regulated MHC class I

gene, *ERAP1,* with the increase in treated versus untreated groups being less in *ERAP1* compared to the other genes.

### ***B2M*-LOH tumors have reduced expression of genes and gene sets corresponding to adaptive immunity**

The impact of genetic alterations in MHC class I structural and non-structural components may have varying effects on tumors and, therefore, may have different therapeutic implications. Thus far, we have explored the effects of mutations in a regulatory component of the MHC class I pathway. Next, we focused on characterizing the impact of genetic defects in *B2M,* a key MHC class I structural component. This work builds off of our earlier work where we identified a greater frequency of *B2M* loss of heterozygosity (LOH) events in non-responsive melanoma biopsies, which correlated with lower *B2M* expression and a greater infiltration of activated NK cells (Chapter 2: Anti-tumor immune responses in *B2M* deficient cancers). Utilizing the same harmonized clinical dataset (15), we further characterized the pre-treatment melanoma biopsies (n=295) with *B2M*-LOH and unaltered status, comparing biopsies of patients with response or no response to ICB (**Supplementary Figure S6**).

To further elucidate the tumor microenvironmental features of *B2M*-LOH tumors, we performed gene set enrichment analysis (GSEA) and differential gene expression using the batch-effect corrected RNAseq data. GSEA was performed using the 'fgsea' tool in R and gene sets were obtained from the Molecular Signatures Database (MSigDB) (25), with gene set pathways from the Hallmark, KEGG, and Reactome databases. For *B2M*-LOH tumors (n=24), there was higher expression of genes and gene sets associated with the toll-like receptor (TLR) cascade (Reactome) and TLR regulation (Reactome), corresponding to elements of innate immunity (**Figure 6A**). For *B2M*-unaltered tumors (n=71), there was higher expression of genes and gene sets associated with both adaptive and innate immunity, corresponding to cytokine-cytokine

receptor interactions (KEGG), allograft rejection (Hallmark), hematopoietic cell lineage (KEGG), and transforming growth factor (TGF)-β signaling (KEGG) (**Figure 6A**). Differential expression analysis was performed using the 'DESeq2' package in R and run comparing *B2M*-LOH (n=24) versus unaltered tumors (n=71) and controlled for cohort group. There were a total of 188 significantly differentially expressed genes, 59 genes were higher in *B2M*-LOH samples, 71 genes were higher in unaltered samples, and 58 genes were similarly expressed in both groups (**Supplementary Table S3** and **Figure 6B**). The gene with the highest adjusted p-value for *B2M*-unaltered tumors was Long Intergenic Non-Protein Coding RNA 1918 (LINC01918), an RNA gene with currently unknown function (GeneCards) (**Supplementary Table S3** and **Figure 6B**). The gene with the highest adjusted p-value for *B2M*-LOH tumors was *HLA-G,* a non-classical MHC class I molecule with several immunosuppressive functions (26).

### *HLA-G* expression is highest in progressive, *B2M*-LOH tumors and positively correlates with NK cell numbers

Tumors with *B2M* LOH had significantly higher differential expression of *HLA-G*, which is involved in dampening the immune response and inhibiting cytotoxic T cell, NK cell, and B cell function (26-28). Thus, we next wanted to determine whether *HLA-G* expression is higher in biopsies with *B2M* LOH and whether there is an association with non-response and NK cell numbers. Indeed, normalized *HLA-G* expression was significantly higher in *B2M*-LOH samples (n=25) compared to unaltered samples (n=75) (p=0.0035) (**Figure 7A**). Additionally, when considering only non-responsive samples (n=59), tumors with *B2M*-LOH (n=19) had significantly higher expression of *HLA-G* relative to unaltered tumors (n=40) (p=0.012) (**Figure 7B**). This was not observed with responsive samples (n=41), where *B2M*-LOH (n=6) and unaltered tumors (n=35) had similar median *HLA-G* expression (p=0.54) (**Figure 7B**). Next, we analyzed the correlation between *HLA-G* expression and total numbers of activated NK cells, as determined through immune cell deconvolution analysis, between responsive and non-responsive samples. Notably, the only

group that had a positive correlation between increasing *HLA-G* expression and increasing numbers of activated NK cells were the progressive, *B2M*-LOH tumors (p=0.015) (**Figure 7C**). For all other groups, responsive, *B2M*-LOH; progressive, *B2M*-unaltered; and responsive, *B2M*-unaltered, there was no discernable trend (**Figure 7C**).

***HLA-G* expression is associated with progressive disease and worse overall survival**

*HLA-G* expression is limited under normal physiological conditions, but it can be expressed on tumors where it is typically associated with worse prognosis (26-28). Thus, we next further explored the role of *HLA-G* in the context of clinical outcomes in these biopsies. Tumors were split based on their expression level of *HLA-G* as low (lower quartile, n=25), intermediate (second and third quartiles, n=50), or high (higher quartile, n=25). Overall, tumors from patients that eventually progressed (n=59) under therapy had significantly higher *HLA-G* expression compared to those that responded (n=41) (p=0.031) (**Supplementary Figure S7A).** Additionally, high *HLA-G* expression was found most often in progressive samples (n=20) compared to responsive samples (n=5) (p=0.0186) (**Table 4**), occurring at a frequency of 65% in non-responders versus 26% in responders (**Supplementary Figure S7B**). Furthermore, high *HLA-G* expression was also associated with worse overall survival when compared to intermediate or low *HLA-G* expression (p<0.001) (**Supplementary Figure S7C**). These results point toward increased *HLA-G* expression in melanoma being associated with worse clinical features.

## Discussion

Among several cancers, loss or dysregulation of the MHC class I antigen processing and presentation machinery continues to be a source of both primary and acquired resistance to ICB therapies (1,2). Although less studied for their role in the MHC class I pathway, *NLRC5* and components of the IFN-γ signaling pathway play a critical part in controlling the expression of surface MHC class I molecules. *NLRC5* activation leads to the induction of MHC class I genes (5,6). Similarly, tumor cell exposure to IFN-γ promotes upregulation of several MHC class I pathway genes (2,7,22). In this work, we focused primarily on the regulatory components and *B2M,* a key structural element of the MHC class I complex. By interrogating the impact of defects in regulatory and structural processes, we have identified potential prognostic markers and gained a greater insight into potential alternative routes for the treatment of MHC class I-defective tumors.

We have characterized genetic alterations in MHC class I pathway genes in pre-treatment biopsies derived from patients with advanced melanoma who were treated with ICB therapies. Furthermore, we interrogated the transcriptomic profiles and other tumor-associated features of MHC class I-altered versus unaltered tumors. First, we demonstrated that among our samples, *NLRC5* and *CIITA*, were among the top mutated genes of the MHC class I pathway. Additionally, it was observed that these mutations trended toward being mutually exclusive from one another when taking into account non-silent mutations and all mutations (silent and non-silent). It was interesting to note that the most recurrently mutated genes included two transcriptional regulators of antigen presentation, *NLRC5,* the master transcriptional activator of MHC class I genes, and *CIITA,* the master transcriptional activator of class II genes that can also regulate class I gene transcription (6,16-18). This was similarly noted in the melanoma cell line panel where *NLRC5* was among the top three mutated genes and *CIITA* was among the top ten mutated genes. This

observation further highlights their critical role in tumor-immune interactions. We also found that the majority of non-silent mutations clustered within the NACHT domain coding region for both genes. Furthermore, tumors with *NLRC5* non-silent mutations had lower median expression of *NLRC5* and NLRC5-regulated MHC class I genes. Additionally, when looking exclusively at *NLRC5* mutant tumors, those with progressive disease status presented with lower transcript expression and often had mutations that led to amino acid changes within the NACHT domain. These results indicate that non-silent mutations in *NLRC5,* particularly those occurring within the NACHT domain, are associated with lower transcript levels and worse clinical features. This has clinical implications as *NLRC5*-NACHT domain mutations can be used prognostically to predict outcomes under ICB therapies.

From a therapeutic standpoint, we have identified two key things, one being that *NLRC5* and *CIITA* mutations do not appear to co-occur within the same sample and that IFN-γ can modulate MHC class I gene expression even among *NLRC5* mutant tumors. The exclusivity of *NLRC5* and *CIITA* mutations opens avenues for potentially leveraging *CIITA* to induce MHC class I expression in tumors with *NLRC5* mutations or *NLRC5* loss. To date, studies demonstrating CIITA induction of class I genes have been limited and have largely been restricted to animal models (17,18). We have shown that in human melanoma cell lines, IFN-γ exposure led to over a thousand-fold increase in *CIITA* transcript levels from a baseline of nearly zero. Thus, suggesting that among patient samples, *CIITA* can be activated to promote expression of antigen presentation genes. However, additional studies are required to verify this and to identify factors other than IFN-γ that can be used promote *CIITA* activation. Similarly, among the cell lines, we also demonstrated that IFN-γ exposure led to greater expression of MHC class I genes, particularly among the *NLRC5* mutant samples. This suggests that strong external signals activating *NLRC5* may be able to bypass the overwhelming majority of dysfunctional proteins and induce additional surface MHC

class I expression even in the setting of genetic alterations. Similarly, these findings merit further experimental validation. Nonetheless, this offers a viable therapeutic intervention worth exploring given the high frequency of *NLRC5* mutations among tumors.

When further characterizing the effects of the altered structural component, *B2M,* in this same melanoma clinical cohort, we identified that biopsies with *B2M* LOH had lower signatures associated with adaptive immunity compared to *B2M*-unaltered tumors. Furthermore, our previous findings showed that tumors with *B2M* LOH were associated with progressive disease and lower *B2M* expression (Chapter 2: Anti-tumor immune responses in *B2M* deficient cancers). These findings are similar to what has been previously found in the literature and with what is expected in tumors with a compromised MHC class I antigen presentation pathway, and thus, a compromised CD8+ T-cell anti-tumor response (5,11,13). We also previously reported that these tumors had higher amounts of activated NK cells (Chapter 2: Anti-tumor immune responses in *B2M* deficient cancers), which are not restricted by MHC class I and can therefore target tumors that lack surface MHC class I expression (29,30). Interestingly, we have now demonstrated that these *B2M*-LOH samples also have greater expression of *HLA-G,* an immunosuppressive non-classical MHC class I molecule capable of inhibiting NK cell function (26-28). Additionally, we found that among these tumors, there was a positive correlation between increasing *HLA-G* expression and increasing numbers of activated NK cells. Hence, based on our findings, we postulate that with a decrease or loss of *B2M* expression, through LOH or another mechanism, NK cells become the main mediators of tumor eradication. However, with increased selective pressure, there may be a compensatory increase in tumor *HLA-G* expression to curb NK cell cytotoxic activity, thereby allowing for continued tumor immune escape in the context of ICB therapies. Another noteworthy observation among these samples was that high *HLA-G*

expression, independent of *B2M* status, strongly correlated with progressive disease and lower overall survival.

In this cohort, we have identified a critical role of *HLA-G* with regard to *B2M*-dysfunction and independently thereof. Physiological *HLA-G* expression is typically limited to pregnancy in the context of maternal-fetal tolerance (26,27). However, it is often expressed among several cancers, including melanoma, breast cancer, and glioblastoma, where it is associated with increased aggressiveness, immune evasion, and metastasis (27,28). Although *HLA-G* blockade is considered a possible viable therapeutic target, due to a low potential for adverse effects given its physiological expression profile, more needs to be unraveled regarding the exact mechanism by which HLA-G inhibits immune cell activity (26-28). Our findings suggest that HLA-G may be implicated in modulating tumor-NK cell interactions, particularly in the context of *B2M* deficiency. This notion is supported by a study that found that in HER-2 positive breast cancer, HLA-G interactions with KIR2DL4 on NK cells mediated resistance to trastuzumab (31). Similar to other reports, among this melanoma cohort, we found that higher *HLA-G* expression was associated with worse clinical features (27,28). Therefore, we propose that *HLA-G* expression in melanoma could be used as a prognostic marker to predict overall outcomes and response to ICB therapies. Furthermore, we propose that targeting *HLA-G* in the context of low B2M/MHC class I expression can offer a therapeutic option for tumors that cannot rely on CD8+ T cells for an effective anti-tumor response. In these situations, once HLA-G is blocked, immune cells that are inhibited by HLA-G, such as NK cells, may then be able to eradicate the tumors.

In this work, we have summarized the key findings regarding genetic alterations in major regulatory and structural components of the MHC class I pathway. We have focused on

observations that have direct clinical and therapeutic implications in order to help identify alternative avenues for the treatment of melanomas with deficient or diminished MHC class I expression. To the best of our knowledge, this work is the first study reporting on the mutual exclusivity of *NLRC5* and *CIITA,* and that begins to explore their parallel role in antigen presentation. This is also the first study to report on the clinical difference between *NLRC5*-NACHT domain and non-NACHT domain mutations. In addition, this is the first report of a potential association between *B2M* status and HLA-G expression. To conclude, tumors with MHC class I defects that are no longer targetable via CD8+ T cells require alternate therapeutic interventions. In the scenario of altered regulatory components, the redundancy of the MHC class I regulatory pathway can be exploited to restore surface MHC class I expression and thus re-establish a CD8+ T cell anti-tumor immune response. In the context of unrestorable loss of MHC class I expression, such as through aberrations of structural components, other tumor-immune cell interactions must be modulated to restore anti-tumor immunity independent of CD8+ T cells.

## Methods

### Melanoma clinical cohort

A harmonized clinical cohort of biopsies from patients with melanoma treated with ICB-based therapies was used for analysis (15). This dataset contains clinical response outcomes and whole-exome sequencing (WES) and bulk RNA-sequencing (RNAseq) data across seven clinical trials of patients with advanced melanoma who were treated with anti-PD-1 monotherapy, anti-CTLA-4 monotherapy, or combination therapy (15). The clinical dataset has been harmonized across all cohorts for somatic variant detection and gene expression profiling. The clinical information is described as the best overall response (BOR) per sample following the Response Evaluation Criteria in Solid Tumors (RECIST) v1.1 (23). The categories are as follows: complete response (CR), partial response (PR), stable disease (SD), and progressive disease (PD), with CR/PR referring to patients who responded and PD referring to patients who did not respond to therapy (23). For this study, only clinical trials that had both WES and RNAseq data were included: Liu *et al.* (13), CheckMate 038 (32), CheckMate 064 (33), and CheckMate 067 (34), and any individual sample that lacked WES data was excluded. For the analysis of MHC class I pathway genetic mutations, only pre-treatment tumor samples of cutaneous, mucosal, acral, and unknown origin with greater than 10% tumor purity (Sequenza) (35) and full clinical response annotation were analyzed. For *B2M* genetic alteration analysis, uveal melanoma samples were included and samples with SD designation were excluded for more direct responder versus non-responder comparisons as previously described (Chapter 2: Anti-tumor immune responses in *B2M* deficient cancers).

### MHC class I somatic mutations

WES data of samples with greater than 10% tumor purity (n=242) were analyzed to identify somatic mutations in MHC class I genes in baseline biopsy samples (**Supplementary Table S1**).

Somatic variants were determined by comparing WES data from baseline tumor biopsies to patient-matched normal blood WES (15). Single nucleotide variants (SNVs) and small insertions and deletions (indels) were called with Mutect2, VarScan2, Strelka, and SomaticSniper and were considered true variants if they were called by two of the four variant callers (15). Tumors were considered mutant if they had SNVs and indels with a Variant Effect Predictor (VEP) designation of high or moderate according to Ensembl (https://useast.ensembl.org/info/genome/variation/prediction/predicted_data.html). The MHC class I gene list was generated with the Kyoto Encyclopedia of Genes and Genomes (KEGG) (https://www.genome.jp/kegg/) and Reactome (https://reactome.org/) pathway databases and includes "KEGG Antigen Processing and Presentation" and "Reactome Interferon Gamma Signaling." Additionally, *NLRC5* was also incorporated into the list since it is directly involved in regulating the MHC class I pathway (6), for a total of 164 MHC class I pathway genes.

**Mutant versus wildtype tumors**

Baseline melanoma tumors were considered mutant if they had non-silent mutations, corresponding to: stop gained, stop lost, start lost, frameshift, splice donor, splice acceptor, inframe deletion, inframe insertion, missense, and protein altering variants. Gene expression analysis in mutant versus wildtype tumors was done using the normalized log-CPM file that was batch-effect corrected with ComBat-seq (36). Differences in gene expression between groups were determined and visualized in R by comparing the medians using a Wilcoxon test and were considered significantly different if the p-values were less than 0.05. For variants that led to amino acid changes, mutation location across the chromosome or protein was visualized with lollipop plots that were generated using the 'ggplot2' R package (https://ggplot2.tidyverse.org/). Chromosomal position was determined through the GeneCards (https://www.genecards.org/Guide/GeneCard) human gene database and the Ensembl (http://useast.ensembl.org/Homo_sapiens/Info/Index) human genome browser.

### *B2M* genetic alterations

Using the WES data of tumors with greater than 10% tumor purity, baseline biopsy samples (n=295) were analyzed for *B2M* genetic alterations. Alterations correspond to copy number alterations (CNAs), loss of heterozygosity (LOH) irrespective of copy number status, and mutations in *B2M.* CNAs and LOH were determined using Sequenza (35) and mutations were determined as described above. For analyses, tumors with *B2M* gains and clinical SD designation were excluded in order to have clear responders versus non-responder and *B2M*-altered versus *B2M*-unaltered comparisons (**Supplementary Figure S6**). Gene expression analysis in *B2M*-altered versus unaltered tumors was done using the normalized log-CPM file that was batch-effect corrected with ComBat-seq (36).

### Gene set enrichment analysis

Raw RNAseq data was batch-effect corrected using the 'Limma' package in R (37). Gene set enrichment analysis (GSEA) of differentially expressed genes was done with the R package 'fgsea' (https://bioconductor.org/packages/release/bioc/html/fgsea.html). Gene sets were obtained from the Molecular Signatures Database (MSigDB) (25) and run against Hallmark, KEGG, and Reactome pathways. Gene sets with p-values less than 0.05 and adjusted p-values less than 0.25 were considered statistically significant.

### Differential expression analysis

Differential expression analysis was performed using the 'DESeq2' R package (38) comparing altered versus unaltered tumors and controlled for cohort group. Prior to analysis, the raw RNAseq data was batch-effect corrected using the 'Limma' package in R (37). Genes were considered differentially expressed if they had a log2 fold change greater than 1 or less than -1 and an adjusted p-value of less than 0.05.

**Tumor microenvironment analysis**

Immune cell populations were estimated with CIBERSORTx (https://cibersortx.stanford.edu) (39-41) using the LM22 signature matrix of 22 functionally defined human immune cell types to infer cell fractions and total cell numbers as previously described (Chapter 2: Anti-tumor immune responses in *B2M* deficient cancers). Briefly, each cohort was run separately using the raw FPKM file and analyzed per the recommended parameters. Immune cell population differences between samples were visualized and evaluated in R by comparing the medians using a Wilcoxon test. Differences were considered significant if the p-value was less than 0.05.

**Survival analysis**

Patient samples were divided based on their *HLA-G* expression level into groups of low expression (lower quartile, n=25), intermediate expression (interquartiles, n=50), and high expression (highest quartile, n=25). The clinically annotated file that includes overall survival in days was used to generate a survival curve based on *HLA-G* expression group using the packages 'survival' (https://cran.r-project.org/web/packages/survival/index.html) and 'survminer' (https://cran.r-project.org/web/packages/survminer/index.html) in R.

**Human melanoma cell lines**

The patient-derived human melanoma cell lines have been previously characterized and sequenced for mutational status and transcriptomic changes with IFN-γ exposure (24). Raw and analyzed RNAseq data with and without IFN-γ exposure is available at https://www.ncbi.nlm.nih.gov/geo/query/acc.cgi?acc=GSE154996. The variants file and complete mutational status information is available upon request from the corresponding authors.

**Bioinformatics statistical analysis and visualization**

All statistical analyses were done using R/RStudio (v 2022.07.1+554) (http://www.R-project.org/). The MHC class I genes waterfall plot was generated using the 'GenVisR' Bioconductor package (42). All other plots were generated using the 'ggplot2' R package (https://ggplot2.tidyverse.org/). For mutation mutual exclusivity testing, a Fisher's exact test was performed using the 'rstatix' package and fisher_test function in R. For median group comparisons between two groups, a Wilcoxon test was performed and p-values less than 0.05 were considered statistically significant. For median group comparisons between more than two groups, a Kruskal-Wallis test was performed and p-values less than 0.05 were considered statistically significant.

**Data availability**

The sequencing data for the melanoma clinical cohort are from a previous publication (15). The raw sequencing data are available through the Sequence Read Archive (SRA) accession: PRJNA923698 (https://www.ncbi.nlm.nih.gov/sra). The processed harmonized data, including the annotated somatic variants and gene expression profiling, are available at https://github.com/ParkerICI/MORRISON-1-public. Additional data generated in this study are available within the article, supplementary materials, and are available from the corresponding authors upon request.

**Acknowledgments**

This study was funded in part by the Parker Institute for Cancer Immunotherapy (PICI), NIH grants R35 CA197633 and P01 CA168585, the Ressler Family Fund, and the support from Ken and Donna Schultz, Todd and Donna Jones, Karen and James Witemyre, and Thomas Stutz through the Jonsson Cancer Center Foundation, and Jonathan Isaacson through the Melanoma Research Foundation (to A.R.). M.G. is a pre-doctoral fellow supported by the UCLA Tumor Cell Biology Training Program (USHHS Ruth L. Kirschstein Institutional National Research Service Award) T32 CA009056 and the UCLA Medical Scientist Training Program (MSTP) NIH NIGMS Training Grant T32 GM008042. K.M.C. is supported by the Cancer Research Institute Irvington Postdoctoral Fellowship Program, the V Foundation Gil Nickel Melanoma Research Fellowship, and the Parker Institute for Cancer Immunotherapy and V Foundation Bridge Fellows Program.

**Conflict of interest statement**

K.M.C. has received consulting fees from PACT Pharma, Tango Therapeutics, and Geneoscopy LLC, and is a shareholder in Geneoscopy LLC. A.R. has received honoraria from consulting with Amgen, Bristol-Myers Squibb, Chugai, Jazz, Merck, Novartis, RAPT, is or has been a member of the scientific advisory board and holds stock in Advaxis, Appia, Apricity, Arcus, Compugen, CytomX, Highlight, ImaginAb, ImmPact, ImmuneSensor, Inspirna, Isoplexis, Kite-Gilead, Larkspur, Lutris, MapKure, Merus, PACT, Pluto, RAPT, Synthekine and Tango, has received research funding from Agilent and from Bristol-Myers Squibb through Stand Up to Cancer (SU2C), and patent royalties from Arsenal Bio.

**Figure 1**

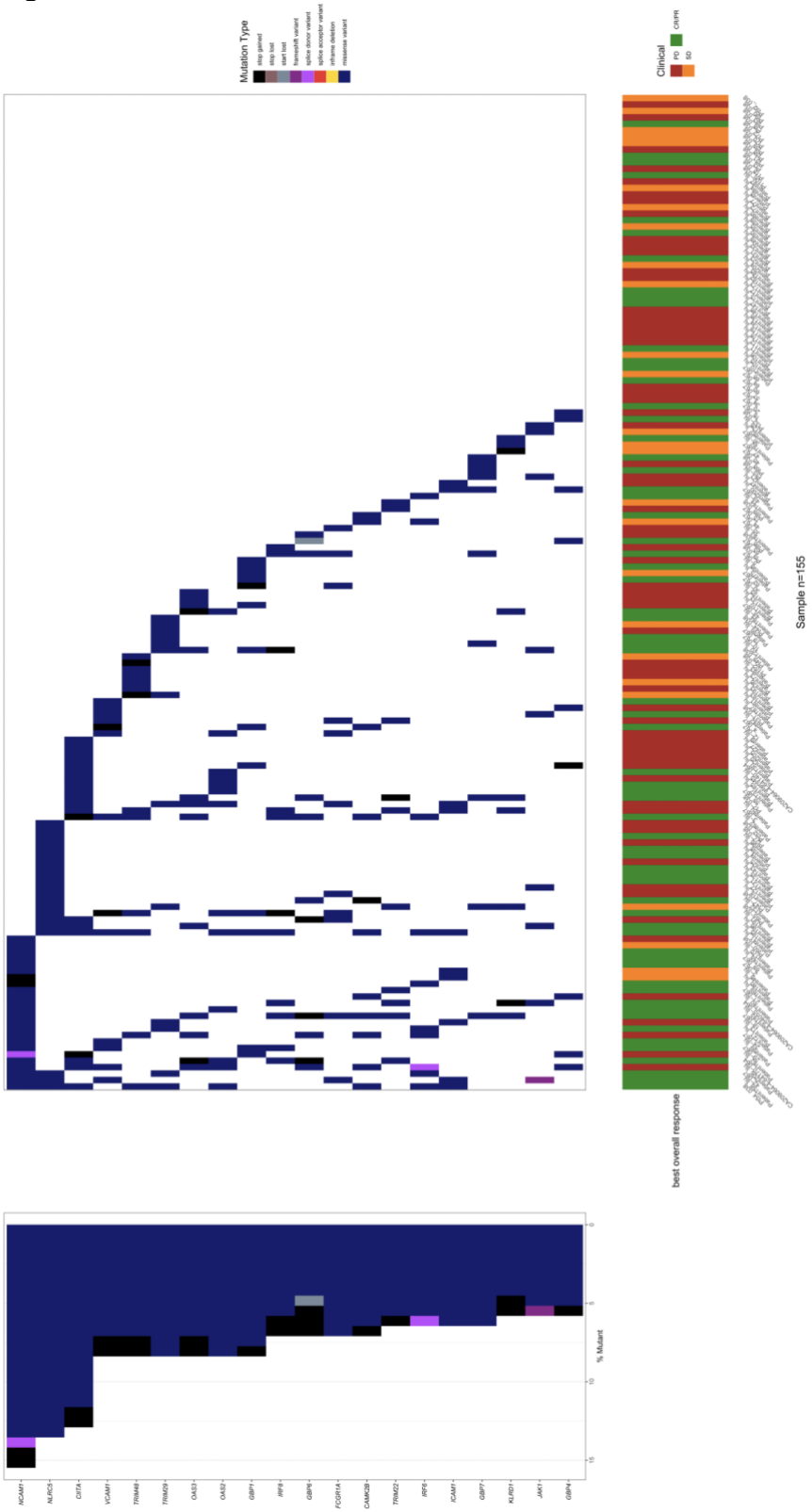
Mutation Type
stop gained
stop lost
start lost
frameshift variant
splice donor variant
splice acceptor variant
inframe deletion
missense variant
Clinical
CR/PR
PD
SD
Sample n=155
best overall response
% Mutant
ICAM1
KLRC3
CIITA
VCAM1
TRIM8
TRIM29
OAS3
OAS2
GBP1
IRF8
GBP6
FCGR1A
CAMK2B
TRIM22
IRF4
ICAM1
GBP7
KLRD1
JAK1
GBP4

**Figure 1: Waterfall plot of the top 20 mutated MHC class I genes.** WES data from baseline melanoma tumors (n=242) was analyzed to identify non-silent mutations in MHC class I structural and regulatory genes (n=164).

**Figure 2**

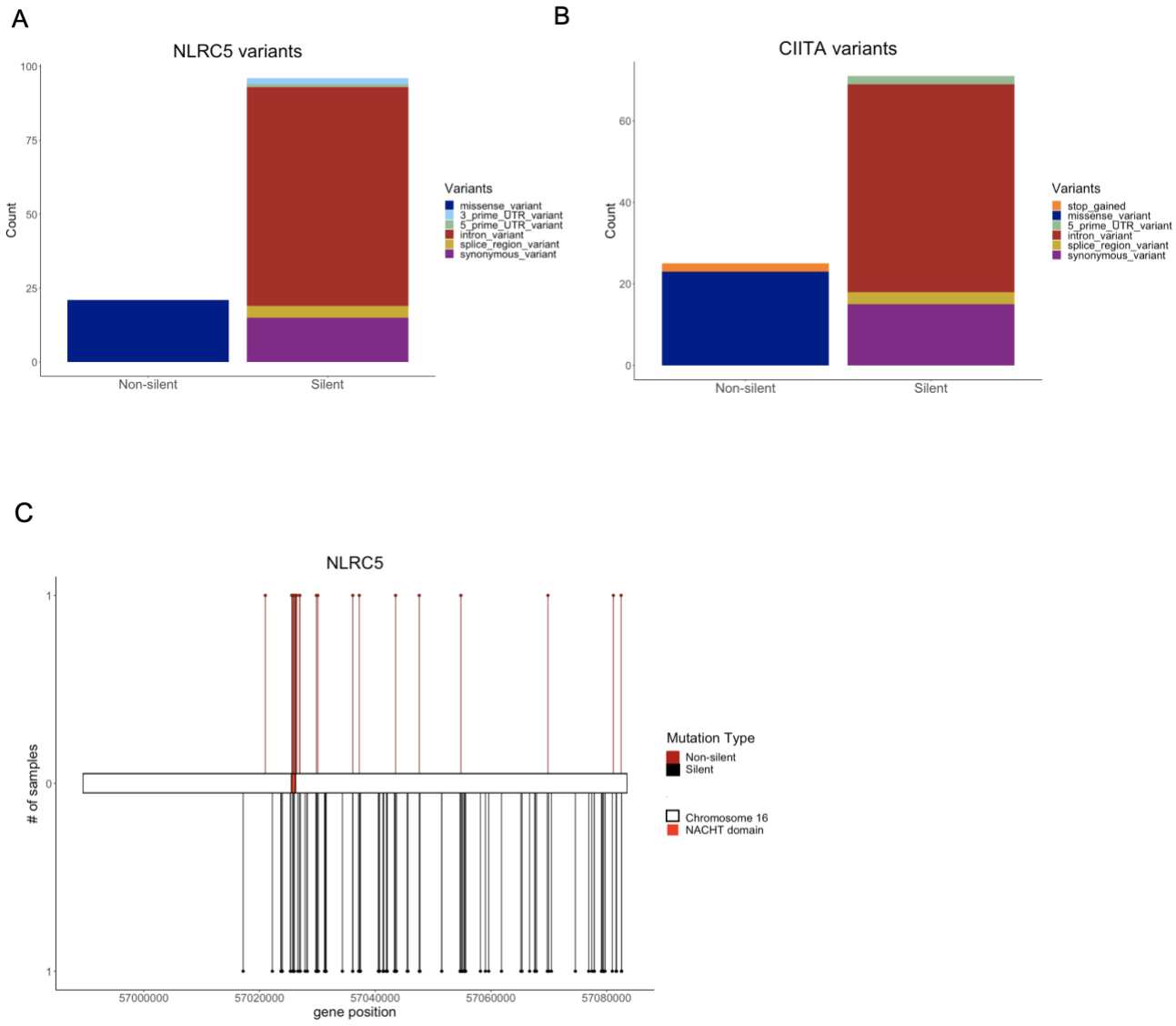
A
NLRC5 variants
Count
100
75
50
25
0
Non-silent
Silent
Variants
missense_variant
3_prime_UTR_variant
5_prime_UTR_variant
intron_variant
splice_region_variant
synonymous_variant
B
CIITA variants
Count
60
40
20
0
Non-silent
Silent
Variants
stop_gained
missense_variant
5_prime_UTR_variant
intron_variant
splice_region_variant
synonymous_variant
C
NLRC5
# of samples
1
0
1
57000000
57020000
57040000
57060000
57080000
gene position
Mutation Type
Non-silent
Silent
Chromosome 16
NACHT domain

**Figure 2 *continued***

D

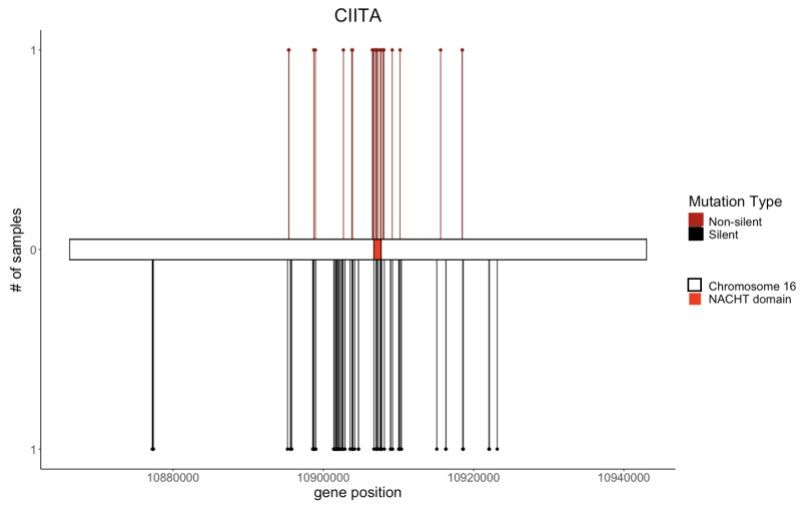


**Figure 2: *NLRC5* and *CIITA* variants.** (A) *NLRC5* silent versus non-silent variants. (B) *CIITA* silent versus non-silent variants. Lollipop plots demonstrating the chromosomal location of silent (black) and non-silent (burgundy) mutations for *NLRC5* (C) and *CIITA* (D). The NACHT domain is shown in bright red.

**Figure 3**

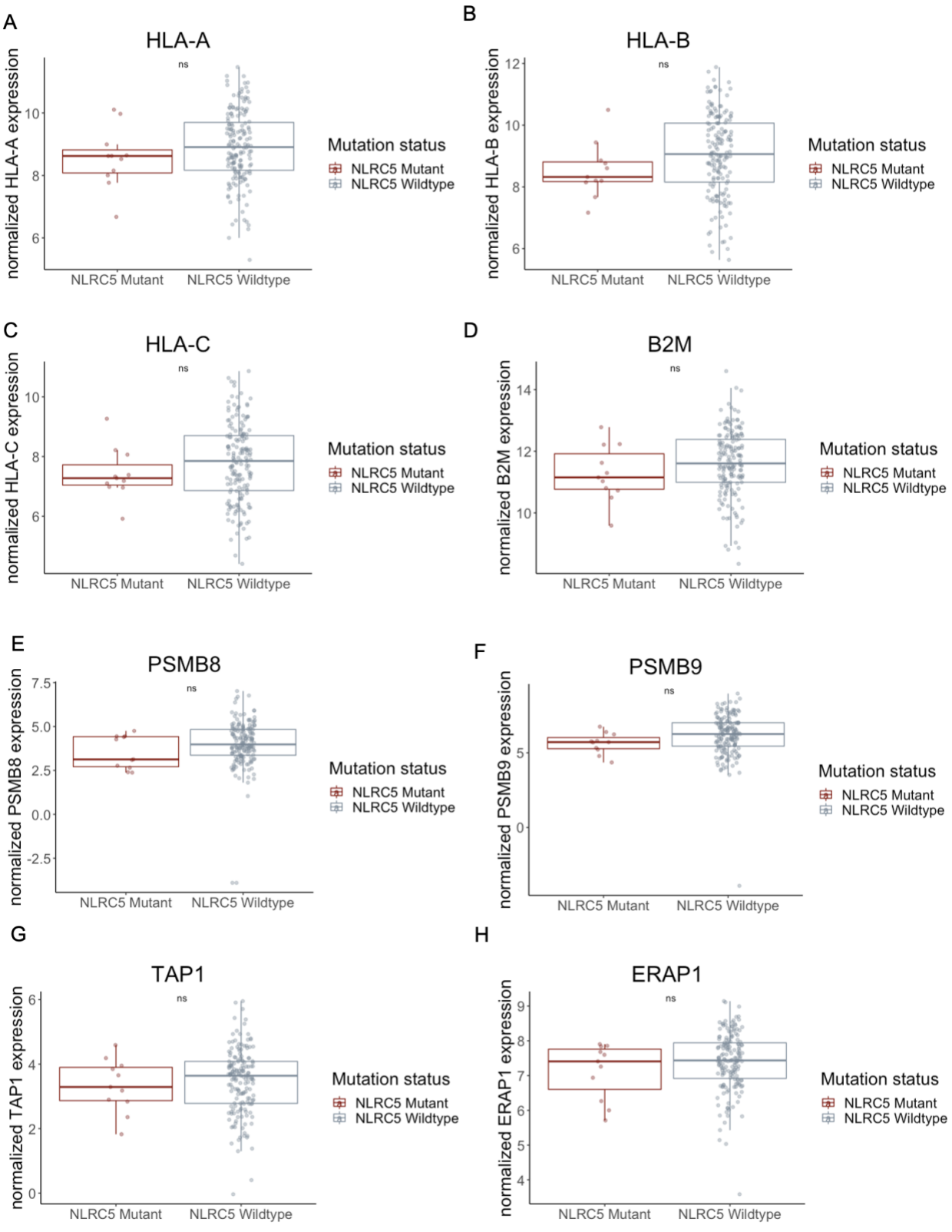
A
HLA-A
normalized HLA-A expression
ns
NLRC5 Mutant
NLRC5 Wildtype
Mutation status
NLRC5 Mutant
NLRC5 Wildtype
B
HLA-B
normalized HLA-B expression
C
HLA-C
normalized HLA-C expression
D
B2M
normalized B2M expression
E
PSMB8
normalized PSMB8 expression
F
PSMB9
normalized PSMB9 expression
G
TAP1
normalized TAP1 expression
H
ERAP1
normalized ERAP1 expression

**Figure 3: Normalized expression of MHC class I pathway genes in *NLRC5* mutant versus wildtype tumors.** (A-G) Normalized expression of NLRC5-regulated MHC class I pathway genes, *HLA-A, HLA-B, HLA-C, B2M, PSMB8, PSMB9,* and *TAP1* in *NLRC5* mutant (n=11) versus wildtype tumors (n=167). (H) Normalized expression of non-NLRC5-regulated MHC class I pathway gene, *ERAP1,* in *NLRC5* mutant (n=11) versus wildtype tumors (n=167). Wilcoxon test, ns= not significant, * $p<0.05$.

**Figure 4**

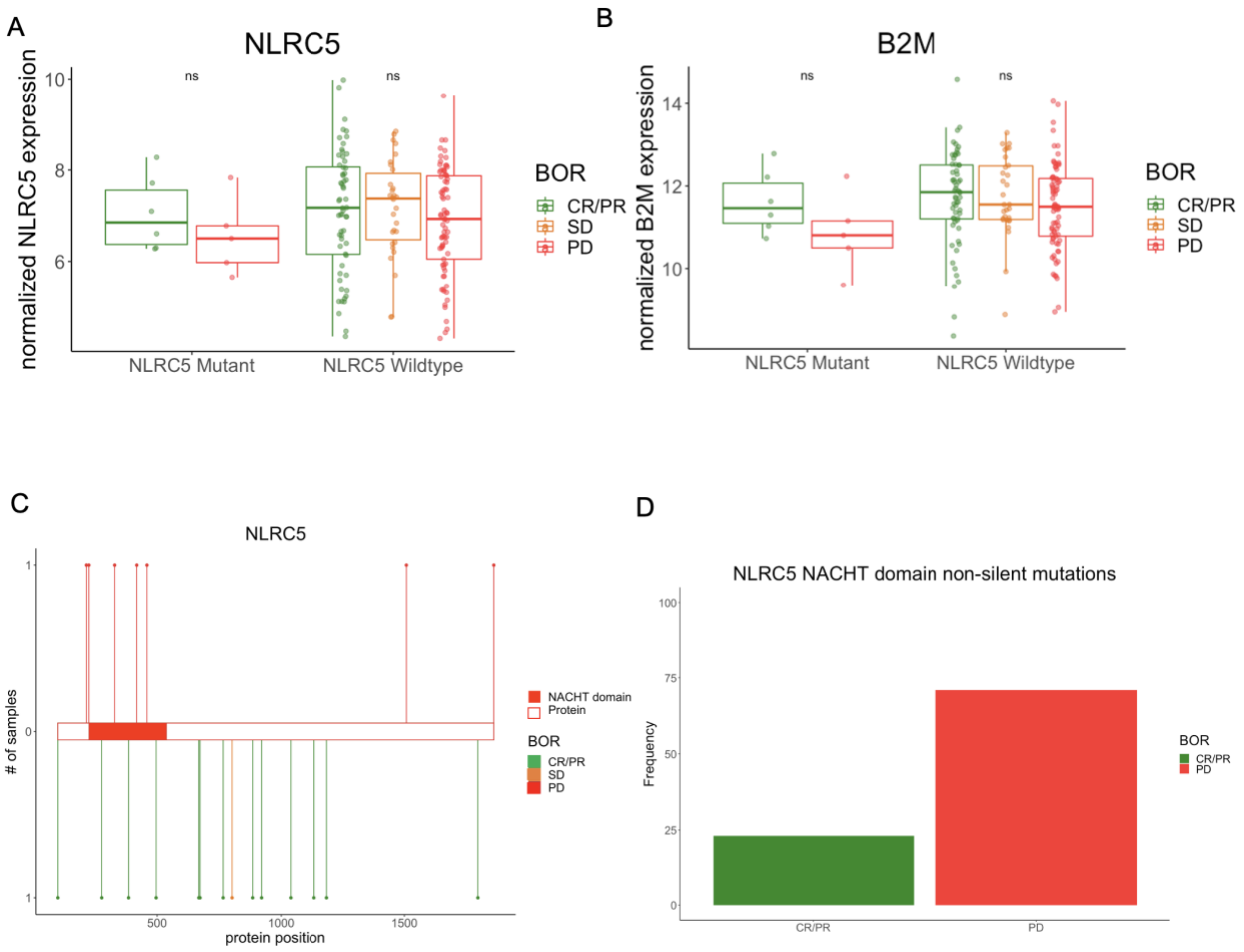


**Figure 4: *NLRC5* mutations by clinical response group.** Normalized *NLRC5* (A) and *B2M* (B) expression in *NLRC5* mutant (n=11) versus wildtype tumors (n=167) split based on clinical response group per the RECIST v1.1 criteria for best overall response (BOR). CR/PR= complete and partial response, SD= stable disease, PD= progressive disease. Wilcoxon test, ns= not significant, * p<0.05. (C) Lollipop plot demonstrating the protein location of *NLRC5* non-silent mutations in responsive versus non-responsive tumors. The NACHT domain is shown in bright red. (D) Frequency of *NLRC5* NACHT domain mutations in responders (n=3/13, 23%) versus non-responders (n=5/7, 71%).

**Figure 5**

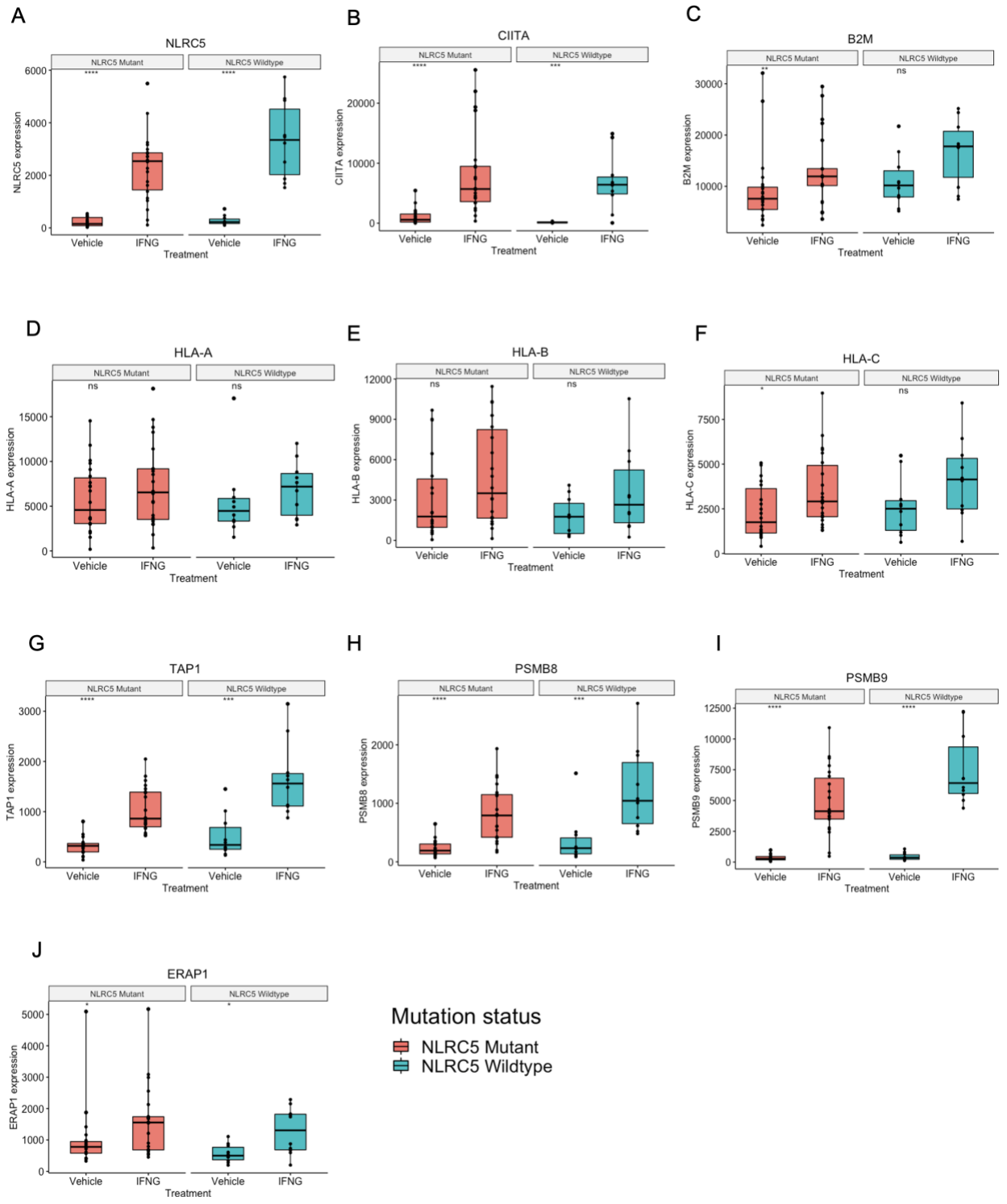
A
NLRC5
NLRC5 Mutant
NLRC5 Wildtype
NLRC5 expression
Vehicle
IFNG
Treatment
B
CIITA
CIITA expression
C
B2M
B2M expression
D
HLA-A
HLA-A expression
ns
E
HLA-B
HLA-B expression
F
HLA-C
HLA-C expression
G
TAP1
TAP1 expression
H
PSMB8
PSMB8 expression
I
PSMB9
PSMB9 expression
J
ERAP1
ERAP1 expression
Mutation status
NLRC5 Mutant
NLRC5 Wildtype

**Figure 5: MHC class I pathway gene expresison in *NLRC5* mutant versus wildtype cell lines by IFN-γ exposure.** (A) Expresison of *NLRC5* in *NLRC5* mutant (n=22) versus wildtype cell lines (n=10) using raw RNAseq data. (B) *CIITA* expression in *NLRC5* mutant versus wildtype cell lines. (C-I) Expression of NLRC5-regulated MHC class I pathway genes, *HLA-A, HLA-B, HLA-C, B2M, PSMB8, PSMB9,* and *TAP1* in *NLRC5* mutant versus wildtype cell lines. (J) Expression of non-NLRC5-regulated MHC class I pathway gene, *ERAP1,* in *NLRC5* mutant versus wildtype cell lines. All groups separated based on 6h of IFN-γ or vehicle exposure. Wilcoxon test, ns= not significant, * $p<0.05$, ** $p<0.01$, *** $p<0.001$, **** $p<0.00001$.

**Figure 6**

A

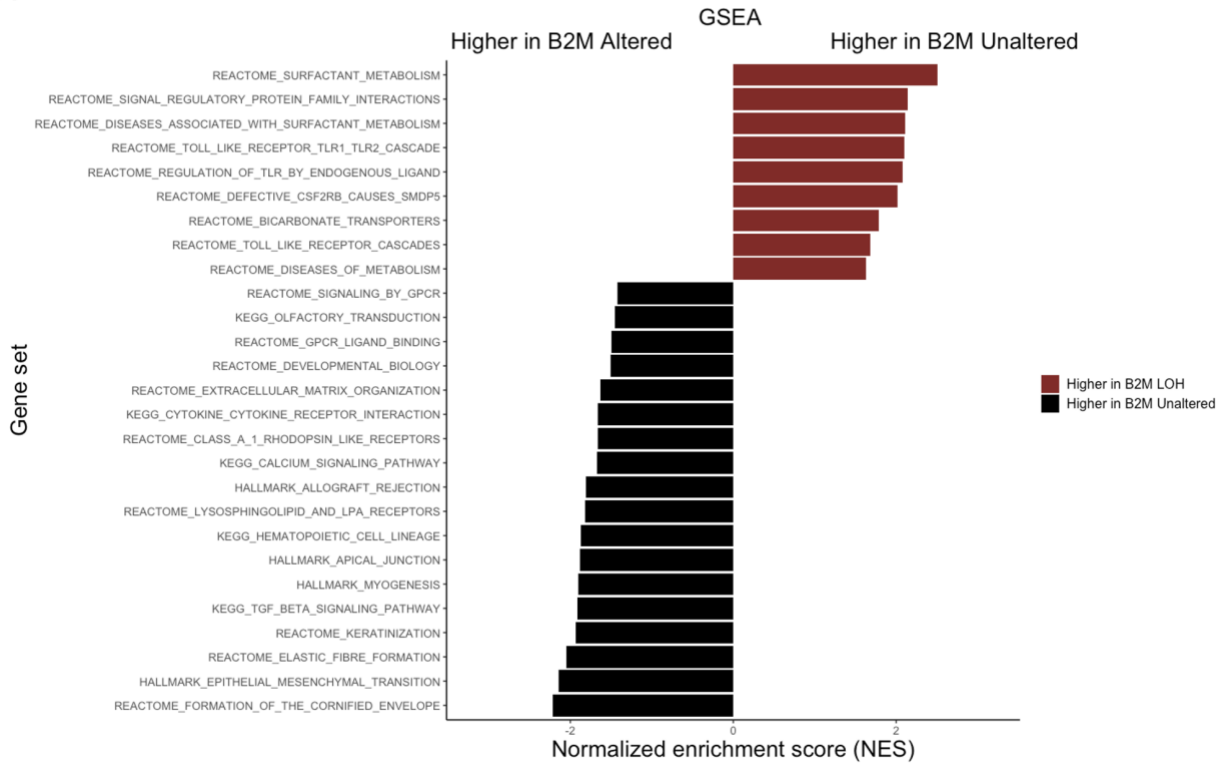
GSEA
Higher in B2M Altered
Higher in B2M Unaltered
REACTOME_SURFACTANT_METABOLISM
REACTOME_SIGNAL_REGULATORY_PROTEIN_FAMILY_INTERACTIONS
REACTOME_DISEASES_ASSOCIATED_WITH_SURFACTANT_METABOLISM
REACTOME_TOLL_LIKE_RECEPTOR_TLR1_TLR2_CASCADE
REACTOME_REGULATION_OF_TLR_BY_ENDOGENOUS_LIGAND
REACTOME_DEFECTIVE_CSF2RB_CAUSES_SMDP5
REACTOME_BICARBONATE_TRANSPORTERS
REACTOME_TOLL_LIKE_RECEPTOR_CASCADES
REACTOME_DISEASES_OF_METABOLISM
REACTOME_SIGNALING_BY_GPCR
KEGG_OLFACTORY_TRANSDUCTION
REACTOME_GPCR_LIGAND_BINDING
REACTOME_DEVELOPMENTAL_BIOLOGY
REACTOME_EXTRACELLULAR_MATRIX_ORGANIZATION
KEGG_CYTOKINE_CYTOKINE_RECEPTOR_INTERACTION
REACTOME_CLASS_A_1_RHODOPSIN_LIKE_RECEPTORS
KEGG_CALCIUM_SIGNALING_PATHWAY
HALLMARK_ALLOGRAFT_REJECTION
REACTOME_LYSOSPHINGOLIPID_AND_LPA_RECEPTORS
KEGG_HEMATOPOIETIC_CELL_LINEAGE
HALLMARK_APICAL_JUNCTION
HALLMARK_MYOGENESIS
KEGG_TGF_BETA_SIGNALING_PATHWAY
REACTOME_KERATINIZATION
REACTOME_ELASTIC_FIBRE_FORMATION
HALLMARK_EPITHELIAL_MESENCHYMAL_TRANSITION
REACTOME_FORMATION_OF_THE_CORNIFIED_ENVELOPE
Gene set
-2
0
2
Normalized enrichment score (NES)
Higher in B2M LOH
Higher in B2M Unaltered

**Figure 6 *continued***

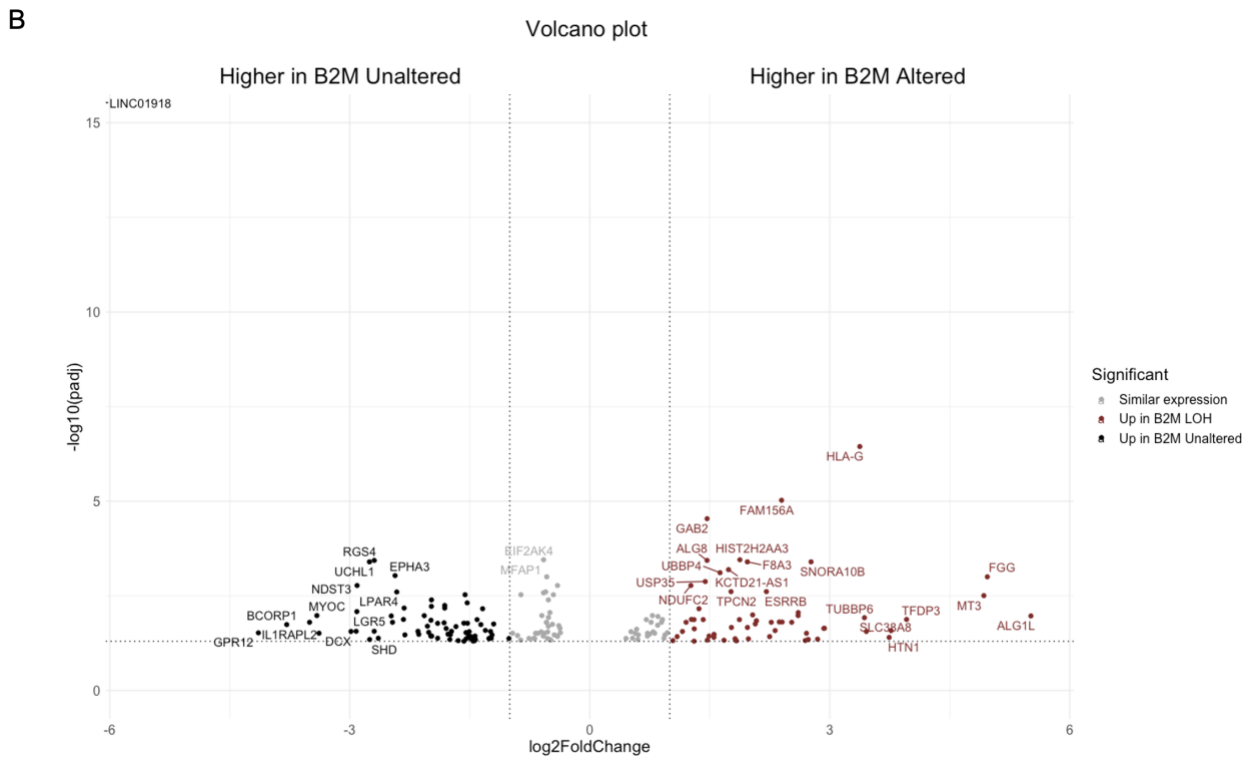


**Figure 6: Differentially expressed genes and gene sets in *B2M*-LOH and unaltered tumors.** (A) Gene set enrichment analysis showing the top most enriched gene sets with a normalized enrichment score of 2 or -2 and p-values less 0.05 and adjusted p-values less than 0.25 in *B2M*-LOH (n=24) versus unaltered tumors (n=71). Black= higher in *B2M*-unaltered, burgundy= higher in *B2M*-LOH. (B) Significantly differentially expressed genes with log2 fold change greater than 1 or less than -1 in *B2M*-LOH (n=24) versus unaltered tumors (n=71). Grey= similar expression between both groups, black= higher in *B2M*-unaltered, burgundy= higher in *B2M*-LOH.

**Figure 7**

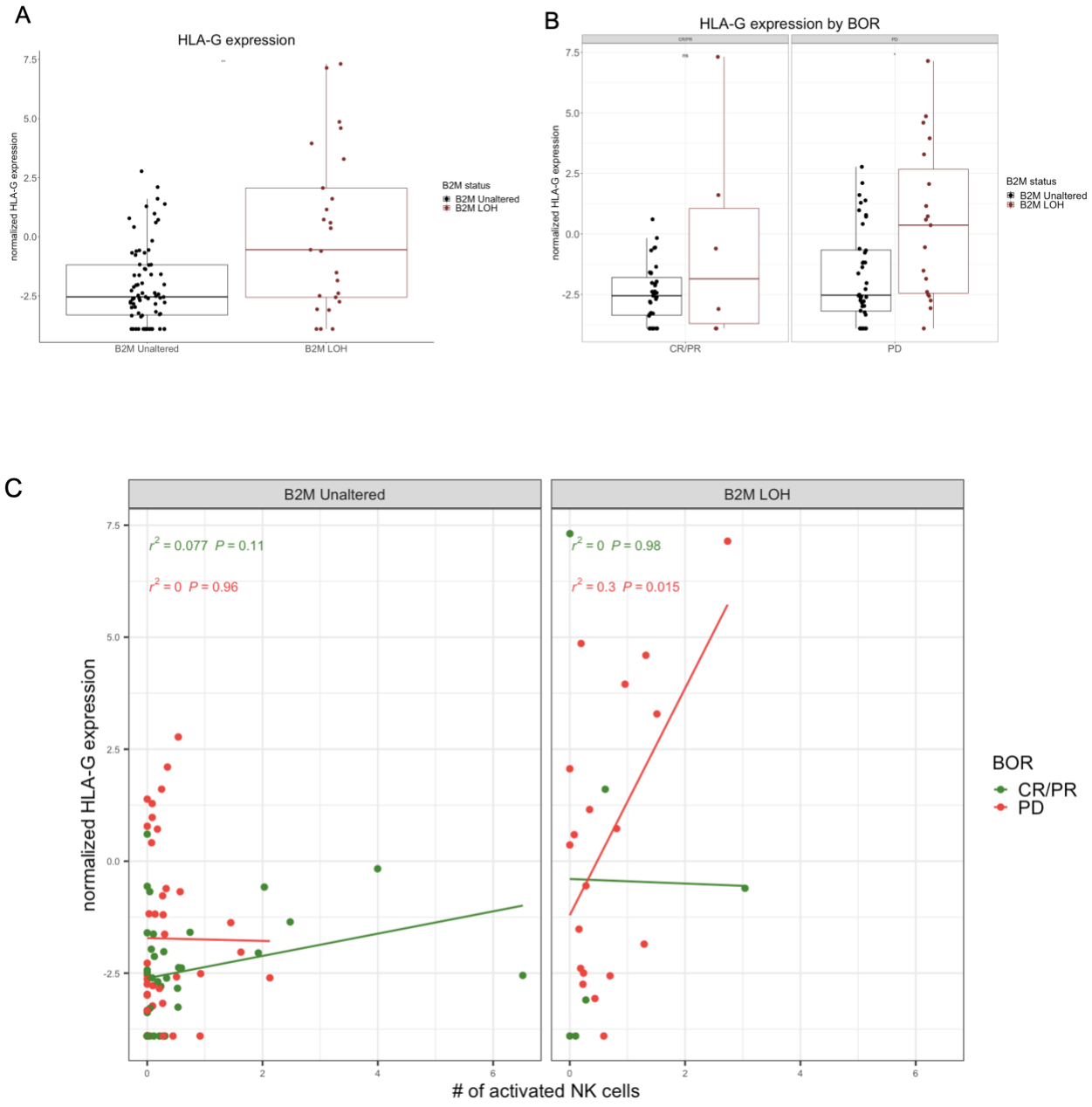
A
HLA-G expression
normalized HLA-G expression
B2M status
B2M Unaltered
B2M LOH
B2M Unaltered
B2M LOH
B
HLA-G expression by BOR
normalized HLA-G expression
B2M status
B2M Unaltered
B2M LOH
CR/PR
PD
C
B2M Unaltered
B2M LOH
r² = 0.077 P = 0.11
r² = 0 P = 0.96
r² = 0 P = 0.98
r² = 0.3 P = 0.015
normalized HLA-G expression
# of activated NK cells
BOR
CR/PR
PD

**Figure 7: *HLA-G* expression.** (A) Normalized *HLA-G* expression in *B2M*-altered (n=25) versus unaltered tumors (n=75). Wilcoxon test, ns= not significant, * p<0.05. (B) Normalized *HLA-G* expression in *B2M*-altered versus unaltered tumors separated by clinical response group. Wilcoxon test, ns= not significant, * p<0.05. (C) Normalized *HLA-G* expression versus numbers of activated NK cells in *B2M*-altered versus unaltered tumors separated by clinical response group; Pearson correlation.

## Table 1

| Association between NLRC5 and CIITA non-silent mutations (n=242) | | | |
|---|---|---|---|
| | **NLRC5 mutant** | **NLRC5 wildtype** | Fisher's exact test |
| **CIITA mutant** | 4 | 16 | p=0.08 |
| **CIITA wildtype** | 17 | 205 | |
| **Total** | 21 | 221 | |

**Table 1: Association between *NLRC5* and *CIITA* non-silent mutations in tumor samples.**

## Table 2

| Association between NLRC5 and CIITA mutations (n=242) | | | |
|---|---|---|---|
| | **NLRC5 mutant** | **NLRC5 wildtype** | Fisher's exact test |
| **CIITA mutant** | 26 | 30 | p=0.00004 |
| **CIITA wildtype** | 34 | 152 | |
| **Total** | 60 | 182 | |

**Table 2: Association between *NLRC5* and *CIITA* mutations in tumor samples.**

## Table 3

| Association of NACHT domain non-silent mutations and progressive disease (n=21) | | | |
|---|---|---|---|
| | **Clinical responder (CR/PR)*** | **Clinical non-responder (PD)** | Fisher's exact test |
| **NACHT mutation** | 3 | 5 | p=0.0555 |
| **Other mutation** | 11 | 2 | |
| **Total** | 13 | 7 | |

**Table 3: Association of *NLRC5* NACHT domain non-silent mutations and progressive disease in tumor samples.**

## Table 4

| Association of HLA-G expression and progressive disease (n=50) | | | |
|---|---|---|---|
| | **Clinical responder (CR/PR)** | **Clinical non-responder (PD)** | Fisher's exact test |
| **HLA-G high** | 5 | 20 | p=0.0186 |
| **HLA-G low** | 14 | 11 | |
| **Total** | 19 | 31 | |

**Table 4: Association of *HLA-G* expression and progressive disease in tumor samples.**

**Supplementary Figure S1**

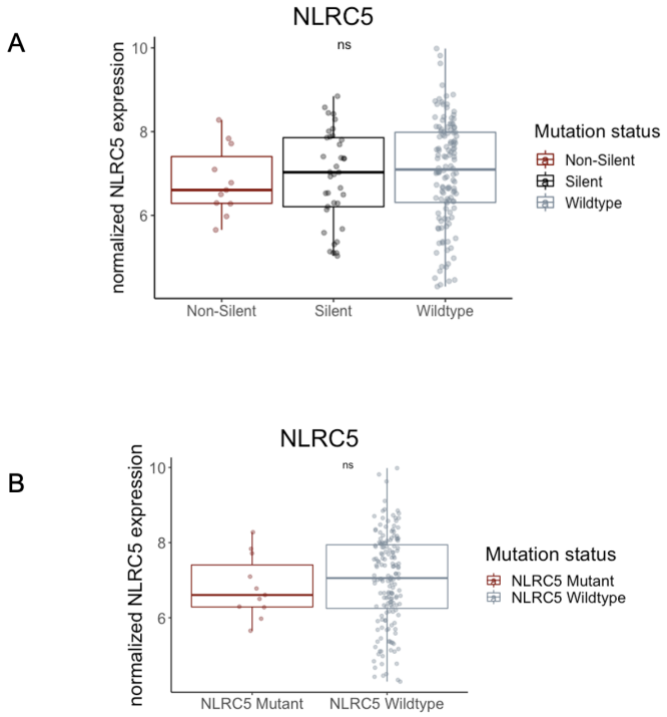


**Supplementary Figure S1: Normalized *NLRC5* expression.** (A) Normalized *NLRC5* expression in *NLRC5* non-silent mutant (n=11), silent mutant (n=37), and wildtype tumors (n=130). (B) Normalized *NLRC5* expression in *NLRC5* mutant (n=11) and wildtype tumors (n=167). Wilcoxon test, ns= not significant, * p<0.05.

**Supplementary Figure S2**

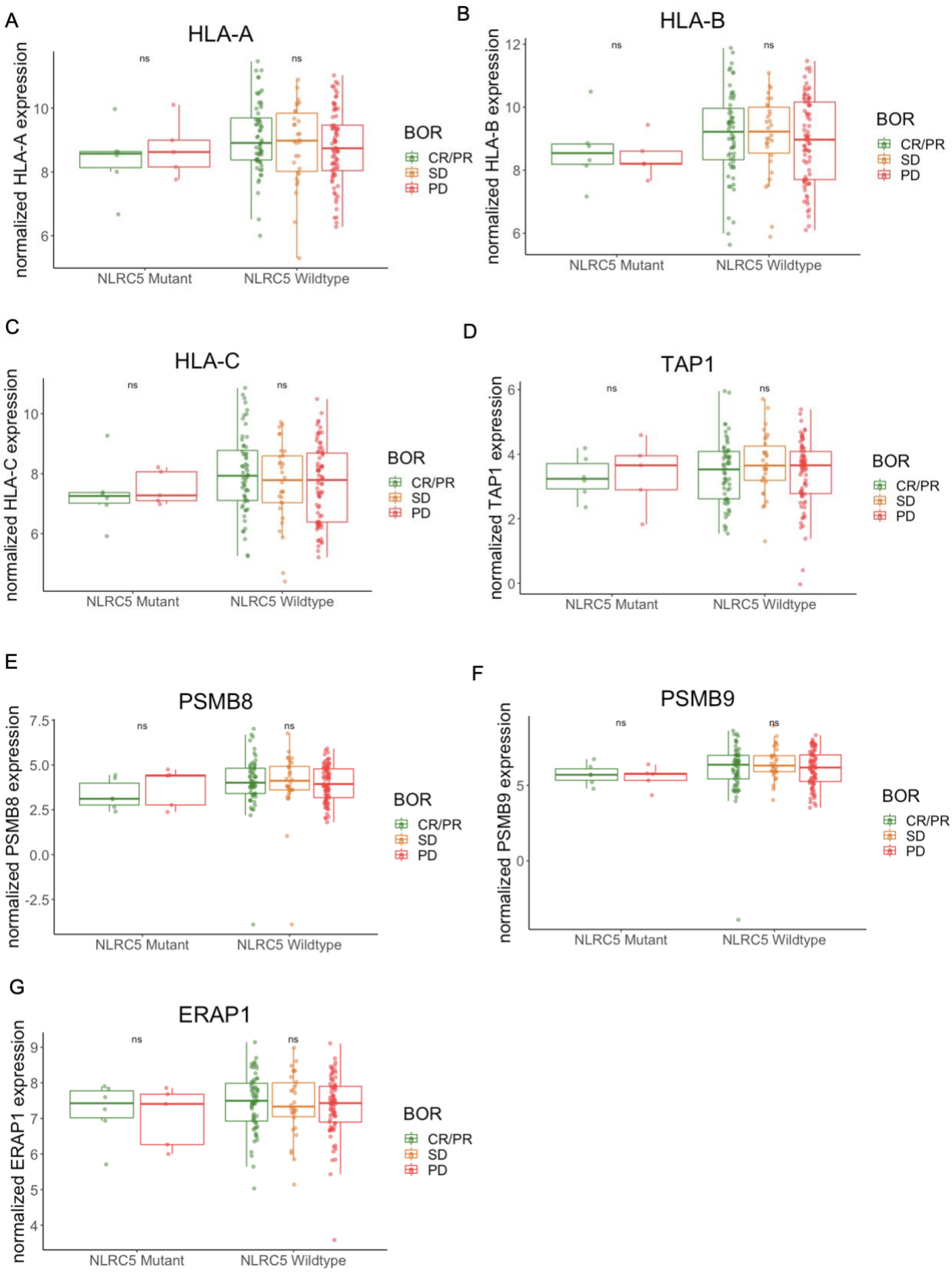

**Supplementary Figure S2: Normalized expression of MHC class I pathway genes in *NLRC5* mutant versus wildtype tumors by clinical response group.** (A-F) Normalized expression of MHC class I pathway genes *HLA-A, HLA-B, HLA-C, B2M, PSMB8, PSMB9,* and *TAP1* in *NLRC5* mutant (n=11) versus wildtype tumors (n=167) split based on clinical response group per the RECIST v1.1 criteria for best overall response (BOR). CR/PR= complete and partial response, SD= stable disease, PD= progressive disease. (G) Normalized expression of non-NLRC5-regulated MHC class I pathway gene, *ERAP1,* in *NLRC5* mutant (n=11) versus wildtype tumors (n=167). Kruskal-Wallis test, ns= not significant, * $p<0.05$.

**Supplementary Figure S3**

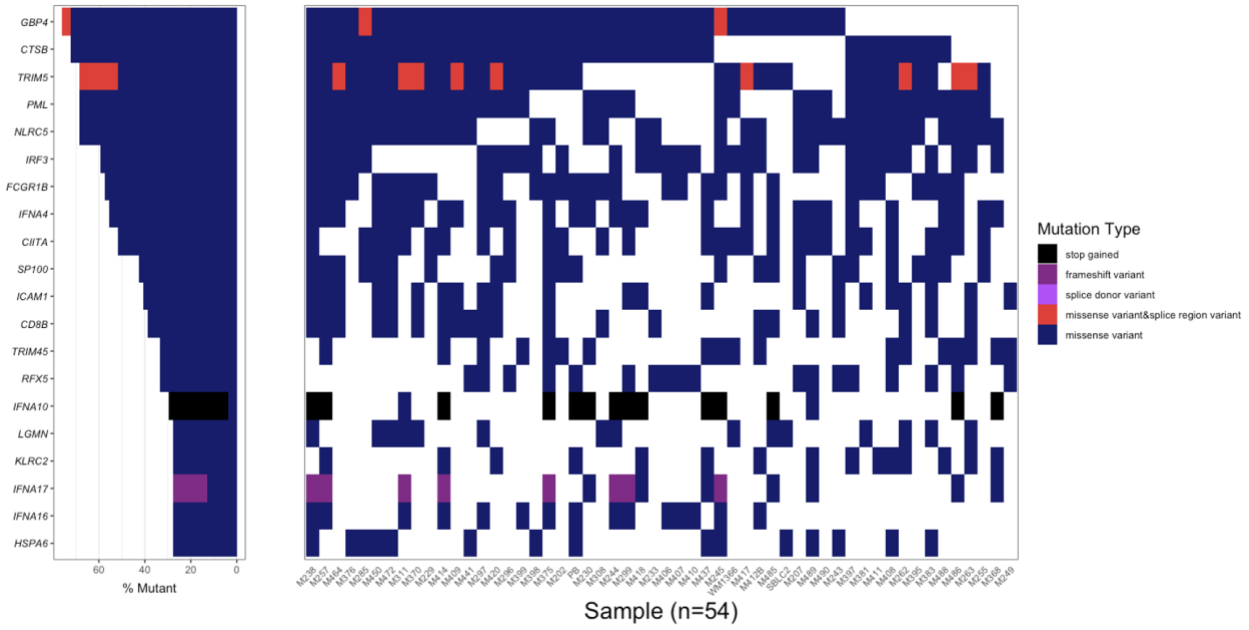


**Supplementary Figure S3: Waterfall plot of the top 20 mutated MHC class I genes in patient-derived melanoma cell lines.** WES data from patient-derived melanoma cell lines (n=54) was analyzed to identify non-silent mutations in MHC class I structural and regulatory genes (n=164).

**Supplementary Figure S4**

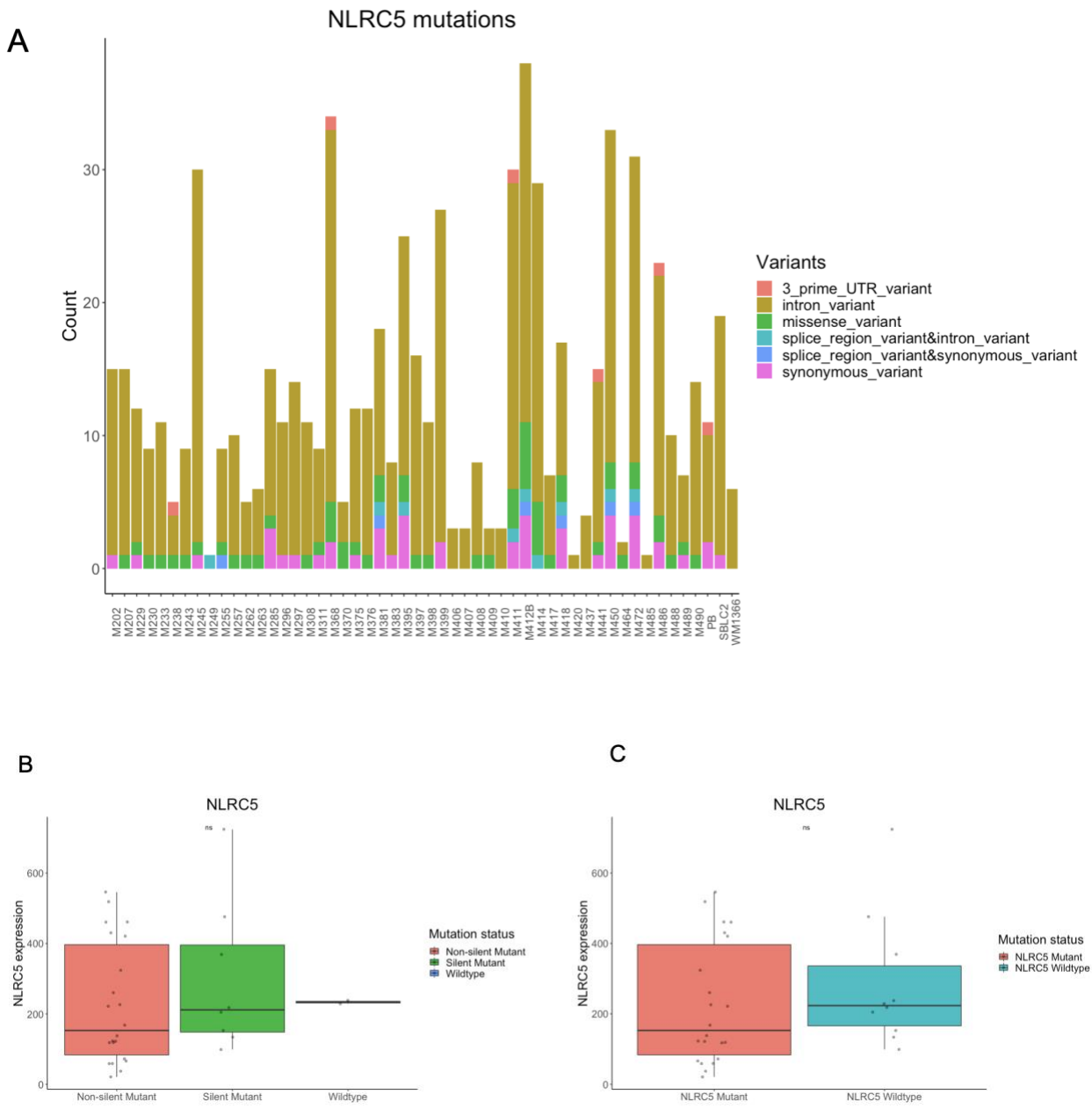

**Supplementary Figure S4: *NLRC5* mutations in melanoma cell lines.** (A) *NLRC5* variant distribution in patient-derived melanoma cell lines (n=52) showing all mutations. (B) Normalized *NLRC5* expression in cell lines with *NLRC5* non-silent (n=22), silent (n=8), or no mutations (n=2). (C) Normalized *NLRC5* expression in *NLRC5* mutant (n=22) versus wildtype cell lines (n=10). Kruskal-Wallis test, ns= not significant, * $p<0.05$. Wilcoxon test, ns= not significant, * $p<0.05$.

## Supplementary Figure S5

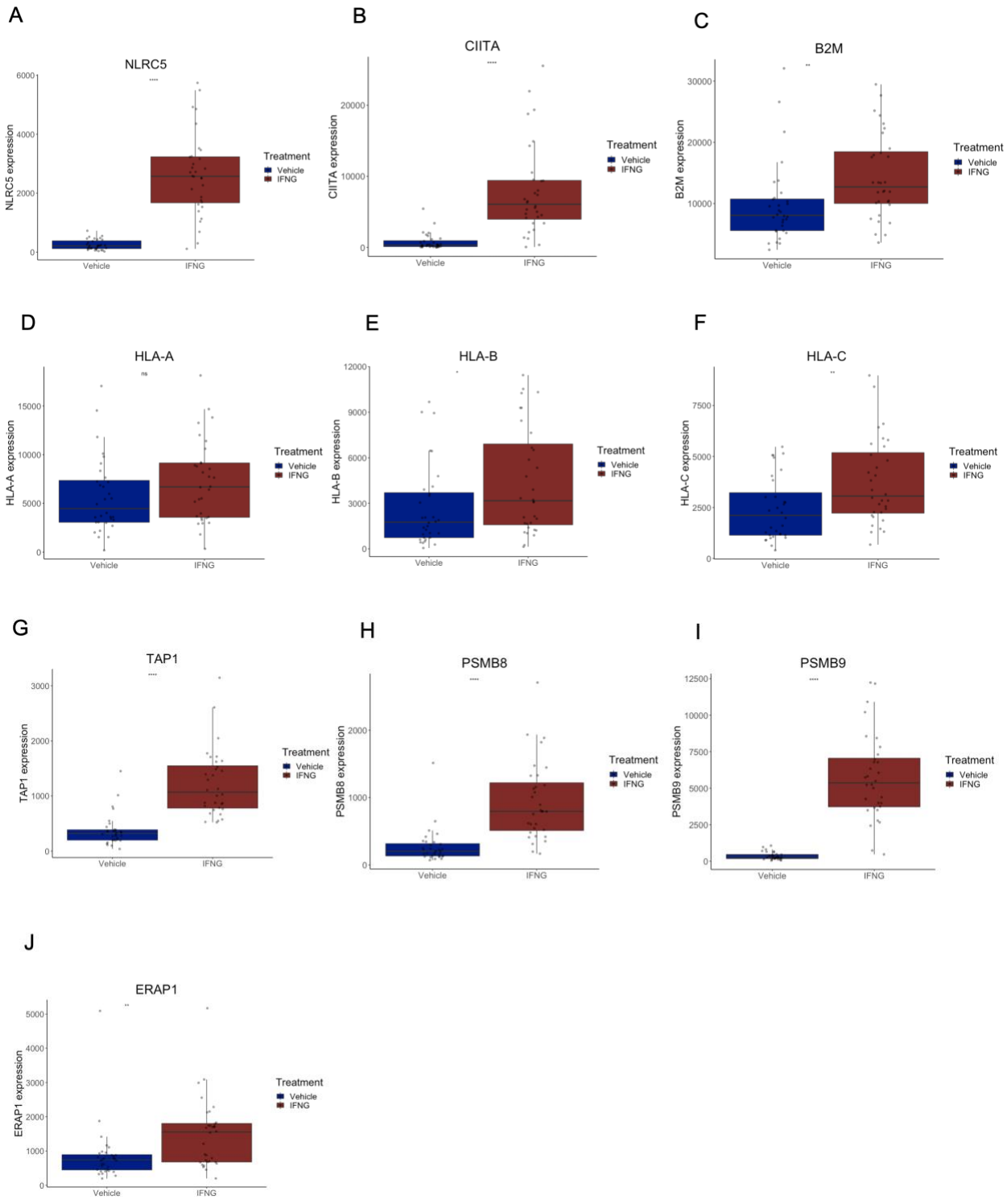

**Supplementary Figure S5: Normalized expression of MHC class I pathway genes by IFN-γ exposure.** (A) Normalized expresison of *NLRC5* in vehicle (n=32) versus IFN-γ-treated cell lines (n=32). (B) Normalized expression of *CIITA.* (C-I) Normalized expression of NLRC5-regulated MHC class I pathway genes, *HLA-A, HLA-B, HLA-C, B2M, PSMB8, PSMB9,* and *TAP1*. (J) Normalized expression of non-NLRC5-regulated MHC class I pathway gene, *ERAP1*. All groups separated based on 6h of IFN-γ or vehicle exposure. Wilcoxon test, ns= not significant, * $p<0.05$, ** $p<0.01$, *** $p<0.001$, **** $p<0.00001$.

**Supplementary Figure S6**

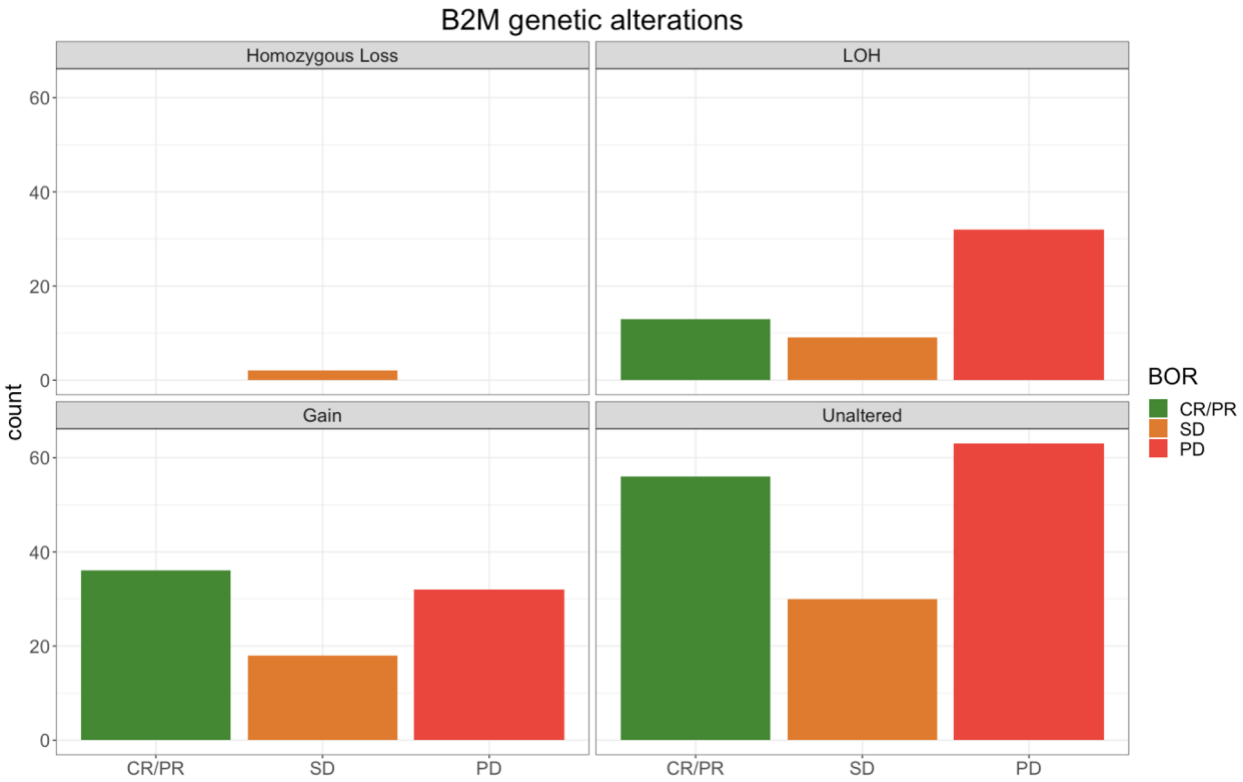


**Supplementary Figure S6: *B2M* genetic alterations.** Summary of *B2M* genetic alterations in the melanoma cohort (n=295). Only *B2M*-LOH and unaltered responder versus non-responder samples with RNAseq data were included for further analysis (n=100).

## Supplementary Figure S7

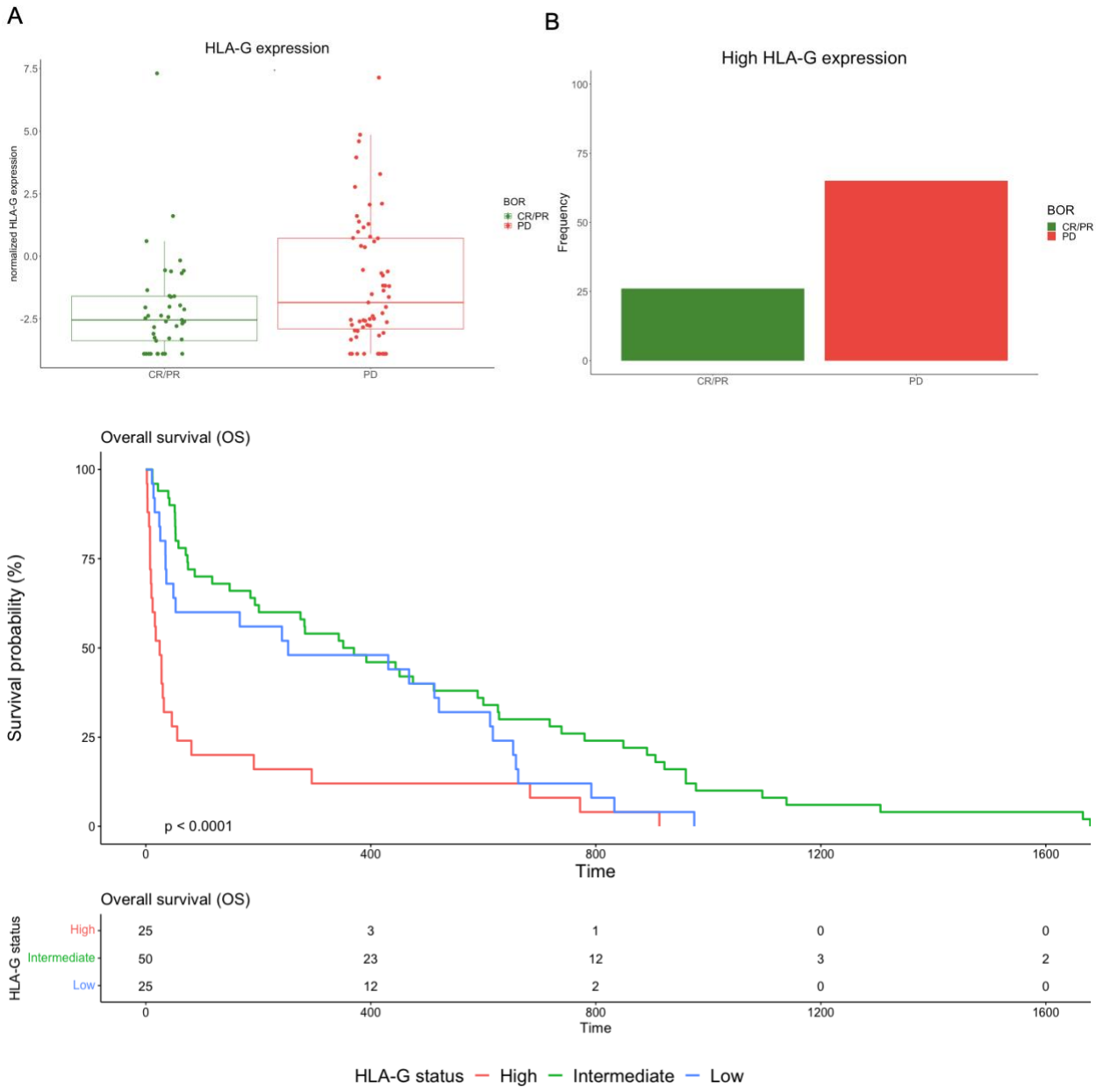

**Supplementary Figure S7: *HLA-G* expression.** (A) Normalized *HLA-G* expression in tumors derived from patients who responded (n=41) or progressed (n=59) during ICB therapy. Wilcoxon test, ns= not significant, * $p<0.05$. (B) Frequency of high *HLA-G* expression in responders (n=20/31, 65%) versus non-responders (n=5/19, 25%). (C) Overalls survival (OS) in patients with low (lower quartile), intermediate (interquartiles), and high (higher quartile) *HLA-G* expression.

**Supplementary Table Index**

**References**


1. Sharma P, Hu-Lieskovan S, Wargo JA, and Ribas A. Primary, Adaptive, and Acquired Resistance to Cancer Immunotherapy. *Cell.* 2017;168(4):707-23.
2. Keenan TE, Burke KP, and Van Allen EM. Genomic correlates of response to immune checkpoint blockade. *Nat Med.* 2019;25(3):389-402.
3. Mpakali A, and Stratikos E. The Role of Antigen Processing and Presentation in Cancer and the Efficacy of Immune Checkpoint Inhibitor Immunotherapy. *Cancers (Basel).* 2021;13(1).
4. Cai L, Michelakos T, Yamada T, Fan S, Wang X, Schwab JH, et al. Defective HLA class I antigen processing machinery in cancer. *Cancer Immunol Immunother.* 2018;67(6):999-1009.
5. Dhatchinamoorthy K, Colbert JD, and Rock KL. Cancer Immune Evasion Through Loss of MHC Class I Antigen Presentation. *Front Immunol.* 2021;12:636568.
6. Kelly A, and Trowsdale J. Genetics of antigen processing and presentation. *Immunogenetics.* 2019;71(3):161-70.
7. Marabelle A, Aspeslagh S, Postel-Vinay S, and Soria JC. JAK Mutations as Escape Mechanisms to Anti-PD-1 Therapy. *Cancer Discov.* 2017;7(2):128-30.
8. Torrejon DY, Abril-Rodriguez G, Champhekar AS, Tsoi J, Campbell KM, Kalbasi A, et al. Overcoming Genetically Based Resistance Mechanisms to PD-1 Blockade. *Cancer Discov.* 2020;10(8):1140-57.
9. Rizvi H, Sanchez-Vega F, La K, Chatila W, Jonsson P, Halpenny D, et al. Molecular Determinants of Response to Anti-Programmed Cell Death (PD)-1 and Anti-Programmed Death-Ligand 1 (PD-L1) Blockade in Patients With Non-Small-Cell Lung Cancer Profiled With Targeted Next-Generation Sequencing. *J Clin Oncol.* 2018;36(7):633-41.

10. Germano G, Lu S, Rospo G, Lamba S, Rousseau B, Fanelli S, et al. CD4 T Cell-Dependent Rejection of Beta-2 Microglobulin Null Mismatch Repair-Deficient Tumors. *Cancer Discov.* 2021;11(7):1844-59.

11. Sade-Feldman M, Jiao YJ, Chen JH, Rooney MS, Barzily-Rokni M, Eliane JP, et al. Resistance to checkpoint blockade therapy through inactivation of antigen presentation. *Nat Commun.* 2017;8(1):1136.

12. Rodig SJ, Gusenleitner D, Jackson DG, Gjini E, Giobbie-Hurder A, Jin C, et al. MHC proteins confer differential sensitivity to CTLA-4 and PD-1 blockade in untreated metastatic melanoma. *Sci Transl Med.* 2018;10(450).

13. Liu D, Schilling B, Liu D, Sucker A, Livingstone E, Jerby-Arnon L, et al. Integrative molecular and clinical modeling of clinical outcomes to PD1 blockade in patients with metastatic melanoma. *Nat Med.* 2019;25(12):1916-27.

14. de Vries NL, van de Haar J, Veninga V, Chalabi M, Ijsselsteijn ME, van der Ploeg M, et al. gammadelta T cells are effectors of immunotherapy in cancers with HLA class I defects. *Nature.* 2023;613(7945):743-50.

15. Campbell KM, Amouzgar M, Pfeiffer SM, Howes TR, Medina E, Travers M, et al. Prior anti-CTLA-4 therapy impacts molecular characteristics associated with anti-PD-1 response in advanced melanoma. *Cancer Cell.* 2023;41(4):791-806 e4.

16. Vijayan S, Sidiq T, Yousuf S, van den Elsen PJ, and Kobayashi KS. Class I transactivator, NLRC5: a central player in the MHC class I pathway and cancer immune surveillance. *Immunogenetics.* 2019;71(3):273-82.

17. Martin BK, Chin KC, Olsen JC, Skinner CA, Dey A, Ozato K, et al. Induction of MHC class I expression by the MHC class II transactivator CIITA. *Immunity.* 1997;6(5):591-600.

18. Ong CEB, Cheng Y, Siddle HV, Lyons AB, Woods GM, and Flies AS. Class II transactivator induces expression of MHC-I and MHC-II in transmissible Tasmanian devil facial tumours. *Open Biol.* 2022;12(10):220208.

19. Shukla A, Cloutier M, Appiya Santharam M, Ramanathan S, and Ilangumaran S. The MHC Class-I Transactivator NLRC5: Implications to Cancer Immunology and Potential Applications to Cancer Immunotherapy. *Int J Mol Sci.* 2021;22(4).

20. Motyan JA, Bagossi P, Benko S, and Tozser J. A molecular model of the full-length human NOD-like receptor family CARD domain containing 5 (NLRC5) protein. *BMC Bioinformatics.* 2013;14:275.

21. Neerincx A, Castro W, Guarda G, and Kufer TA. NLRC5, at the Heart of Antigen Presentation. *Front Immunol.* 2013;4:397.

22. Yoshihama S, Vijayan S, Sidiq T, and Kobayashi KS. NLRC5/CITA: A Key Player in Cancer Immune Surveillance. *Trends Cancer.* 2017;3(1):28-38.

23. Schwartz LH, Litiere S, de Vries E, Ford R, Gwyther S, Mandrekar S, et al. RECIST 1.1-Update and clarification: From the RECIST committee. *Eur J Cancer.* 2016;62:132-7.

24. Grasso CS, Tsoi J, Onyshchenko M, Abril-Rodriguez G, Ross-Macdonald P, Wind-Rotolo M, et al. Conserved Interferon-gamma Signaling Drives Clinical Response to Immune Checkpoint Blockade Therapy in Melanoma. *Cancer Cell.* 2020;38(4):500-15 e3.

25. Liberzon A, Birger C, Thorvaldsdottir H, Ghandi M, Mesirov JP, and Tamayo P. The Molecular Signatures Database (MSigDB) hallmark gene set collection. *Cell Syst.* 2015;1(6):417-25.

26. Carosella ED, Gregori S, and Tronik-Le Roux D. HLA-G/LILRBs: A Cancer Immunotherapy Challenge. *Trends Cancer.* 2021;7(5):389-92.

27. Carosella ED, Rouas-Freiss N, Tronik-Le Roux D, Moreau P, and LeMaoult J. HLA-G: An Immune Checkpoint Molecule. *Adv Immunol.* 2015;127:33-144.

28. Lin A, and Yan WH. Human Leukocyte Antigen-G (HLA-G) Expression in Cancers: Roles in Immune Evasion, Metastasis and Target for Therapy. *Mol Med.* 2015;21(1):782-91.

29. Karre K. NK cells, MHC class I molecules and the missing self. *Scand J Immunol.* 2002;55(3):221-8.

30. Freeman AJ, Vervoort SJ, Ramsbottom KM, Kelly MJ, Michie J, Pijpers L, et al. Natural Killer Cells Suppress T Cell-Associated Tumor Immune Evasion. *Cell Rep.* 2019;28(11):2784-94 e5.

31. Zheng G, Guo Z, Li W, Xi W, Zuo B, Zhang R, et al. Interaction between HLA-G and NK cell receptor KIR2DL4 orchestrates HER2-positive breast cancer resistance to trastuzumab. *Signal Transduct Target Ther.* 2021;6(1):236.

32. Riaz N, Havel JJ, Makarov V, Desrichard A, Urba WJ, Sims JS, et al. Tumor and Microenvironment Evolution during Immunotherapy with Nivolumab. *Cell.* 2017;171(4):934-49 e16.

33. Weber JS, Gibney G, Sullivan RJ, Sosman JA, Slingluff CL, Jr., Lawrence DP, et al. Sequential administration of nivolumab and ipilimumab with a planned switch in patients with advanced melanoma (CheckMate 064): an open-label, randomised, phase 2 trial. *Lancet Oncol.* 2016;17(7):943-55.

34. Wolchok JD, Chiarion-Sileni V, Gonzalez R, Rutkowski P, Grob JJ, Cowey CL, et al. Overall Survival with Combined Nivolumab and Ipilimumab in Advanced Melanoma. *N Engl J Med.* 2017;377(14):1345-56.

35. Favero F, Joshi T, Marquard AM, Birkbak NJ, Krzystanek M, Li Q, et al. Sequenza: allele-specific copy number and mutation profiles from tumor sequencing data. *Ann Oncol.* 2015;26(1):64-70.

36. Zhang Y, Parmigiani G, and Johnson WE. ComBat-seq: batch effect adjustment for RNA-seq count data. *NAR Genom Bioinform.* 2020;2(3):lqaa078.

37. Ritchie ME, Phipson B, Wu D, Hu Y, Law CW, Shi W, et al. limma powers differential expression analyses for RNA-sequencing and microarray studies. *Nucleic Acids Res.* 2015;43(7):e47.

38. Love MI, Huber W, and Anders S. Moderated estimation of fold change and dispersion for RNA-seq data with DESeq2. *Genome Biol.* 2014;15(12):550.

39. Chen B, Khodadoust MS, Liu CL, Newman AM, and Alizadeh AA. Profiling Tumor Infiltrating Immune Cells with CIBERSORT. *Methods Mol Biol.* 2018;1711:243-59.

40. Newman AM, Liu CL, Green MR, Gentles AJ, Feng W, Xu Y, et al. Robust enumeration of cell subsets from tissue expression profiles. *Nat Methods.* 2015;12(5):453-7.

41. Newman AM, Steen CB, Liu CL, Gentles AJ, Chaudhuri AA, Scherer F, et al. Determining cell type abundance and expression from bulk tissues with digital cytometry. *Nat Biotechnol.* 2019;37(7):773-82.

42. Skidmore ZL, Campbell KM, Cotto KC, Griffith M, and Griffith OL. Exploring the Genomic Landscape of Cancer Patient Cohorts with GenVisR. *Curr Protoc.* 2021;1(9):e252.